AD_____

Award Number:
W81XWH-09-1-0090

TITLE:
Combining osteoinductive and antimicrobial therapies to improve healing of contaminated/infected segmental long bone defects

PRINCIPAL INVESTIGATOR:
Chia Soo, M.D.

CONTRACTING ORGANIZATION:
University of Southern California
Los Angeles, California 90095

REPORT DATE:
December 2012

TYPE OF REPORT:
Final

PREPARED FOR: U.S. Army Medical Research and Materiel Command
Fort Detrick, Maryland 21702-5012

REPORT DOCUMENTATION PAGE

Form Approved
OMB No. 0704-0188

1. REPORT DATE	2. REPORT TYPE	3. DATES COVERED
December 2012	Final	15 Dec 2008 – 14 Dec 2012

4. TITLE AND SUBTITLE

Combining osteoinductive and antimicrobial and antimicrobial therapies to improve healing of contaminated/infected segmental long bone defects

5a. CONTRACT NUMBER

5b. GRANT NUMBER
W81XWH-09-1-0090

5c. PROGRAM ELEMENT NUMBER

6. AUTHOR(S)

Chia Soo, M.D. (PI)
Zhong Zheng, PhD, Xinli Zhang, M.D., Ph.D., Kang Ting, D.M.D.

E-Mail: bsoo@ulca.edu

5d. PROJECT NUMBER

5e. TASK NUMBER

5f. WORK UNIT NUMBER

7. PERFORMING ORGANIZATION NAME(S) AND ADDRESS(ES)

University of Southern California, Los Angeles, CA 90095

8. PERFORMING ORGANIZATION REPORT NUMBER

9. SPONSORING / MONITORING AGENCY NAME(S) AND ADDRESS(ES)
U.S. Army Medical Research and Materiel Command
Fort Detrick, Maryland 21702-5012

10. SPONSOR/MONITOR'S ACRONYM(S)

11. SPONSOR/MONITOR'S REPORT NUMBER(S)

12. DISTRIBUTION / AVAILABILITY STATEMENT
Approved for Public Release; Distribution Unlimited

13. SUPPLEMENTARY NOTES

14. ABSTRACT
BMP2-coupled Nanosilver-PLGA composite grafts have been shown to successfully repair grossly infected segmental defects. However, BMP2–regenerated bones are known to have cyst-like bone voids and extensive amounts of fatty tissue. In this study, we hypothesize that addition of the osteoinductive growth factor Nell-1 to the BMP2-coupled Nanosilver-PLGA composite grafts will achieve higher quality bone and faster rates of fusion. Nell-1+BMP2 were added to Nanosilver PLGA scaffolds and implanted into 6 mm rat femoral defects contaminated with 108 S. aureus Mu50. High resolution faxitron images were obtained at 2, 4, 6, 8, 10, and 12 weeks. F emurs were harvested at 12 weeks post-operation. MicroCT analysis, histology, and immunohistochemistry were performed. Nell-1+BMP2 showed faster healing of femoral defects by 8 weeks post-operation compared to 12 weeks in the previous study with BMP2 alone. Progressive mineralization was seen starting at 4 weeks, with 100% fusion achieved by 8 weeks. MicroCT 3D reconstructions showed robust bone formation with no c yst formation. Histology showed densely packed woven and lamellar bone. Nell-1+BMP2 appear to have synergistic effects. The combination of BMP2+Nell-1 improved bone formation over either cytokine alone, and is a promising combination therapy for faster healing of contaminated bone loss.

15. SUBJECT TERMS
Osteoinductive molecules, bone morphogenetic proteins, Nell-1, demineralized bone matrix, segmental long bone defects, osteoconductive, scaffolds, infection, antimicrobials

16. SECURITY CLASSIFICATION OF:			17. LIMITATION OF ABSTRACT	18. NUMBER OF PAGES	19a. NAME OF RESPONSIBLE PERSON
a. REPORT	b. ABSTRACT	c. THIS PAGE			USAMRMC
U	U	U	UU	57	19b. TELEPHONE NUMBER *(include area code)*

Table of Contents

Title: Combining osteoinductive and antimicrobial therapies to improve healing of contaminated/infected segmental long bone defects

PI: Chia Soo

Start date: Dec. 15, 2008

Grant No.: W81XWH-09-1-0090

INTRODUCTION:

Blast weapons such as rocket propelled grenades, mortars, and improvised explosive devices (IEDs) can cause devastating extremity injuries that destroy soft tissue and bone as well as produce significant wound contamination and the potential for secondary infection (*1*). Current approaches for bone regeneration of large defects utilize a combination of autograft, allograft, synthetic, and/or recombinant protein based materials. However, all these techniques can be associated with prolonged times for fracture healing with high failure rates, especially in contaminated/infected wounds. Thus, the development of more efficient osteoinductive and osteoconductive therapeutics that can decrease fracture healing time and reduce the incidence of delayed unions or nonunions, while concurrently preventing bacterial colonization and infection, could save substantial military medical and personnel resources by accelerating the return of military personnel to full duties. Exogenous bone morphogenetic proteins (BMPs) (Medtronic InFUSE® Bone Graft) application to open tibial fractures has already demonstrated feasibility of a single pronged approach to bone regeneration (*2*). However, the high doses of BMP2 required for successful bone regeneration may reflect in part the inefficiencies of a monotherapy approach to complex bone regeneration scenarios. In our preliminary studies, we found that Nell-1 [Nel-like molecule-1; Nel (a protein strongly expressed in **n**eural tissue encoding **e**pidermal growth factor **l**ike domain)] is osteoinductive *in vivo* and that Nell-1 induces bone quantity similar to BMP2 in orthotropic locations. Importantly, Nell-1 induces osteoprogenitor cells and bone marrow stromal cells (BMSCs) to form bone of better quality and maturity than BMP2. Our preliminary data demonstrated exciting additive or synergistic effects of combined Nell-1 + BMP2 on bone regeneration that far exceeds the bone regenerative capacity and quality of BMP2 alone.

With regards to infection prevention and control, the antimicrobial properties of silver have long been recognized. Silver is used to reduce bacterial colonization/infection in a broad range of devices such as vascular and urinary catheters (*3*), endotracheal tubes, and implantable prostheses (*4*). Previous studies revealed that nanosilver (Ag^{NANO}) of defined size appears to be bactericidal without discernable *in vitro* toxicity to osteoblasts (*5-7*). Moreover, in mouse wounds, Tian et al. showed more rapid healing and less scar after addition of silver nanoparticles (*8*). These results strongly suggest that a combo-therapy of Nell-1 + BMP2 and Ag^{NANO} could substantially increase the rate of osseous defect healing—resulting in decreased costs and adverse effects. Overall, we anticipate Nell-1 + BMP2 to deliver improved bone quantity/quality *vs*. BMP2 monotherapy.

BODY:

THE APPROVED AND ADJUNCTIVE TASKS ARE LISTED BELOW:

Task 1: To optimize Nell-1 + BMP2 mediated long bone regeneration (Months 1-31)

a. Optimize Nell-1 + BMP2 dose in a femoral trepanation defect model (Months 1-12)

b. Optimize Nell-1 + BMP2 dose in an adductor thigh muscle model (Months 4-16)

c. Optimize Nell-1 + BMP2 dose in a femoral segmental defect model (Months 13-31)

Task 2: To determine if nanocrystalline silver impacts optimized Nell-1 + BMP2 long bone regeneration (Months 1-36)

a. Determine bactericidal doses of nanocrystalline silver (Ag^{NANO}) *in vitro* (Months 1-9)

b. Determine cytotoxic doses of Ag^{NANO} *in vitro* (Months 1-4)

c. Effect of Ag^{NANO} on Nell-1 + BMP2 in critical femoral segmental defects (Months 23-36)

Task 3: To maintain optimized Nell-1 + BMP2 long bone regeneration in contaminated/infected wounds (Months 7-48)

a. Determine bacteria inoculum dose to produce localized femoral segmental infection (Months 7-24)

b. Implantation of Nell-1+BMP2+Ag^{NANO} in infected critical femoral segmental defects (Months 30-48)

Adjunctive Task: To create nanocrystalline silver-based infection-resistant hardware device to promote bone formation in contaminated/infected wounds (Months 16-36)

Rationale: In fact, a lot of infections are thought to occur by invading bacteria at the time of surgery (*9-11*). These bacteria adhere to foreign bodies like prostheses and other osteosynthetic devices and form biofilms that block the penetration of antibiotics and host immune responses in order to promote the survival of bacteria within these biofilms (*12, 13*). The basic principles of contamination/infection control have been either physically removing the infected hardware and host tissues (*e.g.*, by surgical debridement or vacuum-assisted wound closure devices) or killing and/or preventing growth of the bacteria (*e.g.*, by antibiotics and antiseptics) (*14*). Thus, to control surgical implant-associated infections, removal of infected devices, multiple debridement surgeries, and long-term systemic antibiotic therapy are generally required (*15-20*). As a result, the treatment of a surgical implant infection requires extensive medical and surgical care, increasing patient morbidity and resulting in longer disability, rehabilitation and healthcare costs. Moreover, even with all of these treatments, it is exceedingly difficult to clear the infection because the existing devascularized bone and other necrotic tissues are ideal matrixes for bacteria to adhere and survive (*12, 21*). Soon after an implant is surgically placed, a conditioning layer composed of host-derived adhesins (including fibrinogen, fibronectin, collagen, *etc.*) covers the surface of the implant (*12*). This layer favors adherence of free-floating (planktonic) bacteria, which subsequently divide, secrete exopolysaccharide matrix, and form a three-dimensional (3D) biofilm that contains tightly attached (sessile) bacteria (*12*). Once the biofilm forms, the infection is extremely difficult to treat because the biofilms block the penetration of immune cells (such as macrophages) and antibiotics (*12, 22-25*). Since the treatment of infected implanted materials is exceedingly difficult, strategies aimed at preventing the infection and biofilm from forming in the first place is critical to the future success of the implant. Recently, antibiotics have been directly coated onto or covalently-linked to the prosthetic materials in order to prevent bacteria from infecting the implants at the time of surgery (*26-34*). However, implant-associated infections involve a broad spectrum of bacteria, including Gram-positive *Staphylococcus aureus*, *Staphylococcus epidermidis* and *Streptococci* species, and Gram-negative *Pseudomonas* and *Enterobacter* species (*35, 36*). Since antibiotics often have a narrow spectrum (*37*), they are not effective against all types of bacteria that may cause these infections, and they may also promote antibiotic resistance (*14*). This is especially relevant because there are an increasing number of infections caused by multi-drug-resistant bacteria, especially methicillin-resistant *S. aureus* (MRSA) and methicillin-resistant *S. epidermidis* (MRSE) (*38-40*). Given these limitations of antibiotic therapy, a principle challenge is to develop implant materials possessing inherent broad-spectrum antimicrobial activity that will help prevent implant-associated infections among both Wounded Warriors and the civilian population. In orthopaedic literature, electrically generated silver ions have been successfully used to treat chronic osteomyelitis and infected non-unions (*41-43*). Galvanic deposition of elementary silver on the surface of megaprostheses implanted after orthopaedic tumor resections has also been described in a series of 20 patients without apparent systemic or local toxicity (*44*). Producing infection-resistant hardware device is important because of its high potential to impact bone regeneration/replacement treatments and prevent implant-associated

infection. Therefore, we proposed the **Adjunctive Task** to establish an Ag^{NANO}- based infection-resistant hardware device.

a. Optimize Ag^{NANO}-coating *in vitro* (Months 16-24)

b. Implantation of Ag^{NANO}-coated hardware in infected femoral canal (Months 25-36)

PROGRESS OF OUR RESEARCH

Our three-year study has shown the feasibility of using combotherapy Nell-1 + BMP2 + Ag^{NANO} to successfully heal infected femoral segmental defects. During the first year, we optimized Nell-1 + BMP2 dose in an orthotopic bone model (femoral trepanation defect), which was approved as **Task 1a**. During the second year, we optimized Nell-1 + BMP2 dose in a femoral segmental defect model, as **Task 1c**, as well as establish an infected femoral defect model in which to test our combotherapy, as **Tasks 2a, b**, and **c**. In addition, we have determined bacteria inoculum dose to produce localized femoral segmental infection, as Task 3a. Moreover, we create Ag^{NANO}-coated hardwire, which presents both antimicrobial and osteoinductive properties *in vitro*, as **Adjunctive Task a**. During the third and final year, we demonstrated Ag^{NANO}-coated hardwire promoted new bone formation and inhibited bacterial infection in a rat femoral canal model, as **Adjunctive Task b**. Moreover, our data also showed efficacy of Nell-1 + BMP2 + Ag^{NANO} in an infected FSD model, as **Task 3b**.

Year 1: Dec. 15, 2008 – Dec. 15, 2009 (Months 1-12)

A complete description of the accomplished tasks of Months 1-12 were presented in the first year report. Briefly, **Tasks 1a** and **Task 1c**, as well as optimization of cylindrical poly(lactic-*co*-glycolic acid) (PLGA) graft creation with nanosilver were completed. **Task 1c** was completed ahead of schedule, in place of **Task 1b**, which was approved for removal from the Approved Tasks as **Task 1c** is a more relevant model to focus on.

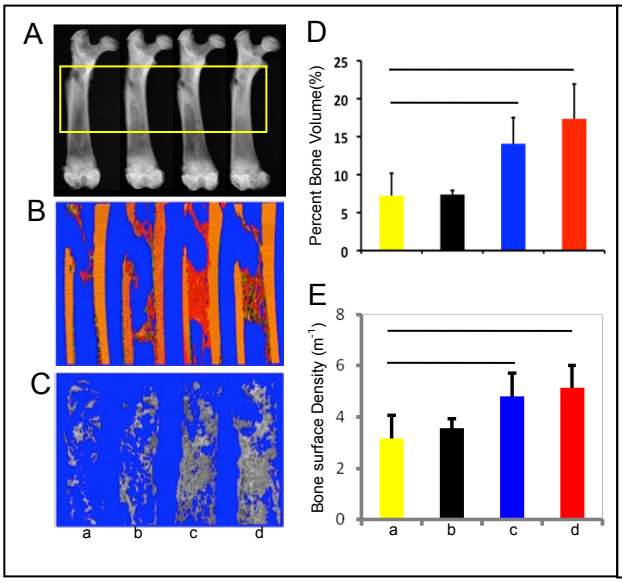

Figure 1. Task 1a: Optimize Nell-1 + BMP2 in a femoral trepanation defect model. Bone marrow injection with PBS, BMP2, Nell-1, and Nell-1 + B MP2. Proteins were lyophilized onto tricalcium phosphate particles (TCP), then injected into femur as shown from left to right (a: control with PBS + TCP; b: 15 µg BMP2; c: 30 µg Nell-1; d: 30 µg Nell-1 + 15 µg BMP2). The X-ray scanning (A) and the 3D sagittal sectioning (B) showed new bone formation (orange>black>green>red from the greatest to least mineralized tissue) with cortical bone in orange. 3D trabecular bone (C) showed trabecular bone present inside the marrow. Bone volume (D) and surface density (E) measurements demonstrate that Nell-1 and Nell-1 + BMP2 induced more bone formation and higher quality of bone compared to PBS control (a) or BMP2 alone (b). *, $p < 0.05$. However, there is no significant different between Nell-1 alone (c) and Nell-1 + BMP2 (d) at $p < 0.05$.

Task 1a utilized a noncritical-sized, 1.5-mm diameter circular femoral diaphysis trepanation defect to rapidly screen and compare multiple Nell-1 + BMP2 dose combinations with BMP2 standards for orthotopic bone healing under low mechanical stress. The trepanation defect was performed as previously described by Niedhart et al. (*45-47*), performing bilateral defects per animal to minimize the number of animals needed for Nell-1 + BMP2 dose optimization. Results are as shown in **Figure 1**.

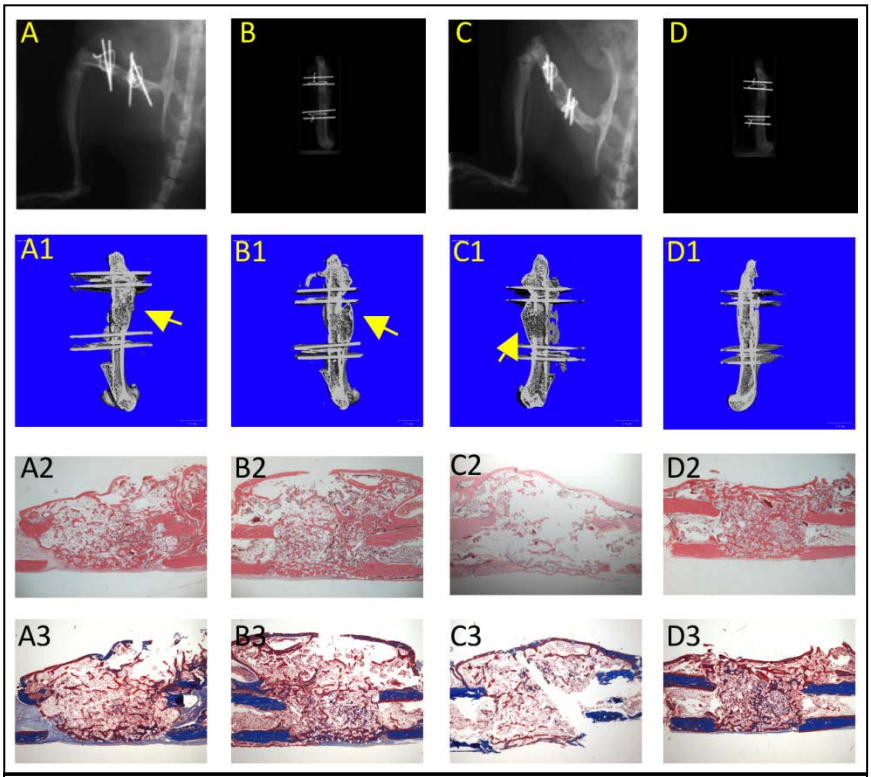

Figure 2. Task 1c: Optimize Nell-1 + BMP2 in a femoral segmental defect model. Nell-1 reduced the BMP2 induced cyst formation during femoral segmental long bong defect regeneration. A, A1, A2, A3: 300 µg/ml BMP2 only; B, B1, B2, B3: 300 µg/ml BMP2 + 100 µg/ml Nell-1; C, C1, C2, C3: 600 µg/ml BMP2 only; D, D1, D2, D3: 600 µg/ml BMP2 + 600 µg/ml Nell-1; A, B, C, D: X-ray; A1, B1, C1, D1: CT analysis; A2, B2, C2, D2: HE staining, 12 x; A3, B3, C3, D3: Masson trichrome staining, 12x. X-ray analysis showed that 300 µg/ml BMP2 only (A), 300 µg/ml BMP2 + 100 µg/ml Nell-1 (B), 600 µg/ml BMP2 only (C), and 600 µg/ml BMP2 + 600 µg/ml Nell-1 (D) can induce 100% bone healing. Meanwhile, also induced cyst formation (yellow arrows) as a side effect. Applying Nell-1 with BMP2 at the same time reduced the cyst formation (B1 and D1), especially at the higher ratio of Nell-1/BMP2 (D1). HE staining (B2 and D2) and Masson trichrome staining (B3 and D3) also revealed that Nell-1 + BMP2 combo treatment induced more novel bone generation relative to the same dose of BMP2 only (HE: A2, C2; Masson trichrome: A3, C3), respectively.

Task 1c utilized a critical sized 6 mm femoral segmental defect in rats to establish Nell-1 + BMP2 doses in a non-infected model. The femoral segmental defects were created as previously described and established in our laboratory (*48*). Defined Nell-1 + BMP2 doses in a constant volume were mixed and lyophilized onto 4 mm diameter x 7 mm length porous PLGA cylinders which were placed into the segmental defect. Results are shown in **Figure 2**, in which BMP2 was shown to produce cyst-like bone formation, which was improved by addition of Nell-1.

It is important to have an Ag^{NANO} delivery system that effectively prevents viable bacterial colonization of the implant to avoid creation of a nidus for infection *in vivo*. Thus, the implant was constructed to have uniform distribution of Ag^{NANO} inside and outside of the scaffold, as shown in **Figure 3**. Cylinder graft fabrication was optimized based on solvent casting and particulate leaching procedure as follows: (1) weigh desired QSI-Nano® Silver Powder and mix thoroughly with 15% (w/v) PLGA/chloroform solution to achieve desired concentration; (2) mix the Ag^{NANO}-PLGA thoroughly with 200-300 mm grain size sugar to generate homogenous paste; (3) pack the paste into the mold followed by solvent evaporation and lyophilization to generate a cylinder size of 4 mm diameter x 7 mm height; (4) dissolve the sugar and coat the cylinder with QSI-Nano® Silver Powder which is suspended in 0.05% (v/v) poly-*N*-vinylpyrrolidone (PVP)/PBS buffer; (5) lyophilize and sterilize the cylinder scaffold with 70% ethanol followed by PBS rinsing; (6) lyophilize and keep the cylinder scaffold stored at -20°C. The multi-porous cylinder scaffold is thus generated for implantation (*49-51*). Maximum concentration of Ag^{NANO} using this

technique was found to be 2% (w/w); otherwise, aggregation of nanoparticles occur creating uneven distribution within the scaffold. Further studies utilizing different concentrations of PVP or different types of surfactants to address the issue of nanosilver aggregation would be beneficial, so that grafts can be constructed with higher nanosilver concentrations without nanoparticle aggregation to treat potentially more virulent or poly-microbial bacterial infections.

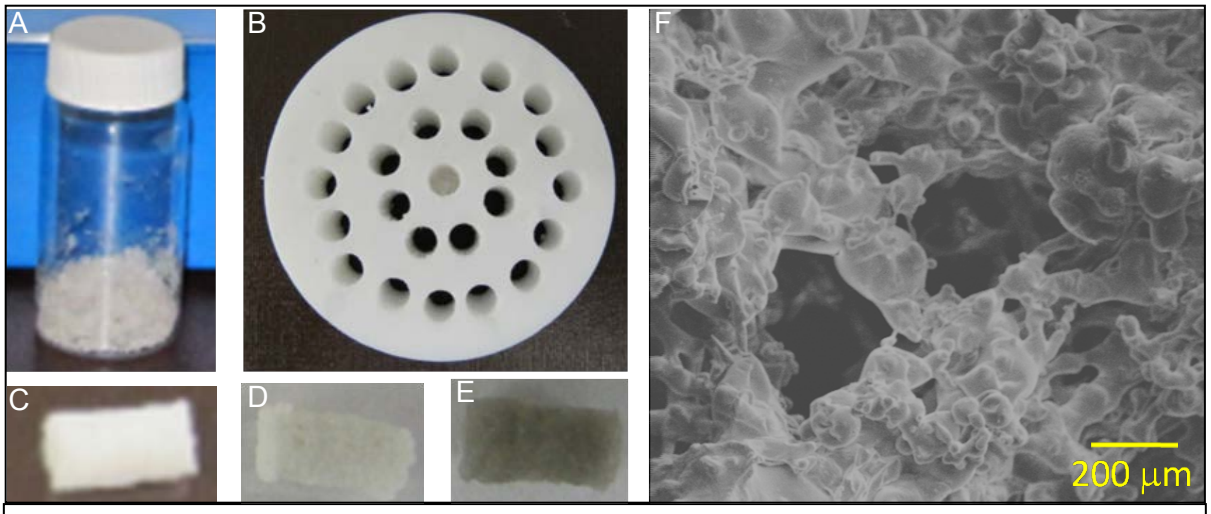

Figure 3. Scaffold fabrication: solvent casting and particulate leaching. A, Ag^{NANO}-PLGA-sugar paste; B, Casting mold; C, Ag^{NANO}-PLGA-sugar formed cylinder scaffold; D, Ag^{NANO}-PLGA cylinder scaffold, after sugar leaching; E, Ag^{NANO}-PLGA cylinder with 1% Ag^{NANO} coating on the surface; and F, TEM showing the structure of the multi-porous Ag^{NANO}-PLGA cylinder scaffold.

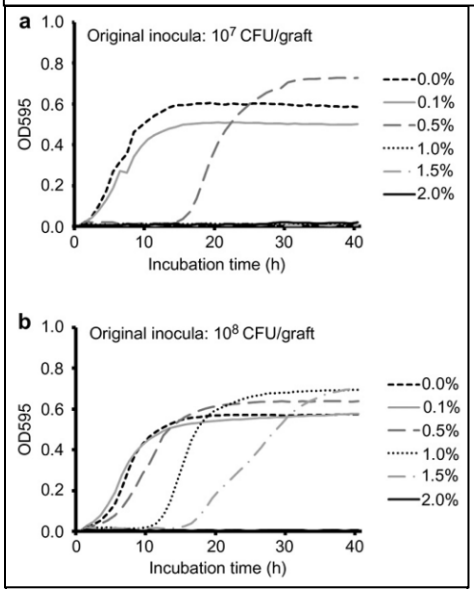

Figure 4. Task 2a: Determine bactericidal doses of nanocrystalline silver (Ag^{NANO}) *in vitro* In vitro antibacterial activity of Ag^{NANO}-PLGA composite grafts. Different inocula (a, 10^7 CFU; b, 10^8 CFU) of *Staphylococcus aureus* Mu50 were injected for microplate proliferation assay.

Year 2: Dec. 15, 2009 – Dec. 15, 2010 (Months 12-24)

A complete description of the accomplished tasks of Months 12-24 was presented in the second year report. Briefly, **Tasks 2a**, **Task 3a**, **Task 2b**, **Task 2c** and **Adjunctive Task a** were completed.

Vancomycin-resistant MRSA clinical strain *Staphylococcus aureus* Mu50 (ATCC 700699) was used to create a bacterial infection model, and was tested against the less virulent SA113 strain (ATCC 35556). *In vitro* testing of the antimicrobial activity of the different doses of nanosilver was done using a microplate proliferation assay for the completion of **Task 2a**. The cylindrical scaffolds were incubated with 10^7 or 10^8 bacterial colony forming units (CFU) of Mu50 in 200 μl of brain heart infusion broth (BHIB; BD, Sparks, MD) in each well of a 96-well microplate (Corning Inc., Corning, NY) at 37°C for 1 hour to allow adherence of the microorganisms to the graft surface. After incubation,

scaffolds were rinsed with phosphate buffered saline (PBS) to remove loosely attached surface cells, and then incubated in 200μl PBS with 0.25% glucose, 0.2% $(NH_4)_2SO_4$, and 1% sterile BHIB for 18 hours at 37°C in another 96-well microplate. During this second incubation step, the viable bacteria attached to the surface or within the scaffolds multiplied and released colony counterparts into the well. After removal of the scaffolds, 100 μl released bacteria were transferred into another 96-well microplate and then amplified by adding 100 μl fresh BHIB for another 40 hours at 37°C. Proliferation of the released daughter cells was monitored at a wavelength of 595 nm online by Tecan Infinite f200 microplate reader (Tecan, Durham, NC) to generate a time-proliferation curve for each well of the microplate. If bacteria were partially or completely inactivated by the scaffold, they were able to seed only a few or even no daughter cells resulting in lagging or absence of bacterial growth. Our results are shown in **Figure 4**; control PLGA scaffolds without nanosilver did not inhibit proliferation of *S. aureus* Mu50 *in vitro*, while dose dependent bactericidal activity was observed in nanosilver PLGA (NS/PLGA) grafts. Grafts with 0.1% nanosilver did not affect 10^7 or 10^8 CFU *S. aureus* Mu50 proliferation, however, when the concentration of nanosilver was increased to 0.5%, bacterial proliferation was delayed in both inoculum densities. Higher concentrations at 1.0% and 1.5% NS/PLGA grafts were even more effective against *S. aureus* Mu50, completely inhibiting proliferation of the lower inoculum of 10^7 CFU and retarding proliferation of 10^8 CFU. At the established ceiling concentration of 2.0% nanosilver, bacterial proliferation of up to 10^8 CFU was completely inhibited *in vitro.* Less consistent results were obtained using the SA113 strain; thus we utilized the Mu50 strain for our remaining experiments.

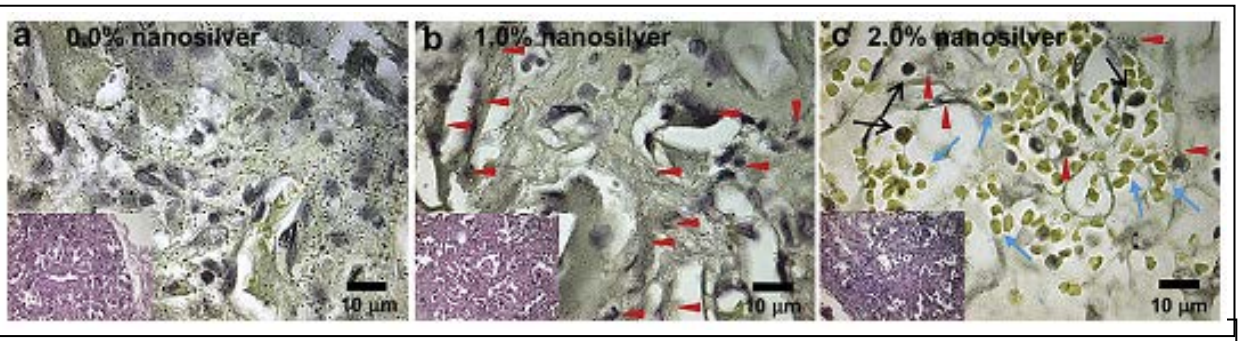

Figure 5. Task 3a: Determine bacteria inoculum dose to produce localized femoral segmental infection. *In vivo* antibacterial activity of nanosilver particle-PLGA composite grafts. After 2-week contamination with 10^8 CFU *S. aureus* Mu50, rat femoral segmental defects with implanted grafts were harvested, fixed, decalcified, embedded, sectioned and stained with Taylor modified Brown and Brenn gram stain as well as H&E (insert figures). Compared to serious bacterial infection (black dots) found in control PLGA grafts (a), 1.0% nanosilver-PLGA composite grafts significantly reduced bacterial survival to colonized collation (b, red arrows). On the other hand, only limited bacterial colonies (red arrows) were observed in 2.0% nanosilver particle-PLGA composite grafts *in vivo* (c), and more red blood cells (blue arrows) were found in the grafts instead of phagocytes (black arrows).

Using bactericidal findings from **Task 2a**, inoculum doses of Mu50 were tested to further define our *in vivo* infected femoral segmental defect model, as **Task 3a**. We found that 10^8 CFU *S. aureus* Mu50 induced continuous infection in a rat femoral segmental defect model with control PLGA grafts implantation *in vivo*. Phagocytes were the predominant cells found in grafts with 0.0% and 1.0% nanosilver. On the other hand, only limited bacterial colonies were observed in 2.0% NS/PLGA grafts *in vivo*, and more red blood cells were found in the grafts instead of phagocytes at 2 weeks post implantation. Results are depicted in **Figure 5**.

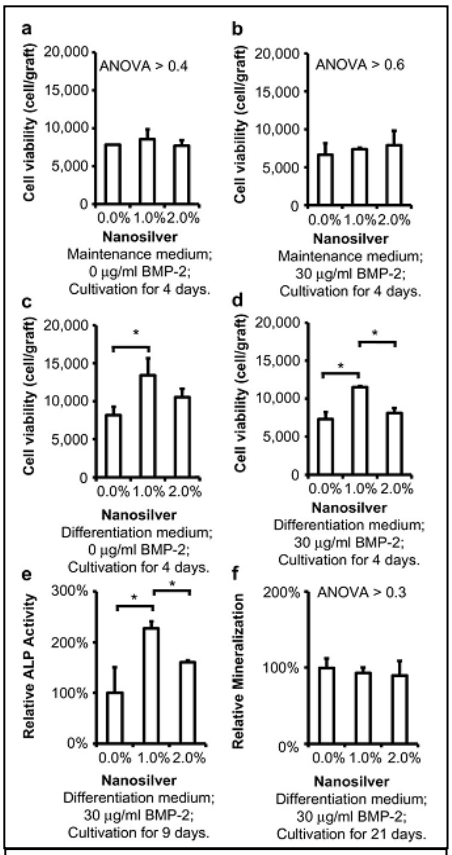

Figure 6. Task 2b: Determine cytotoxic doses of Ag^{NANO} *in vitro*. *In vitro* cytotoxicity of nanosilver particle-PLGA composite grafts. In maintenance medium, up to 2.0% nanosilver did not affect MC3T3-E1 viability with 0 (a) or 30 μg/ml (b) BMP-2. Interestingly, 1.0% nanosilver-PLGA composite grafts induced MC3T3-E1 proliferation in differentiation medium with 0 (c) or 30 μg/ml (d) BMP-2, as well as its ALP activity (e). Otherwise, no significant difference on mineralization was found between the tested grafts (f). *, $P < 0.05$; $N = 6$ for each test.

For **Task 2b** *in vitro* cytotoxicity evaluation of Ag^{NANO}, passage 18 mouse pre-osteoblastic MC3T3-E1 cell line (subclone 4, ATCC CRL-2593) was employed. Briefly, MC3T3-E1 cells were maintained in α-minimal essential medium (α-MEM) supplied with 10% fetal bovine serum (FBS), 1% HT supplement, 100 units/ml penicillin and 100 mg/ml streptomycin (maintenance medium) at 37°C with 5% CO^2. Five thousand cells were seeded on the bone grafts for testing. All media for cell culture were purchased from Gibco (Invitrogen, Calsbad, CA). Cell viability was estimated by 3-(4,5-dimethylthiazol-2-yl)-2,5-diphenyltetrazolium bromide (MTT) metabolism using commercially available Vybrand® MTT Cell Proliferation Assay Kit (Molecular Probes, Invitrogen, Calsbad, CA) with Tecan Infinite f200 microplate reader. In addition, after cultivation in osteoblastic differentiation medium (maintenance medium supplied with 50 μg/ml ascorbic acid and 10 mM β-glycerophosphate), alkaline phosphatase (ALP) activity and degree of mineralization (assessed by Alizarin Red staining) of MC3T3-E1 cells were also quantified. Our findings, depicted in **Figure 6**, showed that MC3T3-E1 cells grew into the grafts in both maintenance and osteoblastic differentiation medium. Neither BMP2 nor up to 2.0% nanosilver affected the viability of MC3T3-E1 cells in maintenance medium. Interestingly, 1.0% nanosilver led to more ongrowth MC3T3-E1 cell proliferation as well as their ALP activity in osteoblastic difference was found in qualitative mineralization evaluation between the BMP2/NS/PLGA grafts and the non-toxic control group (BMP2/PLGA grafts) *in vitro*.

To test the robustness of our Mu50 bacterial inoculum numbers, as well as to confirm the efficacy of our optimized Ag^{NANO} dosing, and verify its non-toxicity in an *in vivo* model, we employed BMP2/NS/PLGA grafts in our infected femoral segmental defect model in 3 month old Sprague Dawley (SD) rats. Creation of the BMP2/NS/PLGA grafts is as described above and the Year 1 report. Surgical procedure for the femoral segmental defects is as described in **Task 1c**. Post surgery and graft implantation, the animals were followed for 12 weeks prior to sacrifice. They underwent weekly high resolution faxitron imaging evaluation, and post-harvest, □CT was utilized for quantitative and qualitative bone formation analysis. Our results showed, by radiographic images, that none or extremely limited bone regeneration occurred in *S. aureus* Mu50 contaminated defects implanted with control BMP2/PLGA grafts and BMP2/1.0% NS/PLGA grafts, respectively, up to 12 weeks post implantation. In addition, there was a loss of bone within the femoral shaft with regression of the proximal and distal cut

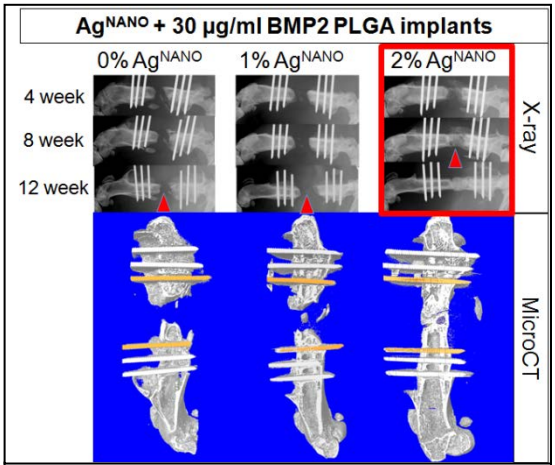

Figure 7. Task 2c: BM2/N2/PLGA graft induced healing in an infected FSD model by 12 weeks. 2D high resolution X-ray and 3D □ reconstruction photos for 10^8 CFU *S. aureus* Mu50 infected rat femoral segmental defects implanted with 0.0% (a), 1.0% (b), and 2.0% (c) nanosilver-PLGA bone grafts coupled with 30 µg/ml BMP-2 at 12 weeks post implantation. Bar =

ends, and significant ectopic bone formation observed in the control group. On the contrary, as early as 6 weeks post implantation, defect fusion resulting from new bone formation was observed in 60% of animals in the group implanted with BMP2/2.0% NS/PLGA grafts. Radiographic findings of bone formation in the femurs were also confirmed by 3D □ CT analysis in **Figure 7**. 3D reconstruction images from the □ CT scan exhibited fusion in the BMP2/2.0% NS/PLGA group, paralleling the quantitative data as well as the 2D radiographic results. In addition, bone mineral density (BMD, $p = 0.036$) and percent bone volume (BV/TV, $p = 0.046$) were found to be significantly greater in the BMP2/2.0% NS/PLGA group compared to the BMP2/PLGA control group.

The quality of newly formed bone was further evaluated by H&E and Masson's trichrome staining, while Taylor modified Brown and Brenn gram staining was employed to identify bacterial residue. Consistent with radiographic analyses, there was minimal evidence of bone regeneration with absence of a bony bridge formation in the contaminated femur defect area implanted with BMP2/PLGA control grafts or BMP-2/1.0% NS/PLGA grafts after 12 weeks, as shown in **Figure 8**. However, despite continued bacterial contamination observed, the number of bacterial colonies was reduced in both groups at 12 weeks compared to tissues harvested after 2 weeks post implantation. In contrast, no *S. aureus* Mu50 survival was evident in the contaminated femurs implanted with BMP2/2.0% NS/PLGA bone grafts after 12 weeks. By eliminating bacteria in the defect, BMP2/2.0% NS/PLGA grafts promoted significantly more bone formation compared to the control group. Furthermore, a mineralized bony bridge connecting the two defect ends was clearly identified by both Masson's trichrome staining and OCN IHC staining. High intensity OCN signals signify that new bone formation was still active in the defect area, especially around the mineralized bridge and in the marrow-like cavities at 12 weeks post implantation.

In the creation of a BMP2/NS/PLGA composite graft, the effect of nanosilver particle on BMP2 was also considered, as nanosilver particles could possibly interfere with essential cellular elements relating to BMP2 osteoinductivity when it binds to thiol groups. Fortunately, up to 2.0% concentration of nanosilver particles did not interrupt bone regeneration induced by BMP2 either *in vitro* or *in vivo* as shown in this study. Not surprisingly, infected defects healed slower compared to non-infected defects, although much faster than infected controls treated without nanosilver. The slower healing time could be attributed to partial BMP2 loss and depletion by bacteria so that the actual BMP2 dose is effectively decreased in an infected defect compared to a non-infected one. Future studies using an alternative system for controlled BMP2 delivery and release, such as via microsphere, should be considered to overcome this problem.

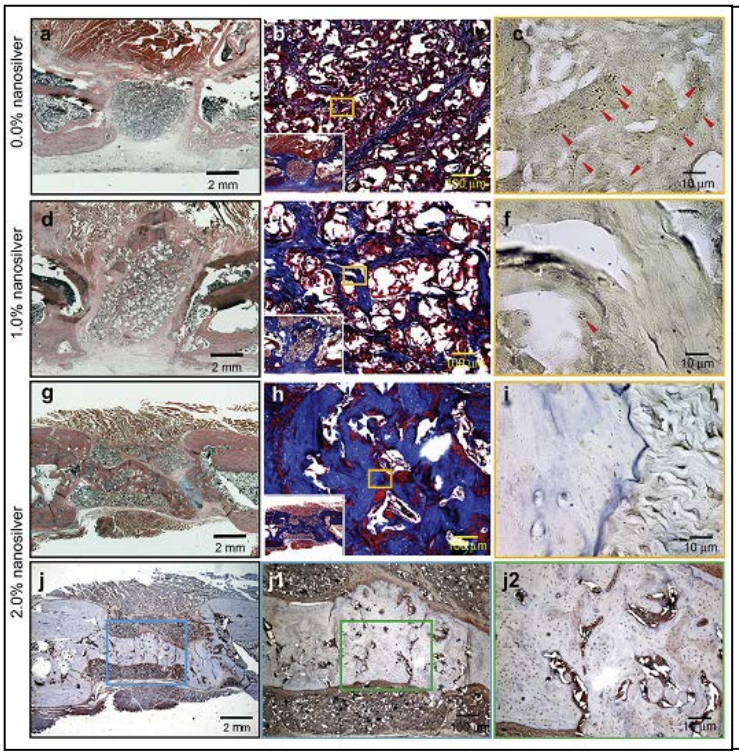

Figure 8. Task 2c: H&E and IHC of 12 week BMP2/NS/PLGA composite grafts. H&E staining (a, d, and g), Masson's trichrome staining (b, e, and h), Taylor modified Brown and Brenn gram stain (c, f, and i) and immunostaining of OCN (j, j1, and j2) of 10^8 CFU *S. aureus* Mu50 contaminated rat femoral segmental defects implanted with 0.0% (a-c), 1.0% (d-f), and 2.0% (g-j2) nanosilver-PLGA bone grafts coupled with 30 mg/ml BMP-2 at 12 weeks post implantation, respectively. Almost no bone regenerated in BMP-2/0.0%-NS/PLGA (control BMP-2 coupled control PLGA) implanted groups (a, and b) with obvious continued bacterial contamination (c, red arrows). Less bone regenerated in the defect area of BMP-2/1.0%-NS/PLGA implanted groups (d and e), while only limited bacterial colonies were observed (f, red arrow). BMP-2/2.0%-NS/PLGA grafts promoted significantly greater bone formation to form a mineralized bony bridge between the two defect ends (g, h, and j) by eliminating bacteria in the defect area (i), Higher magnification figures shows active bone regeneration around the mineralized bridge and in the marrow-like cavities in the bridge (j1, and j2).

The preparation and stabilization of metal nanoparticles represent an open challenge due to the tendency of silver nanoparticles to aggregate. Several polymers have been used to stabilize silver nanoparticles, such as polyethyleneimine (*52*), polyallylamine (*53*), poly(vinyl-pyrrolidone) (*54*), and chitosan (*55*). The nucleophilic character of these polymers (albeit minor) is sufficient for them to bind to the metal particles by donating electrons (*56*). The US Food and Drug Administration (FDA)-approved, biodegradable and biocompatible polymer PLGA has been chosen in **Adjunctive Task a** because the hydrolysable PLGA ester bonds are subject to nucleophilic interactions with incorporated components (*57*), including silver particles. Another advantage of PLGA is that this polymer can be applied onto implants using solvent casting techniques, which allow coating of alloy and even plastic surfaces with polished, irregular or porous materials. For instance, **s**ilver **n**anoparticle (Ag^{NANO})/**P**LGA-coated stainless **s**teel **a**lloy (SNPSA) was simply obtained by incubating 316L steel alloy in Ag^{NANO}/PLGA-chloroform solution. The proportion of Ag^{NANO} refers to the weight ratio of Ag^{NANO} to PLGA. Scanning electromicroscopy (SEM) revealed that a uniform layer of Ag^{NANO}/PLGA was observed on the surface of stainless steel alloy (**Figure 9**). There were no aggregates of Ag^{NANO} in the Ag^{NANO} /PLGA composite layer containing up to 2.0% (w/w) Ag^{NANO} (**Figure 9**).

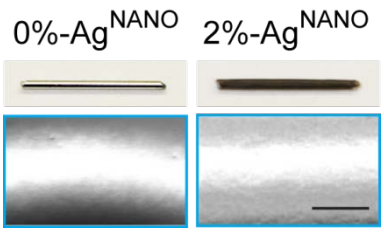

Figure 9. Adjunctive Task a: Morphology of simple Ag^{NANO}/PLGA-coated 316L stainless steel alloy K-wires. Both light microscope (upper panel) and SEM (lower panel) show that up to 2% Ag^{NANO} within PLGA does not result in aggregation. Scale bar: 25 µm.

Bactericidal testing ***in vitro*** was previously done against bacterial-biofilm-forming Gram-positive pathogen *S. aureus* Mu50 and Gram-negative opportunistic pathogen *P. aeruginosa*

PAO-1 (ATCC 15692) (*58, 59*). Bacterial colonization analysis showed that compared with 0%-SNPSA, 1%- and 2%-SNPSAs inhibited initial adherence of *S. aureus* Mu50 (**Figure 10**) and *P. aeruginosa* PAO-1 (**Figure 11**) after 1 h incubation in a bac terial broth in a s ilver-proportion-dependent manner. Quantification of colony formation unit (CFU) demonstrated that, when 0%-SNPSA was incubated with 10^3 CFU *S. aureus* Mu50, almost all the bacteria adhered to the alloy surface in the first hour of incubation, and the number of bacteria markedly increased along with the incubation time (**Figure 10**). This result suggested that *S. aureus* Mu50 extended proliferated on 0%-SNPSA surface after adherence. 1% Ag^{NANO} slightly reduced initial adherence of 10^3 CFU *S. aureus* Mu50 but significantly inhibited its extended proliferation on the coated alloy (**Figure 10**). Initial adherence of 10^3 CFU *S. aureus* Mu50 on 2%-SNPSA was less than 5% (**Figure 10**). Furthermore, none of initial inoculum of 10^3 CFU bacteria survived after 24 h incubation with 2%-SNPSA (**Figure 10**). 2%-SNPSA presented the similar antibacterial properties against 10^3 CFU *P. aeruginosa* PAO-1 as the same initial inoculum of *S. aureus* (**Figure 11**).

In order to further evaluate the effect of silver nanoparticle/PLGA coating on preventing bacterial adherence and biofilm

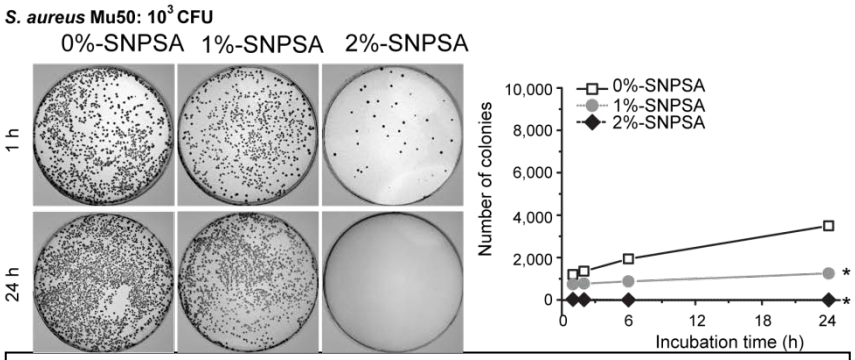

Figure 10. Adjunct Task a: *In vitro* antimicrobial activity of SNPSAs against 10^3 CFU *S. aureus* Mu50. Changes of bacterial colonization after incubation with various SNPSAs revealed that SNPSA inhibited *S. aureus* Mu50 initial adherence and extended proliferation in a silver-proportion-dependent manner *in vitro*. N = 4, *, significant deference compared with 0%-SNPSA, ANOVA < *0.05*, error bars were too small to show.

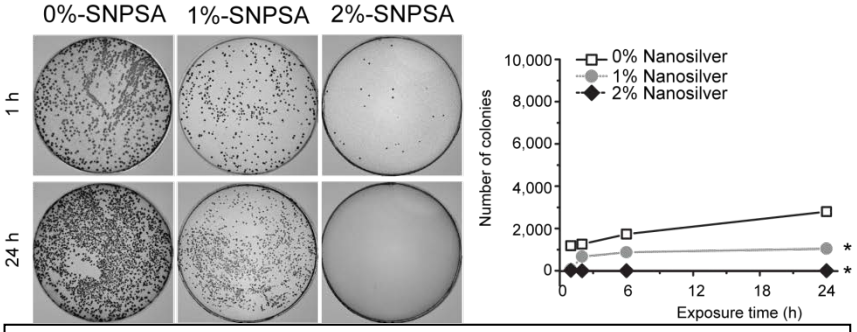

Figure 11. Adjunct Task a: *In vitro* antimicrobial activity of SNPSAs against 10^3 CFU *P. aeruginosa* PAO-1. Changes of bacterial colonization after incubation with various SNPSAs revealed that SNPSA inhibited *P. aeruginosa* PAO-1 initial adherence and extended proliferation in a silver-proportion-dependent manner *in vitro*. N = 4, *, significant deference compared with 0%-SNPSA, ANOVA < *0.05*, error bars were too small to show.

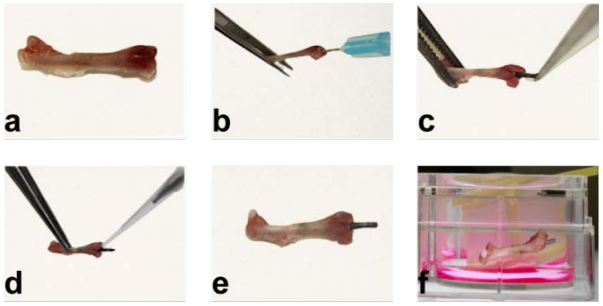

Figure 12. Adjunct Task a: *Ex vivo* antimicrobial model. Femurs isolated from 12-week old male 129/sv mice (**a**) were used for SNPSA *ex vivo* antimicrobial activity test. After locating the femoral intercondylar notch, an intramedullary canal was manually reamed into the distal femur with a 25 gauge n eedle (**b**). A SNPSA K-wire was then placed into the intramedullary canal (**c**) with 2 μl bacteria suspended in PBS (**d**). Then, these femurs (**e**) with implants were placed in 100 mm cell strainer within 6-well culture plate containing 2 ml medium (**f**). In order to avoid direct contact between SNPSA and cell culture medium, the distal femur with a protruding SNPSA was angled superiorly, and the proximal femur was soaked in culture medium.

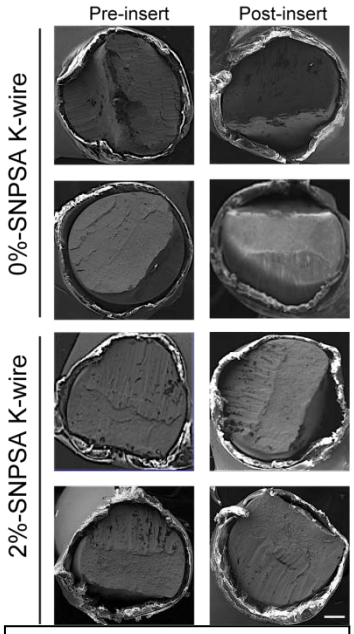

Figure 13. Adjunctive Task a: SEM images of SNPSA K-wires. Placing SNPSA K-wires into the pre-reamed intramedullary canal (See **Figure 12**) did not considerably damage the Ag^{NANO}/PLGA coating. Scale bar: 100 μm.

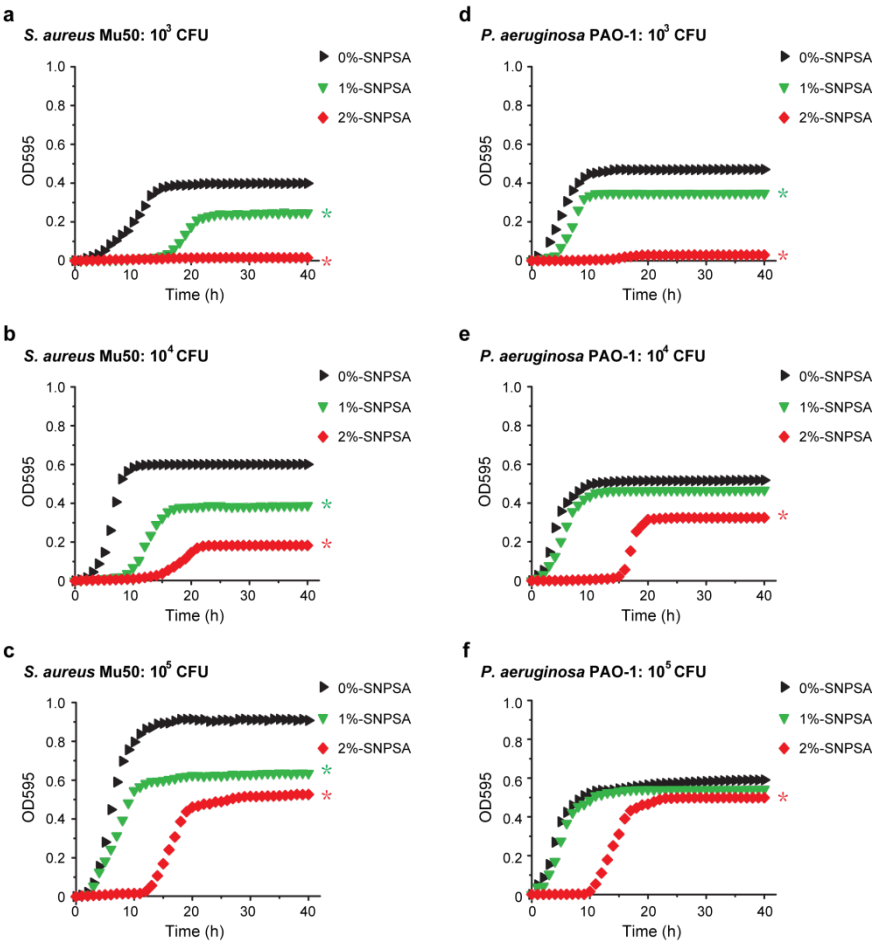

Figure 14.Adjunctive Task a: *Ex vivo* antimicrobial activity of SNPSAs. Using an *ex vivo* antimicrobial model (See Fig. 5), antimicrobial activity of SNPSAs was further investigated against 10^3 (**a**), 10^4 (**b**), and 10^5 (**c**) CFU *S. aureus* Mu50 as well as 10^3 (**d**), 10^4 (**e**), and 10^5 (**f**) CFU *P. aeruginosa* PAO-1 *ex vivo*. After being cultured at 37°C, 5% CO_2, 95% humidity in cell culture incubator for 18 h, SNPSA was removed from the intramedullary canal and incubated in 1 ml nutrient PBS [1 x PBS with 0.25% glucose, 0.2% $(NH4)_2SO_4$, and 1% sterile bacterial growth broth] for 18 h. 100 μl of released bacteria was transferred into a 96 -well microplate and t hen amplified by adding 100
released daughter cells was monitored at a wavelength of 595 nm online by Tecan Infinite f200 microplate reader (Tecan, Durham, NC) to generate a time-proliferation curve for each well of the microplate. SNPSA effectively prohibited bacterial proliferation in a silver-proportion-dependent manner. N = 3, *, significant difference compared with 0%-SNPSA, ANOVA < *0.05*, error bars were too small to show.

formation on the surface of implants, an ***ex vivo*** contamination model (**Figure 12**) was employed with previously reported microplate proliferation assay (*60, 61*). SEM showed that placing SNPSA K-wires into the pre-reamed intramedullary canal did not considerably damage the coating (**Figure 13**). Control 0%-SNPSA did not inhibit *ex vivo* bacterial adherence/proliferation, while silver-proportion-dependent antimicrobial activity was observed in 1%- and 2%-SNPSAs (**Figure 14**). Higher silver proportion at 2% silver nanoparticle was more effective against *ex vivo* adherence/proliferation of 10^4 or 10^5 CFU *S. aureus* Mu50 and *P. aeruginosa* PAO-1 (**Figure 14**), respectively. Furthermore, *ex vivo* adherence/proliferation of 10^3 CFU *S. aureus* Mu50 and *P. aeruginosa* PAO-1 was completely inhibited by 2%-SNPSA (**Figure 14**).

Meanwhile, osteogenic activity of SNPSAs were evaluated *in vitro* to accomplish **Adjunctive Task a** in Year 2. Generally, silver nanoparticles resulted in increased MC3T3-E1 cell proliferation on SNPSAs in a silver-proportion-dependent manner (**Figure 15a**). Interestingly,

along with the culture time, SNPSAs with higher silver proportions promoted cell proliferation more potently (**Figure 15a**). For example, cell proliferation on 2%-SNPSA was 1.17, 1.63, and 1.88 times greater than that on control 0%-SNPSA after 3, 6, and 9 da ys in osteoblastic differentiation medium, respectively. To assay osteoblastic cell function, ALP activity in MC3T3-E1 cells was measured after 9 days in osteoblastic differentiation medium. SNPSAs significantly increased ALP activity of ongrowth cells compared to 0%-silver nanoparticle controls (**Figure 15b**). Furthermore, SNPSAs also significantly promoted ongrowth terminal differentiation of osteoblasts, as indicated by mineralization, during the 21-day culture period (**Figure 15c**). Therefore, SNPSAs exhibited osteoinductive properties in a silver-proportion-dependent manner *in vitro*.

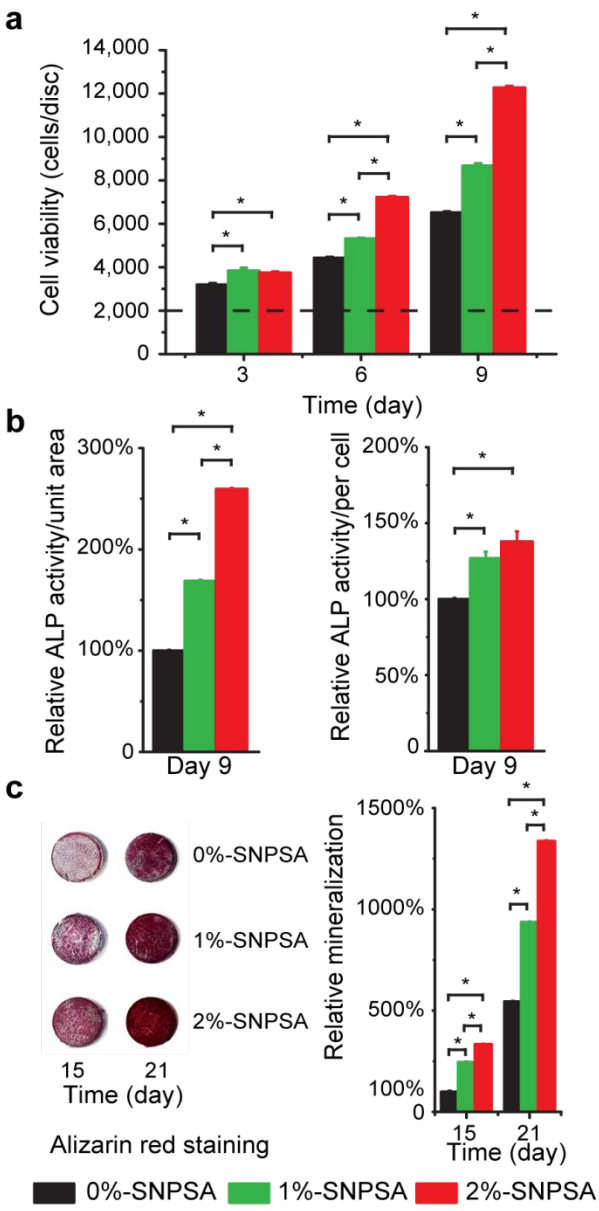

Figure 15. Adjunctive Task a: *In vitro* osteoinductive activity of SNPSAs. SNPSAs significantly promoted MC3T3-E1 cell proliferation (**a**), ALP activity (**b**), as well as mineralization (**c**) in a silver-proportion-dependent manner. Data were normalized to 0%-SNPSA on day 9 (**b**) or on day 15 (**c**). N = 6, *, *P < 0.05*.

Year 3: Dec. 15, 2010 – Dec. 15, 2011 Months 24-36

Adjunctive Task 2 was completed in the final year using an infected rat femoral canal (FC) model. All surgical procedures were approved by the UCLA Office of Animal Research Oversight (protocol #2008-073). Using aseptic technique, a 25 -30 mm longitudinal incision was made over the anterolateral aspect of the left femur of 12-week old male Sprague-Dawley (SD) rats. The femoral shaft was then exposed by separating the vastus lateralis and biceps femoris muscles. Using a micro-driver (Stryker, Kalamazoo, MI), four canals were drilled on each femur with 2-mm interface. SNPSA K-wires were implanted into each predrilled canal. For bacterial inoculation, 10^3 CFU S. aureus Mu50 or P. aeruginosa PAO-1 in 10 ^{5} CFU/ml (10 µl) was pipetted into the canal before implantation. After inoculation, the overlying muscle and fascia were closed with 4-0 Vicryl absorbable suture to secure the implant in place. Following surgery, the animals were housed in separate cages and allowed to eat and d rink ad libitum. Weight bearing was started immediately postoperatively, and t he animals were monitored daily. Buprenorphine was administered for 2 days as an analgesic, but no antibiotic was administered.

No obvious radiographic signs of bone formation were observed in rat FCs implanted with either uncontaminated (**Figure 16**) or bacterially contaminated (**Figure 17**) 0%-SNPSAs up to 8 weeks post-surgery; instead, radiographic evidence of osseous destruction was detected in the contaminated 0%-SNPSA group (**Figure 17**). In contrast, significant bone formation surrounding 2%-SNPSAs implants in rat FCs was observed despite the initial contamination with 10^3 CFU bacteria (**Figures 16**, and **17**). In addition, no osteolysis was observed in the contaminated 2%-SNPSAs group (**Figure 17**). Radiographic findings of bone formation surrounding contaminated 2%-SNPSA implants in rat FCs were also confirmed by 3D microCT analysis (**Figure 17**). Microscopic examination revealed bacterial persistence (**Figure 18a**) accompanied by many inflammatory cells (**Figure 18b**) in the intramedullary tissues around 0%-SNPSA implants in rat FCs 8 weeks after implantation with 10^3 CFU initial bacterial inoculum. In contrast, no bacterial survival was evident around 2%-SNPSA implants under the same conditions (**Figure 18a**), and inflammatory cell infiltration in the intramedullary tissues around the implants was minimal (**Figure 18b**). Thus, 2%-SNPSA implants markedly inhibited bacterial invasion without evoking significant host inflammatory responses *in vivo*. Newly formed bone around SNPSA implants was further evaluated by H&E staining, Trichrome staining, and IHC staining with an antibody against OCN, a marker of mature differentiated osteoblasts, at 8 weeks after implantation with 10^3 CFU initial bacterial inoculum. Only minimal bone formation around the 0%-SNPSA groups was observed (**Figure 18c** and **d**). On the other hand, consistent with radiographic analyses, significant bone formation

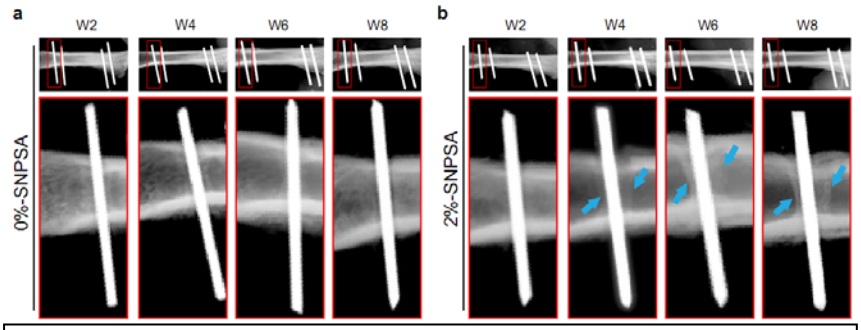

Figure 16. Adjunctive Task b: Radiographic images of uncontaminated 0%- and 2%-SNPSA implants in rat FCs. No obvious signs of bone formation were shown in rat FCs implanted with 0%-SNPSA up to 8 weeks post-surgery (a). In contrast, radiography revealed significant bone formation (blue arrows) around 2%-SNPSAs implanted in rat FCs (b).

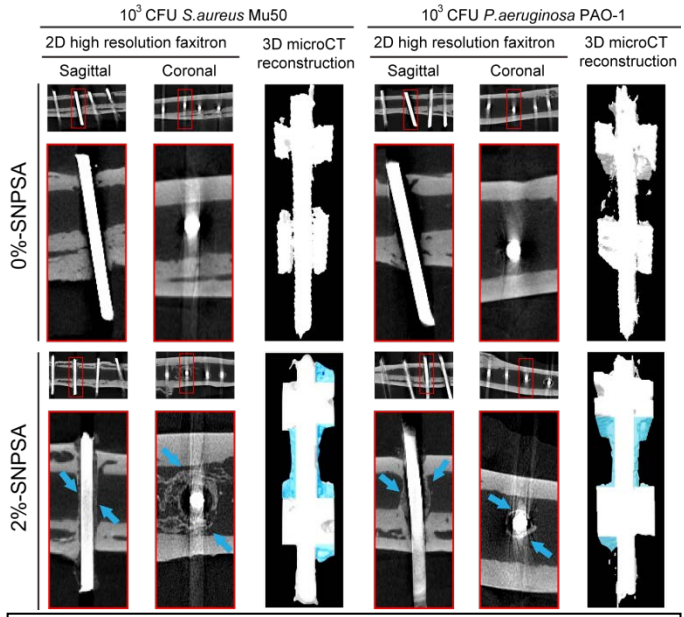

Figure 17. Adjunctive Task b: Radiographic images of contaminated 0%- and 2%-SNPSA implants in rat FCs 8 weeks after implantation. 10^3 CFU *S. aureus* Mu50 or *P. aeruginosa* PAO-1 in 10 ^{5} CFU/ml) was pipetted into the canal before implantation for bacterial invasion. No obvious signs of bone formation were shown in rat FCs implanted with 0%-SNPSA up to 8 weeks post-surgery. In contrast, radiographic analysis revealed significant bone formation around 2%-SNPSAs implanted in rat FCs at week 8 post-implantation (shown as blue rockets in 2D resolution microCT images) without significant osteolysis. Newly formed bone around 2%-SNPSA implants was highlighted in 3D microCT reconstruction images (blue shadows).

was detected around 2%-SNPSA implants (**Figure 18c** and **d**), and intense OCN staining signified that new bone formation was still active around 2%-SNPSA implants at week 8 after implantation (**Figure 18e**). Taken together, 2%-SNPSA implants exhibited significant osteoinductive as well as antibacterial effects *in vivo*.

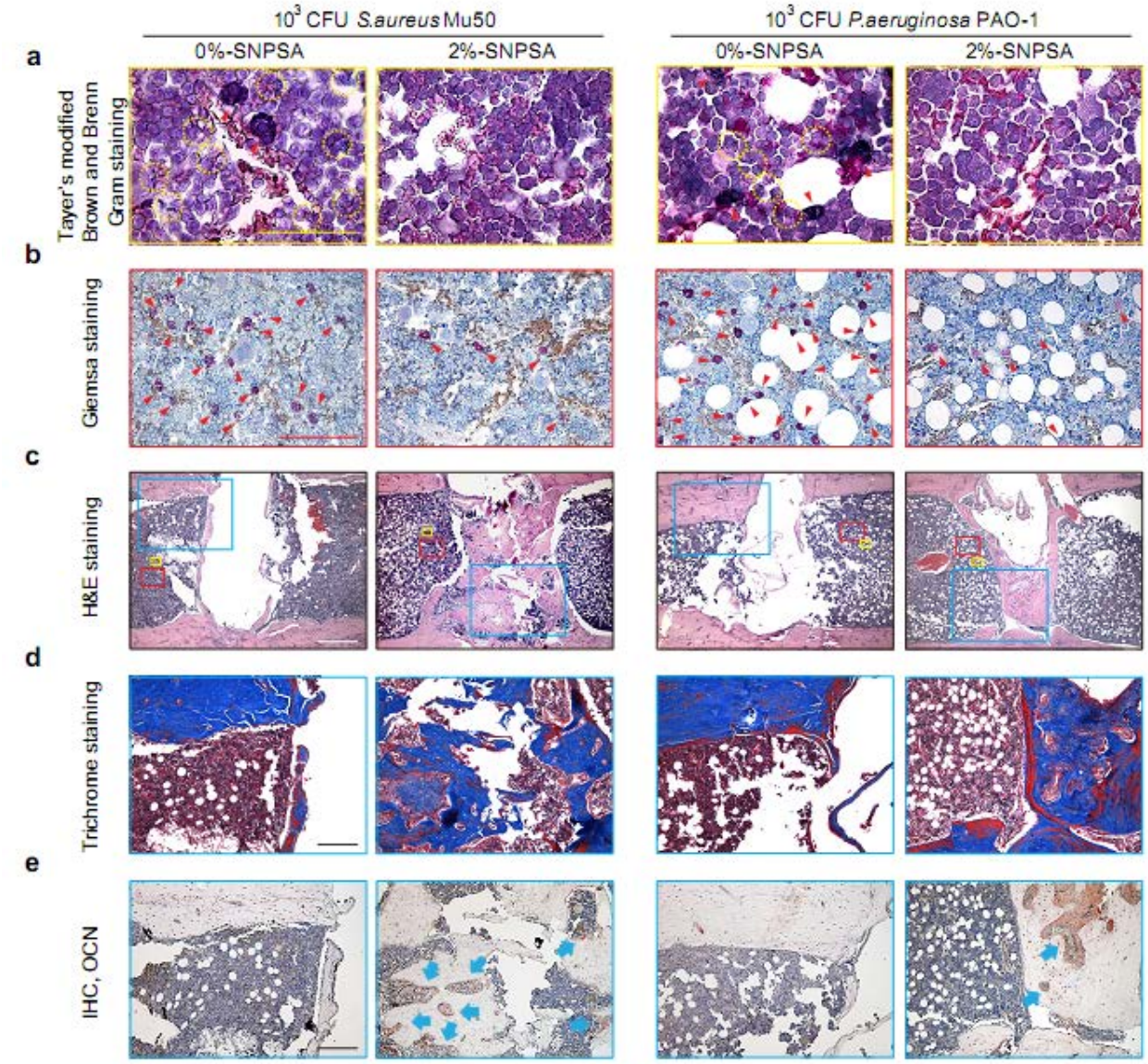

Figure 18. Adjunctive Task b: Histological and IHC analysis of contaminated 0%- and 2%-SNPSA implants in rat FCs at 8 weeks after implantation. 10^3 CFU *S. aureus* Mu50 or *P. aeruginosa* PAO-1 in 10 μl PBS (10^5 CFU/ml) was pipetted into the canal before implantation for bacterial invasion. Taylor-modified Brown and Brenn Gram staining (a) and Giemsa staining (b) revealed bacterial persistence (yellow dotted circles) with massive inflammatory cell infiltration (red arrowheads) in the intramedullary tissue around 0%-SNPSA implants in rat FCs. In contrast, no bacterial survival was evident around 2%-SNPSA implants in the same situation, and inflammatory cell infiltration in the intramedullary tissues around the implants was minimal. Consistent with the radiographic analysis, only minimal bone formation around the 0%-SNPSA groups was observed, whereas significant bone f ormation (blue arrows) was detected around 2%-SNPSA implants, as shown by H &E staining (c), Masson's Trichrome staining (d), and immunostaining of high-intensity OCN signals (e). Yellow scale bar = 50 μm; red scale bar = 100 μm; white scale bar = 500 μm; black scale bar = 200 μm.

Task 3b was also completed in the final year. Using optimized Nell-1 + BMP2 doses from **Task 1c**, and optimized Ag^{NANO} dose from **Task 2b**, the combotherapy Nell-1+BMP2+Ag^{NANO} was implanted in a femoral segmental defect using inoculum doses of *S. aureus* Mu50 optimized in **Task 2a** and **Task 3a**. Due to budget cuts imposed on the project, we had to severely decrease the N number for each treatment group in order to perform all tasks presented within the budget constraints.

Using an implant consisting of 600 μg/ml Nell-1 and 600 μg/ml BMP2, combined with 0%, 1%, and 2% Ag^{NANO} in a cylindrical PLGA scaffold, we were able to show a trend of robust healing of a 6 mm femoral segmental defect infected with an inoculum dose of 10^8 CFU of *S. aureus* Mu50 by 12 weeks post-operation. Bone regeneration with the combotherapy Nell-1+BMP2+Ag^{NANO} showed higher quality bone by high resolution radiographs (**Figure 19**) and 3D μCT analyses (**Figure 20**) compared with BMP2+ Ag^{NANO} alone, which showed formation of bone beyond the original defect space, but was cyst-like in quality, consisting of an outer bony shell and a central bone void that on histology was found to be filled with adipocytes (**Figure 21**).

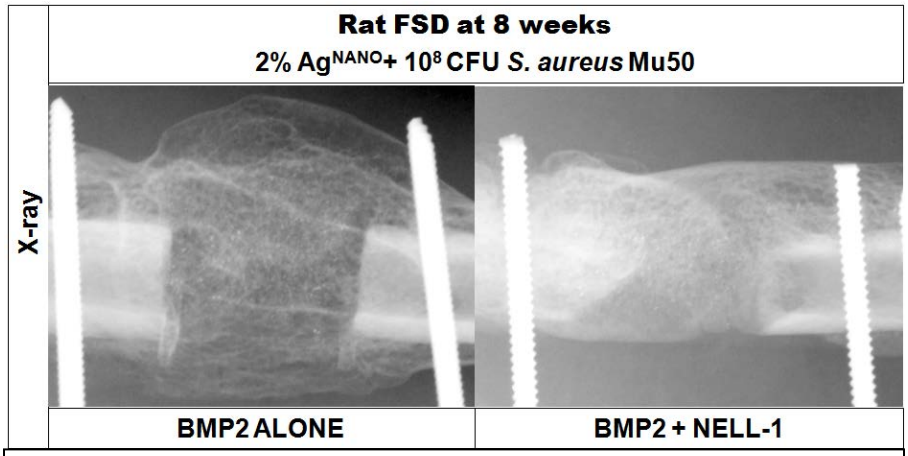

Figure 19. Task 3b: Implantation of Nell-1+BMP2+Ag^{NANO} in infected critical femoral segmental defects. High resolution radiographic images of cyst-like bone formation in defects treated with 600 μg/ml BMP2 alone compared to bone formation treated with 600 μg/ml Nell-1 + 600 μg/ml BMP2 which shows fusion of the defect, with bone limited to the original defect site.

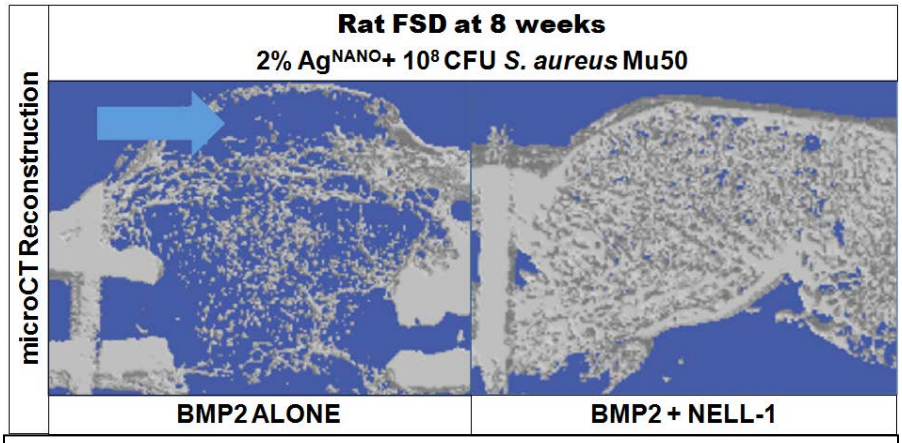

Figure 20. Task 3b: Implantation of Nell-1+BMP2+AgNANO in infected critical femoral segmental defects. 3D μCT reconstruction of FSD samples at 12 weeks, showing cyst-like bone formation in defects treated with 600 μg/ml BMP2 alone compared to bone formation treated with 600 μg/ml Nell-1 + 600 μg/ml BMP2 which shows fusion of the defect, with bone limited to the original defect site.

As stated, a trend showing improvement of BMP2 adverse effects of cyst-like bone formation was observed with addition of Nell-1; however, statistically significant changes in bone volume and bone mineral density was not found between BMP2 alone, and Nell-1 + BMP2. This is likely due to the small N number for each treatment group; a small N number was

necessary in order to complete Task 3b within the reduced budget. Future studies should include additional animals to show definitive findings with statistically significant differences of improved bone healing of infected femoral segmental defects using the combotherapy Nell-1/BMP2/Ag^{NANO}/PLGA graft. In addition, future studies should utilize more virulent strains of bacteria, or multiple bacterial combinations to represent polymicrobial infections seen in clinical scenarios, especially those involving combat extremity injuries.

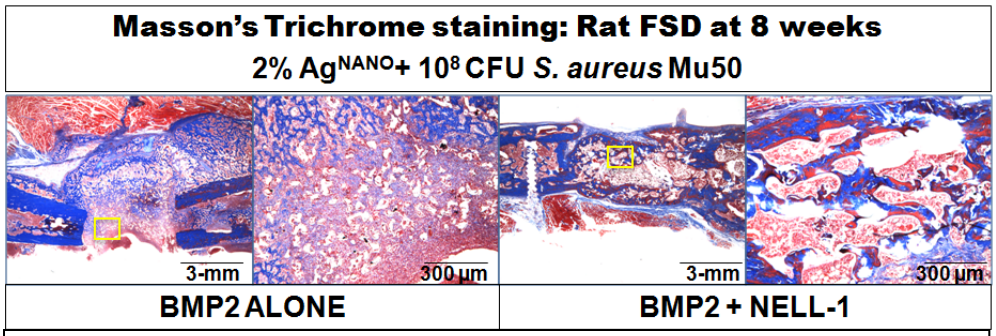

Figure 21. Task 3b: Implantation of Nell-1+BMP2+AgNANO in infected critical femoral segmental defects. Trichrome staining of FSD samples at 12 weeks, confirming cyst-like bone formation in defects treated with 600 g/ml BMP2 alone c with 600 ±1 g/ml Nell g/ml BMP2 which s to the original defect site, consistent with radiographic findings.

KEY RESEARCH ACCOMPLISHMENTS

1. Optimize Nell-1 + BMP2 dose in a femoral trepanation defect model
2. Standardized the procedure for Ag^{NANO}/PLGA cylinders construction
3. Optimize Nell-1 + BMP2 dose in a femoral segmental defect model
4. Determine bactericidal doses of Ag^{NANO} *in vitro*
5. Determine cytotoxic doses of Ag^{NANO} *in vitro*
6. Effect of Ag^{NANO} on BMP2 in critical femoral segmental defects
7. Determine bacteria inoculum dose to produce localized femoral segmental infection
8. Implantation of BMP2+Ag^{NANO} in infected critical femoral segmental defects
9. Implantation of Nell-1 + BMP2 + Ag^{NANO} in infected critical femoral segmental defects
10. Produce the Ag^{NANO}-based hardware devise, which has simultaneous antimicrobial and osteoinductive properties

REPORTABLE OUTCOMES:

Manuscripts:

1. *The use of BMP-2 coupled-nanosilver-PLGA composite grafts to induce bone repair in grossly infected segmental defects.* Z. Zheng, W. Yin, J. N. Zara, W. Li, J. Kwak, R. Mamidi, M. Lee, R. K. Siu, R. Ngo, J. Wang, D. Carpenter, X. Zhang, B. Wu, K. Ting, C. Soo. *Biomaterials* 2010, 31: 9293-9300.
2. *The antimicrobial and osteoinductive properties of silver nanoparticle/poly($_{DL}$-lactic-co-glycolic acid)-coated stainless steel.* Y. Liu, Z. Zheng, J. N. Zara, C. Hsu, D. E. Soofer, K. S. Lee, R. K. Siu, L. S. Miller, X. Zhang, D. Carpenter, C. Wang, K. Ting, C. Soo. *Biomaterials* 2012, 33: 8745-8756.

Conference abstracts:

1. *Nanosilver particles with BMP2 improve bone repair of contaminated segmental defects*. J. Zara, Z. Zheng, W. Yin, M. Lee, J. H. Kwak, R. Siu, X. Zhang, B. Wu, K. Ting, C. Soo. In the 96th American College of Surgeons Annual Clinical Congress, Washington DC, USA, Oct 2010. Selected for podium presentation and received the Excellence in Research Award.
2. *Infected femoral segmental defect model: effects of nanosilver in re-establishing BMP-2 osteoinductivity in infected wounds*. J. Zara, Z. Zheng, W. Yin, W. Li, R. Siu, J. Kwak, R. Ngo, M. Chiang, X. Zhang, K. Ting, C. Soo. Presented at the 2011 Annual Meeting of the Orthopaedic Research Society, Long B each, USA, Jan 2011. Selected for podium presentation.
3. *Synergistic Effects of BMP2 and Nell-1, with NanoSilver for the Healing of Infected Long Bone Defects*. Y Liu, VT Nguyen, JN Zara, AW James, M Chiang, W Yuan, Z Zheng, X Zhang, K Ting, C Soo. Presented at the 97th American College of Surgeons Annual Clinical Congress, San Francisco CA, Oct 2011. Selected for podium presentation.
4. *The use of nanosilver-containing materials for orthopedic application.* Z. Zheng, J. N. Zara, Y. Liu, M. Lee, C. Y. Hsu, K. S. Lee, X. Zhang, K. Ting, C. Soo. In the 2012 Military Health System Research Symposium (MHSRS), Fort Lauderdale, FL, USA, Aug 2012. Selected for poster presentation.
5. *Nanosilver coated stainless steel: an antimicrobial and osteoinductive material for orthopedic device fabrication.* Z. Zheng, Y. Liu, J. N. Zara, M. Chiang, W. Yuan, C. Y. Hsu, D. Soofer., X. Zhang, K. Ting, C. Soo. In the 98th American College of Surgeons Annual Clinical Congress, Chicago, Illinois, USA, Sep 2012. Selected for podium presentation.

CONCLUSIONS:

Our results described above support our hypothesis that Nell-1 can improve BMP2 therapy for bone healing, shown in a femoral trepanation defect model and a femoral segmental defect model, by improving the bone quality obtained with BMP2 alone, which has been shown to elicit cyst-like bone void formation. In addition, employing nanosilver particles, we have successfully regenerated bone in a 6 mm critical-sized defect (total volume ~75 µl) infected with 10^8 CFU vancomycin-resistant MRSA strain Mu50 (i.e., ~10^9 CFU/ml bacteria, which far exceeds the typical 10^5 CFU/ml criteria for invasive tissue infection); contaminated effects that otherwise result in non-union. Meanwhile, our studies demonstrated that Ag^{NANO}-based hardware device exhibited strong bactericidal and osteoinductive properties. Our results also indicated that Ag^{NANO}/PLGA coating is a practical process that is non-toxic, easy to operate, and free of silver nanoparticle aggregation. Since the antibacterial and osteoinductive activities of Ag^{NANO}-based hardware device are silver-proportion-dependent, further improvement of interfacial adhesion of Ag^{NANO} coating to different implant materials, such as stainless steel alloys, titanium and titanium-based alloys, and cobalt alloys, should be investigated and fabricated for clinical application of Ag^{NANO}-based hardware device in orthopedic surgery, especially when permanent implants such as pins and intramedullary rods for the fixation of bone fracture are indicated. Collectively, these results are promising for the future application of bone regeneration therapies combining osteoinductive and antimicrobial components to treat contaminated/infected bone defects, especially in the military population.

REFERENCES:

1. D. Herbert, *Extremity War Injuries: State of the art and future directions*. (Washington, D.C., 2006).

2. S. Govender, e. al., Recombinant human bone morphogenetic protein-2 for treatment of open tibial fractures: a prosepective, controlled, randomized study of four hundred and fifty patients. *J Bone Joint Surg Am* **84-A**, 2123 (2002).

3. C. Seymour, Audit of catheter-associated UTI using silver alloy-coated Foley catheters. *Br J Nurs* **15**, (2006).

4. J. Hardes *et al.*, Lack of toxicological side-effects in silver-coated megaprostheses in humans. *Biomaterials* **28**, 2869 (Jun, 2007).

5. V. Alt *et al.*, In vitro testing of antimicrobial activity of bone cement. *Antimicrob Agents Ch* **48**, 4084 (Nov, 2004).

6. V. Alt *et al.*, An in vitro assessment of the antibacterial properties and cytotoxicity of nanoparticulate silver bone cement. *Biomaterials* **25**, 4383 (Aug, 2004).

7. M. Bosetti, A. Masse, E. Tobin, M. Cannas, Silver coated materials for external fixation devices: in vitro biocompatibility and genotoxicity. *Biomaterials* **23**, 887 (Feb, 2002).

8. J. Tian *et al.*, Topical delivery of silver nanoparticles promotes wound healing. *Chemmedchem* **2**, 129 (Jan, 2007).

9. J. Lee *et al.*, Surgical site infection in the elderly following orthopaedic surgery. Risk factors and outcomes. *J Bone Joint Surg Am* **88**, 1705 (Aug, 2006).

10. E. M. Hetrick, M. H. Schoenfisch, Reducing implant-related infections: active release strategies. *Chem Soc Rev* **35**, 780 (Sep, 2006).

11. D. Campoccia, L. Montanaro, C. R. Arciola, The significance of infection related to orthopedic devices and issues of antibiotic resistance. *Biomaterials* **27**, 2331 (Apr, 2006).

12. R. O. Darouiche, Treatment of infections associated with surgical implants. *N Engl J Med* **350**, 1422 (Apr 1, 2004).

13. B. D. Brause, in *Principle and practice of infectious diseases,* G. L. Mandell, R. G. Douglas, J. E. Bennett, R. Dolin, Eds. (Churchill Livingstong, New York, 2005).

14. L. G. Ovington, The truth about silver. *Ostomy Wound Manage* **50**, 1S (Sep, 2004).

15. P. J. Sanderson, Preventing Infection in Orthopedic Implants. *J Antimicrob Chemoth* **24**, 277 (Sep, 1989).

16. G. J. Taylor, G. C. Bannister, S. Calder, Perioperative wound infection in elective orthopaedic surgery. *J Hosp Infect* **16**, 241 (Oct, 1990).

17. J. K. Koort *et al.*, Efficacy of ciprofloxacin-releasing bioabsorbable osteoconductive bone defect filler for treatment of experimental osteomyelitis due to Staphylococcus aureus. *Antimicrob Agents Chemother* **49**, 1502 (Apr, 2005).

18. M. B. Toma, K. M. Smith, C. A. Martin, R. P. Rapp, Pharmacokinetic considerations in the treatment of methicillin-resistant Staphylococcus aureus osteomyelitis. *Orthopedics* **29**, 497 (Jun, 2006).

19. H. Winkler, K. Kaudela, A. Stoiber, F. Menschik, Bone grafts impregnated with antibiotics as a tool for treating infected implants in orthopedic surgery - one stage revision results. *Cell Tissue Bank* **7**, 319 (2006).

20. C. Allende, M. Mangupli, J. Bagliardelli, P. Diaz, B. T. Allende, Infected nonunions of long bones of the upper extremity: staged reconstruction using polymethylmethacrylate and bone graft impregnated with antibiotics. *Chir Organi Mov* **93**, 137 (Dec, 2009).

21. G. Giavaresi *et al.*, Preliminary investigations on a new gentamicin and vancomycin-coated PMMA nail for the treatment of bone and intramedullary infections: An experimental study in the rabbit. *J Orthop Res* **26**, 785 (Jun, 2008).

22. M. Habash, G. Reid, Microbial biofilms: their development and significance for medical device-related infections. *J Clin Pharmacol* **39**, 887 (Sep, 1999).

23. B. Jansen, G. Peters, Foreign body associated infection. *J Antimicrob Chemother* **32 Suppl A**, 69 (Jul, 1993).

24. J. W. Costerton, Overview of microbial biofilms. *J Ind Microbiol* **15**, 137 (Sep, 1995).

25. J. W. Costerton, Z. Lewandowski, D. E. Caldwell, D. R. Korber, H. M. Lappin-Scott, Microbial biofilms. *Annu Rev Microbiol* **49**, 711 (1995).

26. R. H. Fitzgerald, Jr., Experimental osteomyelitis: description of a canine model and the role of depot administration of antibiotics in the prevention and treatment of sepsis. *J Bone Joint Surg Am* **65**, 371 (Mar, 1983).

27. W. Petty, S. Spanier, J. J. Shuster, Prevention of infection after total joint replacement. Experiments with a canine model. *J Bone Joint Surg Am* **70**, 536 (Apr, 1988).

28. L. Sarda *et al.*, Evaluation of (99m)Tc-ciprofloxacin scintigraphy in a rabbit model of Staphylococcus aureus prosthetic joint infection. *J Nucl Med* **43**, 239 (Feb, 2002).

29. M. Lucke *et al.*, Gentamicin coating of metallic implants reduces implant-related osteomyelitis in rats. *Bone* **32**, 521 (May, 2003).

30. V. Alt *et al.*, The effects of combined gentamicin-hydroxyapatite coating for cementless joint prostheses on the reduction of infection rates in a rabbit infection prophylaxis model. *Biomaterials* **27**, 4627 (Sep, 2006).

31. V. Antoci, Jr., C. S. Adams, N. J. Hickok, I. M. Shapiro, J. Parvizi, Vancomycin bound to Ti rods reduces periprosthetic infection: preliminary study. *Clin Orthop Relat Res* **461**, 88 (Aug, 2007).

32. V. Antoci, Jr. *et al.*, Vancomycin covalently bonded to titanium alloy prevents bacterial colonization. *J Orthop Res* **25**, 858 (Jul, 2007).

33. R. O. Darouiche, M. D. Mansouri, D. Zakarevicz, A. Alsharif, G. C. Landon, In vivo efficacy of antimicrobial-coated devices. *J Bone Joint Surg Am* **89**, 792 (Apr, 2007).

34. N. M. Bernthal *et al.*, A mouse model of post-arthroplasty Staphylococcus aureus joint infection to evaluate in vivo the efficacy of antimicrobial implant coatings. *PLoS One* **5**, e12580 (2010).

35. E. Bouza, P. Munoz, Micro-organisms responsible for osteo-articular infections. *Bailliere's best practice & research. Clinical rheumatology* **13**, 21 (Mar, 1999).

36. D. J. Moojen *et al.*, Identification of orthopaedic infections using broad-range polymerase chain reaction and reverse line blot hybridization. *J Bone Joint Surg Am* **89**, 1298 (Jun, 2007).

37. H. van de Belt *et al.*, Infection of orthopedic implants and the use of antibiotic-loaded bone cements. A review. *Acta Orthop Scand* **72**, 557 (Dec, 2001).

38. D. J. Kilgus, D. J. Howe, A. Strang, Results of periprosthetic hip and knee infections caused by resistant bacteria. *Clin Orthop Relat Res*, 116 (Nov, 2002).

39. K. Hirakawa, B. N. Stulberg, A. H. Wilde, T. W. Bauer, M. Secic, Results of 2-stage reimplantation for infected total knee arthroplasty. *J Arthroplasty* **13**, 22 (Jan, 1998).

40. P. J. James, I. A. Butcher, E. R. Gardner, D. L. Hamblen, Methicillin-resistant Staphylococcus epidermidis in infection of hip arthroplasties. *J Bone Joint Surg Br* **76**, 725 (Sep, 1994).

41. K. Tamura, Some effects of weak direct current and silver ions on experimental osteomyelitis and their clinical application. *Nihon Seikeigeka Gakkai Zasshi* **57**, 187 (Feb, 1983).

42. D. A. Webster, J. A. Spadaro, R. O. Becker, S. Kramer, Silver anode treatment of chronic osteomyelitis. *Clin Orthop Relat Res*, 105 (Nov-Dec, 1981).

43. S. Nand, G. K. Sengar, V. K. Jain, T. D. Gupta, Dual use of silver for management of chronic bone infections and infected non-unions. *J Indian Med Assoc* **94**, 91 (Mar, 1996).

44. J. Hardes *et al.*, Lack of toxicological side-effects in silver-coated megaprostheses in humans. *Biomaterials* **28**, 2869 (Jun, 2007).

45. C. Niedhart *et al.*, The effect of basic fibroblast growth factor on bone regeneration when released from a novel in situ setting tricalcium phosphate cement. *J Biomed Mater Res A* **69A**, 680 (Jun 15, 2004).

46. C. Niedhart *et al.*, Stimulation of bone formation with an in situ setting tricalcium phosphate/rhBMP-2 composite in rats. *J Biomed Mater Res A* **65A**, 17 (Apr 1, 2003).

47. C. Niedhart, U. Maus, E. Redmann, C. H. Siebert, In vivo testing of a new in situ setting beta-tricalcium phosphate cement for osseous reconstruction. *J Biomed Mater Res* **55**, 530 (Jun 15, 2001).

48. C. M. Cowan, C. Soo, K. Ting, B. Wu, Evolving concepts in bone tissue engineering. *Curr Top Dev Biol* **66**, 239 (2005).

49. Y. Deng *et al.*, Poly(hydroxybutyrate-co-hydroxyhexanoate) promoted production of extracellular matrix of articular cartilage chondrocytes in vitro. *Biomaterials* **24**, 4273 (Oct, 2003).

50. Z. Zheng, Y. Deng, X. S. Lin, L. X. Zhang, G. Q. Chen, Induced production of rabbit articular cartilage-derived chondrocyte collagen II on polyhydroxyalkanoate blends. *J Biomater Sci Polym Ed* **14**, 615 (2003).

51. Y. W. Wang, Q. Wu, J. Chen, G. Q. Chen, Evaluation of three-dimensional scaffolds made of blends of hydroxyapatite and poly(3-hydroxybutyrate-co-3-hydroxyhexanoate) for bone reconstruction. *Biomaterials* **26**, 899 (Mar, 2005).

52. J. Dai, M. L. Bruening, Catalytic nanoparticles formed by reduction of metal ions in multilayered polyelectrolyte films. *Nano Letters* **2**, 497 (2002).

53. P. L. Kuo, W. F. Chen, Formation of silver nanoparticles under structured amino groups in pseudo-dendritic poly(allylamine) derivatives. *J Phys Chem B* **107**, 11267 (Oct 16, 2003).

54. H. Yu *et al.*, Preparation and antibacterial effects of PVA-PVP hydrogels containing silver nanoparticles. *J Appl Ploym Sci* **103**, 125 (2007).

55. A. Travan *et al.*, Non-cytotoxic silver nanoparticle-polysaccharide nanocomposites with antimicrobial activity. *Biomacromolecules* **10**, 1429 (Jun 8, 2009).

56. A. Henglein, Physicochemical Properties of Small Metal Particles in Solution - Microelectrode Reactions, Chemisorption, Composite Metal Particles, and the Atom-to-Metal Transition. *J Phys Chem-Us* **97**, 5457 (May 27, 1993).

57. M. L. Houchin, E. M. Topp, Chemical degradation of peptides and proteins in PLGA: A review of reactions and mechanisms. *J Pharm Sci-Us* **97**, 2395 (Jul, 2008).

58. B. W. Holloway, Genetic recombination in Pseudomonas aeruginosa. *J Gen Microbiol* **13**, 572 (Dec, 1955).

59. Z. Shan *et al.*, Identification of two new genes involved in twitching motility in Pseudomonas aeruginosa. *Microbiology* **150**, 2653 (Aug, 2004).

60. Z. Zheng *et al.*, The use of BMP-2 coupled - Nanosilver-PLGA composite grafts to induce bone repair in grossly infected segmental defects. *Biomaterials* **31**, 9293 (Dec, 2010).

61. V. Alt *et al.*, An in vitro assessment of the antibacterial properties and cytotoxicity of nanoparticulate silver bone cement. *Biomaterials* **25**, 4383 (Aug, 2004).

APPENDICES:

Manuscripts:

1. *The use of BMP-2 coupled-nanosilver-PLGA composite grafts to induce bone repair in grossly infected segmental defects.* Z. Zheng, W. Yin, J. N. Zara, W. Li, J. Kwak, R. Mamidi, M. Lee, R. K. Siu, R. Ngo, J. Wang, D. Carpenter, X. Zhang, B. Wu, K. Ting, C. Soo. *Biomaterials* 2010, 31: 9293-9300.
2. *The antimicrobial and osteoinductive properties of silver nanoparticle/poly($_{DL}$-lactic-co-glycolic acid)-coated stainless steel.* Y. Liu, Z. Zheng, J. N. Zara, C. Hsu, D. E. Soofer, K. S. Lee, R. K. Siu, L. S. Miller, X. Zhang, D. Carpenter, C. Wang, K. Ting, C. Soo. *Biomaterials* 2012, 33: 8745-8756.

Conference abstracts:

3. *Nanosilver particles with BMP2 improve bone repair of contaminated segmental defects*. J. Zara, Z. Zheng, W. Yin, M. Lee, J. H. Kwak, R. Siu, X. Zhang, B. Wu, K. Ting, C. Soo. In the 96th American College of Surgeons Annual Clinical Congress, Washington DC, USA, Oct 2010.
4. *Infected femoral segmental defect model: effects of nanosilver in re-establishing BMP-2 osteoinductivity in infected wounds*. J. Zara, Z. Zheng, W. Yin, W. Li, R. Siu, J. Kwak, R. Ngo, M. Chiang, X. Zhang, K. Ting, C. Soo. Presented at the 2011 Annual Meeting of the Orthopaedic Research Society, Long Beach, USA, Jan 2011.
5. *Synergistic Effects of BMP2 and Nell-1, with NanoSilver for the Healing of Infected Long Bone Defects*. Y Liu, VT Nguyen, JN Zara, AW James, M Chiang, W Yuan, Z Zheng, X Zhang, K Ting, C Soo. Presented at the 97th American College of Surgeons Annual Clinical Congress, San Francisco CA, Oct 2011.
6. *The use of nanosilver-containing materials for orthopedic application.* Z. Zheng, J. N. Zara, Y. Liu, M. Lee, C. Y. Hsu, K. S. Lee, X. Zhang, K. Ting, C. Soo. In the 2012 Military Health System Research Symposium (MHSRS), Fort Lauderdale, FL, USA, Aug 2012.
7. *Nanosilver coated stainless steel: an antimicrobial and osteoinductive material for orthopedic device fabrication.* Z. Zheng, Y. Liu, J. N. Zara, M. Chiang, W. Yuan, C. Y. Hsu, D. Soofer., X. Zhang, K. Ting, C. Soo. In the 98th American College of Surgeons Annual Clinical Congress, Chicago, Illinois, USA, Sep 2012.

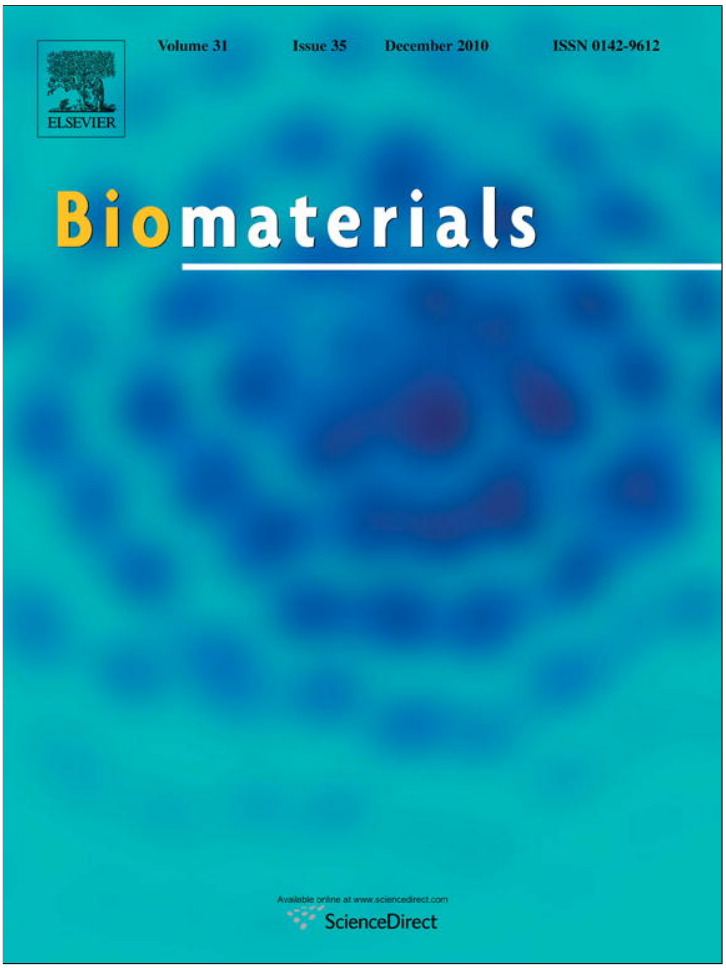

Biomaterials 31 (2010) 9293–9300

Contents lists available at ScienceDirect

Biomaterials

journal homepage: www.elsevier.com/locate/biomaterials

The use of BMP-2 coupled – Nanosilver-PLGA composite grafts to induce bone repair in grossly infected segmental defects

Zhong Zheng [a,1], Wei Yin [b,c,1], Janette N. Zara [d], Weiming Li [b,e], Jinny Kwak [b], Rachna Mamidi [f], Min Lee [d], Ronald K. Siu [b,d], Richard Ngo [g], Joyce Wang [h], Doug Carpenter [i], Xinli Zhang [b], Benjamin Wu [b,d,j], Kang Ting [b,**], Chia Soo [a,*]

[a] Department of Orthopaedic Surgery, David Geffen School of Medicine, University of California, Los Angeles, CA 90095-1759, United States
[b] Department of Craniofacial Research Institute, University of California, Los Angeles, Los Angeles, CA 90095, United States
[c] Department of Endodontics & Periodontics, College of Stomatology, Dalian Medical University, Dalian, Liaoning 116044, PR China
[d] Department of Bioengineering, University of California, Los Angeles, Los Angeles, CA 90095, United States
[e] Department of Orthopaedics, the First Clinical Hospital of Harbin Medical University, Harbin, Heilongjiang 150081, PR China
[f] Department of Biochemistry, University of California, Los Angeles, Los Angeles, CA 90095, United States
[g] Department of Molecular, Cell and Developmental Biology, Los Angeles, Los Angeles, CA 90095, United States
[h] School of Medicine, University at Buffalo, Buffalo, NY 14260, United States
[i] QuantumSphere, Inc., Santa Ana, CA 92705,United States
[j] Department of Materials Science and Engineering, University of California, Los Angeles, Los Angeles, CA 90095, United States

ARTICLE INFO

Article history:
Received 27 July 2010
Accepted 19 August 2010
Available online 22 September 2010

Keywords:
Bone repair
Antimicrobial
Nanosilver particle
Bone morphogenetic protein 2 (BMP-2)

ABSTRACT

Healing of contaminated/infected bone defects is a significant clinical challenge. Prevalence of multi-antibiotic resistant organisms has renewed interest in the use of antiseptic silver as an effective, but less toxic antimicrobial with decreased potential for bacterial resistance. In this study, we demonstrated that metallic nanosilver particles (with a size of 20–40 nm)-poly(lactic-*co*-glycolic acid) (PLGA) composite grafts have strong antibacterial properties. In addition, nanosilver particles-PLGA composite grafts did not inhibit adherence, proliferation, alkaline phosphatase activity, or mineralization of ongrowth MC3T3-E1 pre-osteoblasts compared to PLGA controls. Furthermore, nanosilver particles did not affect the osteoinductivity of bone morphogenetic protein 2 (BMP-2). Infected femoral defects implanted with BMP-2 coupled 2.0% nanosilver particles-PLGA composite grafts healed in 12 weeks without evidence of residual bacteria. In contrast, BMP-2 coupled PLGA control grafts failed to heal in the presence of continued bacterial colonies. Our results indicate that nanosilver of defined particle size is bactericidal without discernable *in vitro* and *in vivo* cytotoxicity or negative effects on BMP-2 osteoinductivity, making it an ideal antimicrobial for bone regeneration in infected wounds.

1. Introduction

Healing of contaminated/infected bone defects is in essence a "race" between infectious organisms that seek to contaminate, colonize, and ultimately infect the implanted bone graft versus the body's own endogenous tissues that seek to grow into the osseous defect via osteogenesis and neovascularization in the formation of a functional bony union. The need for bone grafts to repair significant bone loss in a non-sterile wound poses an additional challenge as the bone graft can serve as a nidus for infection. In fact, implantation of bone graft materials such as autograft bone or allograft is contra-indicated in actively infected wounds [1,2]. Bone graft infections are devastating complications requiring multiple debridement surgeries, local antibiotic bead implantation, and long-term systemic antibiotic treatment to eradicate infection prior to reconstructive re-grafting attempts [1,3]. This leads to significant medical costs for surgeries, antibiotic therapy, and lost productivity as well as major patient morbidity related to multiple surgeries, adverse antibiotic reactions, development of multi-resistant bacteria, and decreased quality of life [4]. Therefore, it would be advantageous to have tissue engineered bone graft devices that simultaneously

* Corresponding author. University of California, Los Angeles, David Geffen School of Medicine, Department of Orthopaedic Surgery, MRL 2641, Box 951759, 675 Charles E Young Drive, South, Los Angeles, CA 90095-1759, United States. Fax: +1 310 206 7783.
** Corresponding author.
E-mail address: bsoo@ucla.edu (C. Soo).
[1] These contributed equally to this study.

0142-9612/$ – see front matter © 2010 Elsevier Ltd. All rights reserved.
doi:10.1016/j.biomaterials.2010.08.041

control infection while promoting bone regeneration in order to avoid multiple surgeries and delayed reconstruction.

Bone repair is a highly concerted process involving osteogenic stem cells, osteoconductive surfaces, and osteoinductive growth factors that are severely disrupted by bacterial toxins and host inflammatory responses—thus, controlling infection is a key factor in successful regeneration in non-sterile bone defects. Creation of a favorable microenvironment for bone repair in this clinical setting would require a resorbable, biocompatible bone graft device with osteoinductive, osteoconductive, and antimicrobial properties. Although there are many advantages to using autologous graft, major drawbacks to this strategy include the extra surgery time for harvesting autologous bone, morbidity at the donor site including post-operative pain, hypersensitivity, pelvic instability, paresthesia, and infection [5–7], as well as limited availability of bone at the donor site. Meanwhile, allogeneic grafts can introduce infection risks and are less effective than autograft bone. Therefore, synthetic materials that are simultaneously osteoinductive and antimicrobial are potentially better therapeutic adjuncts for infected wounds. Poly(lactic-*co*-glycolic acid) (PLGA) has been used for decades in clinical applications, including prosthetic devices, implants [8], and microspheres for drug delivery [9,10] because it is a USA Food and Drug Administration (FDA)-approved biodegradable and biocompatible polymer [9], that can be manufactured as a porous material with various surface textures. Meanwhile, bone morphogenetic protein 2 (BMP-2) is a proven strong osteoinductive factor, and used for the treatment of many bone fractures and bone defects [8,11,12]. Therefore, the combination of a BMP-2 coupled PLGA graft has potential to be an ideal clinically applicable bone scaffold.

Current antimicrobials used locally in bone graft infections are antibiotics, which generally bind to specific chemical targets that exist in bacteria but not in humans [13]. However, this binding specificity for a given antibiotic also narrows the number of bacterial species and strains that are susceptible to a given antibiotic, and contributes significantly to the development of antibiotic resistance [14]. This issue is made more serious by the increasing number of infections caused by multi-drug resistant bacteria [15], prompting a search for antimicrobial alternatives. For example, gentamicin is the most frequently used antibiotic in bone tissue engineering due to its relatively minimal cytotoxic effects with local implantation [16]. However, during the last decade, there has been an increase in the number of deep periprosthetic infections caused by resistant bacteria, such as methicillin-resistant *Staphylococcus aureus* (MRSA) or methicillin-resistant *Staphylococcus epidermidis* (MRSE) [15,17–19], with several of them exhibiting multi-antibiotic drug resistance [20].

Silver, an antiseptic targeting a broad spectrum of $Gram^+$ and $Gram^-$ bacteria such as MRSE, MRSA and even vancomycin-resistant strains [14,20–22], has been used in different fields of medicine for years [23–28]. By binding and disrupting multiple components of bacterial structure/metabolism [23,29], silver is less likely to promote bacterial resistance than antibiotics. Bacterial resistance to silver [30] requires at least three separate mutations in three different bacterial systems—all within one generation of bacteria [23], and so far silver-resistant bacteria do not play a major role in hospital microbial germ flora [20]. Owing to advances in nanotechnology, it is now possible to produce pure silver particles at the nanoscale. The advantage of nanoparticles is their greater surface to mass ratio. Thus, nanosilver particles offer greater solubility and chemical reactivity, and higher antibacterial activity compared to conventional silver preparations [21,22]. The purpose of this study was to create BMP-2 coupled nanosilver-PLGA composite (BMP-2/NS/PLGA) bone grafts as infected bone segmental defect adjunctive therapy. Antibacterial activity against bacteria and cytotoxicity of nanosilver coupled BMP-2/NS/PLGA grafts were studied *in vitro* and *in vivo*. Furthermore, an infected femoral defect model was utilized to evaluate the efficacy of BMP-2/NS/PLGA bone graft *in vivo*.

2. Materials and methods

2.1. Nanosilver

Nanosilver used in this study is in 20–40 nm silver particle form (QSI-Nano® Silver) obtained from QuantumSphere, Inc. (Santa Ana, CA).

2.2. Bone graft

Bone grafts were manufactured using a combination of published leaching techniques [31,32]. Briefly, the desired amount of nanosilver was mixed thoroughly with 17.5% (w/v) PLGA [85:15 poly(DL-lactic-*co*-glycolic acid), inherent viscosity: 0.64 dl/g in chloroform; Durect Co., Pelham, AL]-chloroform solution. The concentration of silver refers to the weight ratio of nanosilver mixed with PLGA. This solution was then poured onto a bed of sieved sugar particles with a size of 200–300 μm to generate a homogenous paste (Supplemental Fig. 1a), which was then stacked into a Teflon mold (Supplemental Fig. 1b) to generate 4 mm diameter × 7 mm length cylindrical grafts (Supplemental Fig. 1c). The grafts were placed in a chemical hood for 12 h and lyophilized for 4 h, followed by repeated washing with large amounts of distilled water to leach the sugar. After the sugar-leaching process, the microporous grafts were air dried, sterilized in 70% alcohol and air dried again in a biosafety cabinet. The surface morphology of the grafts was evaluated using scanning electron microscopy (SEM, JEOL JSM-6700, Tokyo, Japan) [33]. Prior to SEM analysis, the samples were mounted on aluminum stubs and carbon coated. In addition, for *in vitro* cytotoxicity assay and *in vivo* animal model studies, 30 μg/ml BMP-2 in a total volume of 75 μl was injected into the graft and lyophilized to create a BMP-2/NS/PLGA bone graft.

2.3. In vitro antimicrobial activity

Vancomycin-resistant MRSA clinical strain *S. aureus* Mu50 (ATCC 700699) was used in a bacterial infection model. *In vitro* testing of the antimicrobial activity of the different doses of nanosilver was done using a microplate proliferation assay [20,34]. Specifically, the grafts were incubated with 10^7 or 10^8 bacterial colony forming units (CFU) in 200 μl of brain heart infusion broth (BHIB; BD, Sparks, MD) in each well of a 96-well microplate (Corning Inc., Corning, NY) at 37 °C for 1 h to allow adherence of the microorganisms to the graft surface. After incubation, grafts were rinsed with phosphate buffered saline (PBS) to remove loosely attached surface cells, and then incubated in 200 μl PBS with 0.25% glucose, 0.2% $(NH_4)_2SO_4$, and 1% sterile BHIB for 18 h at 37 °C in another 96-well microplate. During this second incubation step, the viable bacteria attached to the surface or within the grafts start to multiply and to release colonial counterparts into the well. After removal of the grafts, 100 μl released bacteria were transferred into another 96-well microplate and then amplified by adding 100 μl fresh BHIB for another 40 h at 37 °C. Proliferation of the released daughter cells were monitored at a wavelength of 595 nm online by Tecan Infinite f200 microplate reader (Tecan, Durham, NC) to generate a time-proliferation curve for each well of the microplate. If bacteria were partially or completely inactivated by the graft, they were able to seed only a few or even no daughter cells resulting in lagging or absence of bacterial growth [20]. In addition, general *S. aureus* strain SA113 (ATCC 35556) was also evaluated.

2.4. In vitro cytotoxicity testing

Passage 18 mouse pre-osteoblastic MC3T3-E1 cell line (subclone 4, ATCC CRL-2593) was employed for *in vitro* cytotoxicity evaluation of nanosilver-PLGA composite (NS/PLGA) grafts. MC3T3-E1 cells were maintained in α-minimal essential medium (α-MEM) supplied with 10% fetal bovine serum (FBS), 1% HT supplement, 100 units/ml penicillin and 100 μg/ml streptomycin (maintenance medium) at 37 °C with 5% CO_2. Five thousand cells were seeded on the bone grafts for testing. All media for cell culture were purchased from Gibco (Invitrogen, Calsbad, CA). Cell viability was estimated by 3-(4,5-dimethylthiazol-2-yl)-2,5-diphenyltetrazolium bromide (MTT) metabolism using commercially available Vybrand® MTT Cell Proliferation Assay Kit (Molecular Probes, Invitrogen, Calsbad, CA) with Tecan Infinite f200 microplate reader. In addition, after cultivation in osteoblastic differentiation medium (maintenance medium supplied with 50 μg/ml ascorbic acid and 10 mM β-glycerophosphate), alkaline phosphatase (ALP) activity and degree of mineralization (assessed by Alizarin Red staining) of MC3T3-E1 cells were also quantified [35,36].

2.5. Rat femoral segmental defect model

All surgical procedures were approved by the UCLA Chancellor's Animal Research Committee (2008-073). To standardize bone regeneration characteristics, 16–18 week old male Sprague-Dawley (SD) rats were randomly divided into groups of eight. Animals were anesthetized by isoflurane inhalation. With use of aseptic technique, a 25–30 mm longitudinal incision was made over the anterolateral aspect of the femur.

The femoral shaft was then exposed by separating the vastus lateralis and biceps femoris muscles. A polyethylene plate (length: 23 mm; width: 4 mm; height: 4 mm) was placed on the anterolateral surface of the femur. The plate contained six pre-drilled holes to accommodate 0.9 mm diameter threaded Kirschner wires. Taking the plate as a template, six threaded Kirschner wires were drilled through the plate and both cortices. With a small oscillating saw blade (Stryker, MI, USA), a 6-mm critical-sized mid-diaphyseal defect was created. The volume of the defect was approximately 75 μl. A bone graft injected with 10^8 CFU *S. aureus* Mu50 in 75 μl 20% gelatin gel was implanted into the defect. The overlying muscle and fascia were then closed with 4–0 Vicryl absorbable suture to secure the implant in place. Following surgery, the animals were housed in separate cages and allowed to eat and drink ad libitum. Weight bearing was started immediately postoperatively, and animals were monitored daily. Buprenorphine was administered for 2 days as an analgesic, but no antibiotic was administered.

2.6. Radiograph and three-dimensional micro-computerized tomography scanning

At 2, 4, 6, 8, 10, and 12 weeks post implantation, high-resolution lateral radiographs were obtained while the animals were under isoflurane sedation. Animals were euthanized at 12 weeks post implantation. The femurs were dissected, harvested, and fixed in 10% buffered formalin (Fisher Scientific, Fair Lawn, NJ). Following fixation for a minimum of 48 h, samples were scanned using high-resolution micro-computerized tomography (microCT; Skyscan 1172, Skyscan Belgium) at an image resolution of 16.1 μm (55 kVp and 181 μA radiation source with a 0.5 mm aluminum filter). 2D and 3D high-resolution reconstruction images were performed using the softwares provided by the manufacturer, and bone mineral density (BMD) and percent bone volume (BV/TV) were assessed to quantify newly formed bone bridge [37,38].

2.7. Histological and immunohistochemical evaluation

Following 3D microCT scanning, the specimen was decalcified using Cal-Ex solution (Fisher) for seven to nine days, washed with running tap water for 3–4 h and then transferred to a 75% ethanol solution, followed by embedding in paraffin. 5-μm sagittal sections of each specimen were obtained. Hematoxylin and eosin (H&E) and Masson's trichrome [39] staining were used for morphology estimation. Meanwhile, Taylor modified Brown and Brenn gram staining [40] was used to detect bacterial growth in the tissue. In addition, immunohistochemical (IHC) staining of osteocalcin (OCN) was also used for bone maturity evaluation [41,42].

2.8. Statistical analysis

The results were graphically depicted as the mean ± the standard deviation (SD). Two-tailed *t*-test and one-way ANOVA were performed (SPSS 13.0 for Windows, SPSS, Chicago, IL) to detect statistically significant differences. P value < 0.05 was considered statistically significant.

3. Results

3.1. Nanosilver coupled on PLGA bone graft

The microstructure of NS/PLGA grafts was analyzed by SEM. Aggregates or particles sintered together were not present in the silver (metal)-PLGA (polymer) composite grafts containing up to 2.0% silver (Fig. 1a–c). On the other hand, nanosilver particles aggregated in the composite grafts at higher silver concentrations (Fig. 1d). Because the bioactivity of silver is mostly based on generation and/or release of oxidative silver [14], asymmetric distribution of nanosilver particles will result in uneven local concentration of oxidative silver followed by variable local antibacterial activity and cytotoxicity. Therefore, the ceiling concentration of nanosilver in this study was established as 2.0%.

3.2. Antibacterial activity of nanosilver

Control PLGA grafts with no nanosilver did not inhibit proliferation of *S. aureus* Mu50 *in vitro*, while dose dependent bactericidal activity was observed in NS/PLGA grafts (Fig. 2). Grafts with 0.1%

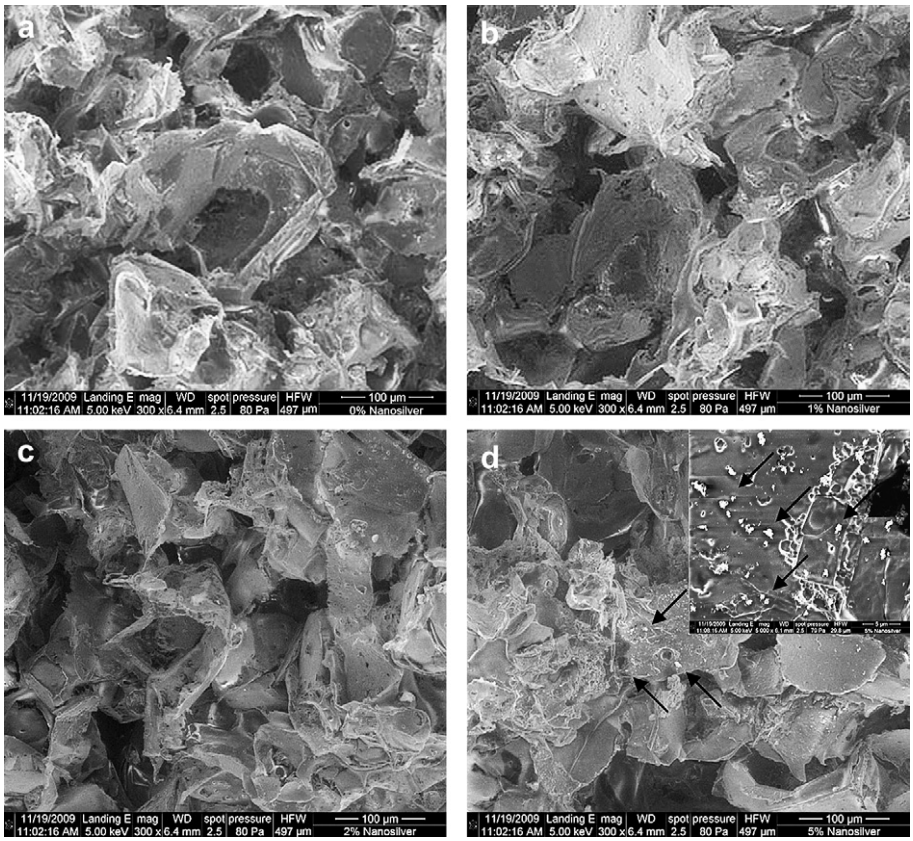

Fig. 1. Scanning electron microscopy of bone grafts. Compared to control PLGA grafts (a), no significant difference was found in nanosilver-PLGA composite grafts with 1.0% (b) and 2.0% (c) nanosilver particles. However, particles aggregated (arrows) in the composite grafts with 5.0% nanosilver (d).

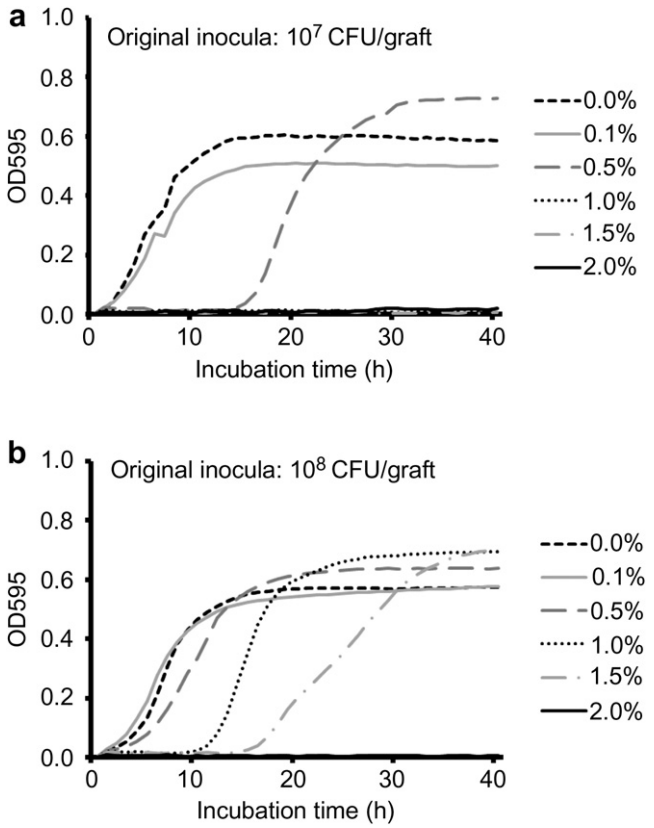

Fig. 2. *In vitro* antibacterial activity of nanosilver particle-PLGA composite grafts. Different inocula (a, 10^7 CFU; b, 10^8 CFU) of *Staphylococcus aureus* Mu50 were injected for microplate proliferation assay.

nanosilver did not affect 10^7 or 10^8 CFU *S. aureus* Mu50 proliferation, however, when the concentration of nanosilver was increased to 0.5%, bacterial proliferation was delayed in both inoculum densities. Higher concentrations at 1.0% and 1.5% NS/PLGA grafts were even more effective against *S. aureus* Mu50, completely inhibiting proliferation of the lower inoculum of 10^7 CFU and retarding proliferation of 10^8 CFU. At the established ceiling concentration of 2.0% nanosilver, bacterial proliferation of up to 10^8 CFU was completely inhibited *in vitro* (Fig. 2).

In addition, our studies on another strain *S. aureus* SA113, wildly used as a model for virulence [43,44] exhibited the following: (1) 0.1% nanosilver-PLGA composite grafts delayed *S. aureus* SA113 proliferation at 10^6 CFU inoculation, while proliferation was completely inhibited by grafts with 0.5–2.0% nanosilver at the same condition; and (2) 2.0% NS/PLGA grafts completely inhibited *S. aureus* SA113 proliferation of as high as 10^{12} CFU inoculation (Supplemental Fig. 2).

Similar to the *in vitro* studies described above, 10^8 CFU *S. aureus* Mu50 induced continuous infection in a rat femoral segmental defect model with control PLGA graft implantation *in vivo* (Fig. 3a), while grafts with 1.0% nanosilver significantly reduced *S. aureus* Mu50 survival (Fig. 3b). Phagocytes were the predominant cells found in grafts with 0.0% and 1.0% nanosilver (Fig. 3a and b). On the other hand, only limited bacterial colonies were observed in 2.0% NS/PLGA grafts *in vivo*, and more red blood cells were found in the grafts instead of phagocytes at 2 weeks post implantation (Fig. 3c).

3.3. Cytotoxicity

Mouse pre-osteoblastic MC3T3-E1 cells grew into the grafts in both maintenance and osteoblastic differentiation medium (Fig. 4). Neither BMP-2 nor up to 2.0% nanosilver affected the viability of MC3T3-E1 cells in maintenance medium (Fig. 4a and b). Interestingly, 1.0% nanosilver led to more ongrowth MC3T3-E1 cell proliferation (Fig. 4c and d) as well as their ALP activity (Fig. 4e) in osteoblastic differentiation medium. In addition, no significant difference was found in qualitative mineralization evaluation between the BMP-2/NS/PLGA bone grafts and the non-toxic control group (BMP-2/PLGA bone grafts) *in vitro* (Fig. 4f).

Furthermore, *in vivo* studies also revealed that bone regenerated on BMP-2/NS/PLGA bone grafts as well as it did in uncontaminated rat femoral defect controls, indicating good biocompatibility of BMP-2/NS/PLGA grafts (Supplemental Fig. 3).

3.4. Implantation of BMP-2/NS/PLGA bone graft in infected critical femoral segmental defects

3.4.1. Radiography

Radiographic images showed none or extremely limited bone regeneration in *S. aureus* Mu50 contaminated defects implanted with control BMP-2/PLGA grafts and BMP-2/1.0% NS/PLGA grafts, respectively, up to 12 weeks post implantation (Fig. 5). In addition, there was a loss of bone within the femoral shaft with regression of the proximal and distal cut ends, and significant ectopic bone formation observed in the control group. On the contrary, as early as 6 weeks post implantation, defect fusion resulting from new bone formation was observed in 60% of animals in the group implanted with BMP-2/2.0% NS/PLGA grafts (Fig. 5). Radiographic findings of

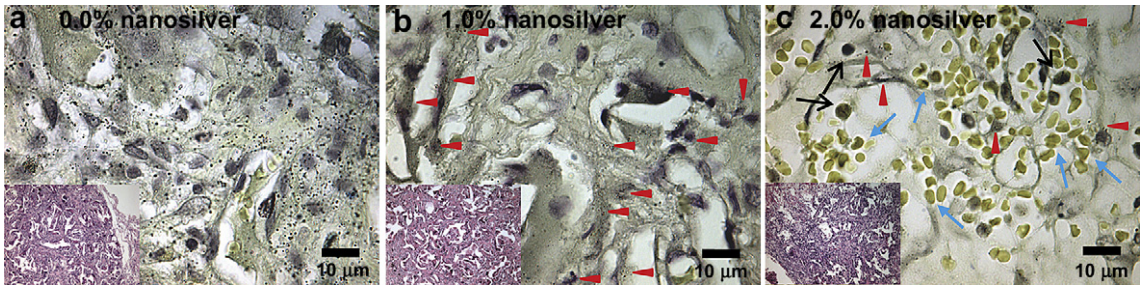

Fig. 3. *In vivo* antibacterial activity of nanosilver particle-PLGA composite grafts. After 2-week contamination with 10^8 CFU *S. aureus* Mu50, rat femoral segmental defects with implanted grafts were harvested, fixed, decalcified, embedded, sectioned and stained with Taylor modified Brown and Brenn gram stain as well as H&E (insert figures). Compared to serious bacterial infection (black dots) found in control PLGA grafts (a), 1.0% nanosilver-PLGA composite grafts significantly reduced bacterial survival to colonized collation (b, red arrows). On the other hand, only limited bacterial colonies (red arrows) were observed in 2.0% nanosilver particle-PLGA composite grafts *in vivo* (c), and more red blood cells (blue arrows) were found in the grafts instead of phagocytes (black arrows).

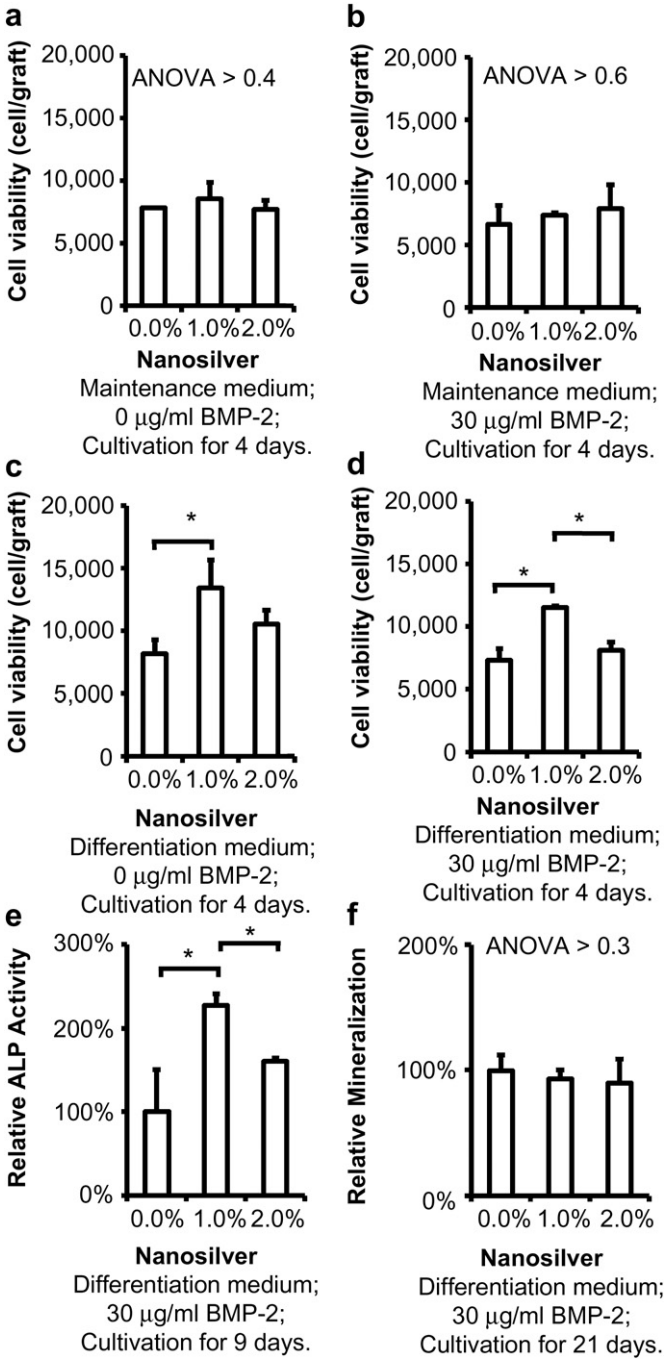

Fig. 4. *In vitro* cytotoxicity of nanosilver particle-PLGA composite grafts. In maintenance medium, up to 2.0% nanosilver did not affect MC3T3-E1 viability with 0 (a) or 30 μg/ml (b) BMP-2. Interestingly, 1.0% nanosilver-PLGA composite grafts induced MC3T3-E1 proliferation in differentiation medium with 0 (c) or 30 μg/ml (d) BMP-2, as well as its ALP activity (e). Otherwise, no significant difference on mineralization was found between the tested grafts (f). *, $P < 0.05$; $N = 6$ for each test.

bone formation in the femurs were also confirmed by 3D microCT analysis (Supplemental Fig. 4). 3D reconstruction images from the microCT scan exhibited fusion in the BMP-2/2.0% NS/PLGA group, paralleling the quantitative data as well as the 2D radiographic results. In addition, bone mineral density (BMD, $P < 0.04$) and percent bone volume (BV/TV, $P < 0.05$) were found to be significantly greater in the BMP-2/2.0% NS/PLGA group compared to the BMP-2/PLGA control group.

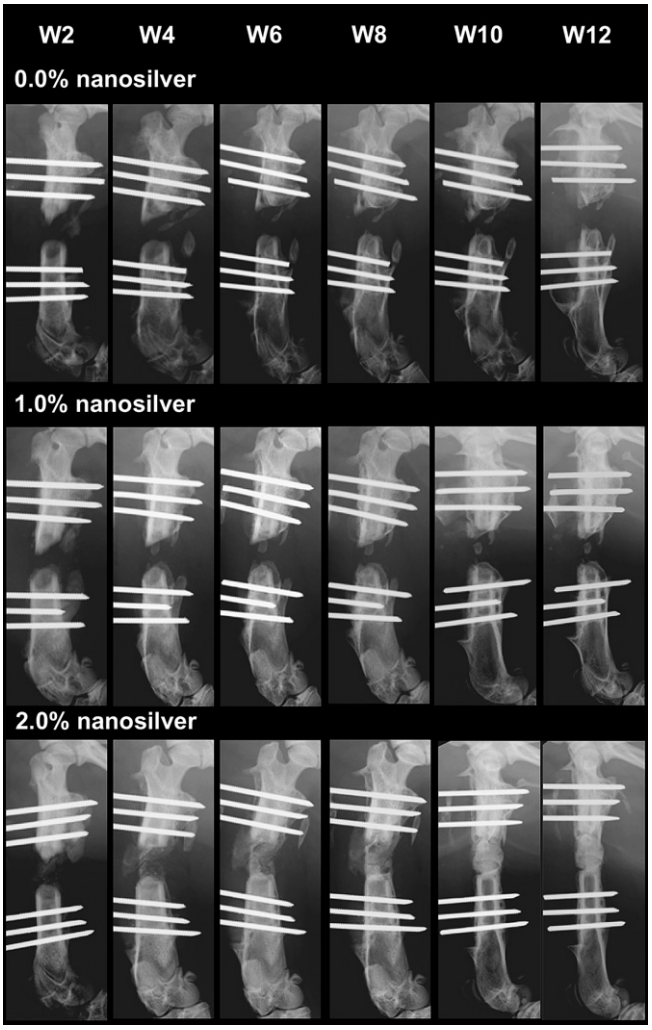

Fig. 5. Radiographic images of 10^8 CFU *S. aureus* Mu50 infected rat femoral segmental defects implanted with 0.0% (a), 1.0% (b), and 2.0% (c) nanosilver-PLGA bone grafts coupled with 30 μg/ml BMP-2.

3.4.2. Histological and IHC analysis

The quality of newly formed bone was further evaluated by H&E and Masson's trichrome staining, while Taylor modified Brown and Brenn gram staining was employed to identify bacterial residue. Consistent with radiographic analyses, there was minimal evidence of bone regeneration with absence of a bony bridge formation in the contaminated femur defect area implanted with BMP-2/PLGA control grafts (Fig. 6a and b) or BMP-2/1.0% NS/PLGA grafts (Fig. 6d and e) after 12 weeks. However, despite continued bacterial contamination observed, the number of bacterial colonies was reduced in both groups at 12 weeks (Fig. 6c and f) compared to tissues harvested after 2 weeks post implantation. In contrast, no *S. aureus* Mu50 survival was evident in the contaminated femurs implanted with BMP-2/2.0% NS/PLGA bone grafts after 12 weeks (Fig. 6i). By eliminating bacteria in the defect, BMP-2/2.0% NS/PLGA grafts promoted significantly more bone formation compared to the control group (Fig. 6g and h, Supplemental Fig. 4). Furthermore, a mineralized bony bridge connecting the two defect ends was clearly identified by both Masson's trichrome staining and OCN IHC staining (Fig. 6h and j). High intensity OCN signals signify that new bone formation was still active in the defect area, especially around the mineralized bridge and in the marrow-like cavities (Fig. 6j–j2) at 12 weeks post implantation.

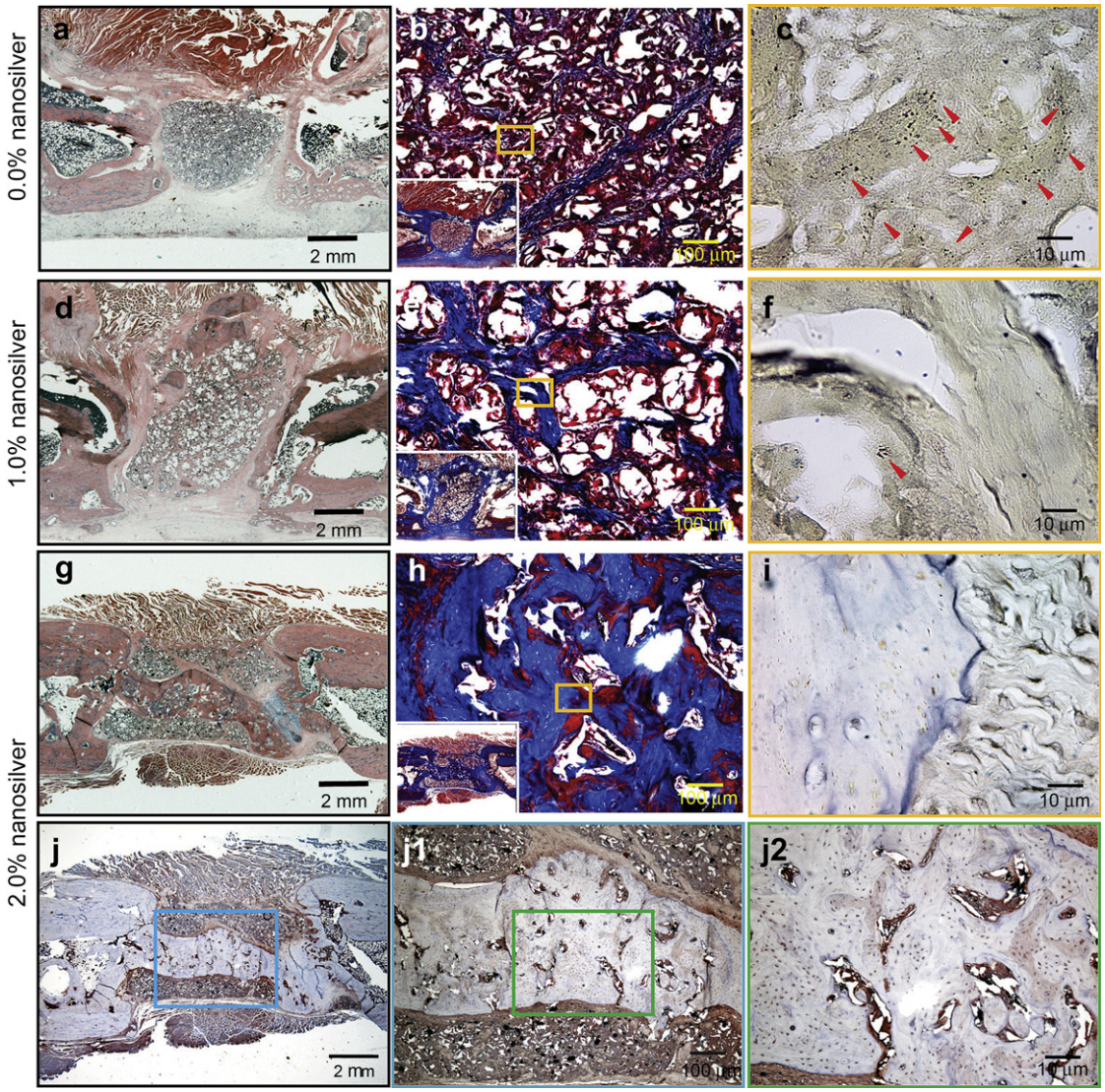

Fig. 6. H&E staining (a, d, and g), Masson's trichrome staining (b, e, and h), Taylor modified Brown and Brenn gram stain (c, f, and i) and immunostaining of OCN (j, j1, and j2) of 10^8 CFU *S. aureus* Mu50 contaminated rat femoral segmental defects implanted with 0.0% (a–c), 1.0% (d–f), and 2.0% (g–j2) nanosilver-PLGA bone grafts coupled with 30 μg/ml BMP-2 at 12 weeks post implantation, respectively. Almost no bone regenerated in BMP-2/0.0%-NS/PLGA (control BMP-2 coupled control PLGA) implanted groups (a, and b) with obvious continued bacterial contamination (c, red arrows). Less bone regenerated in the defect area of BMP-2/1.0%-NS/PLGA implanted groups (d and e), while only limited bacterial colonies were observed (f, red arrow). BMP-2/2.0%-NS/PLGA grafts promoted significantly greater bone formation to form a mineralized bony bridge between the two defect ends (g, h, and j) by eliminating bacteria in the defect area (i), Higher magnification figures show active bone regeneration around the mineralized bridge and in the marrow-like cavities in the bridge (j1, and j2).

4. Discussion

Infection of bone graft devices is considered a devastating complication. The major critical barrier to progress is the absence of an integrated approach to infection control and bone regeneration for the bone graft device. Clinically, bone graft devices implanted into infected wounds need to prevent bacterial infection while promoting cellular ingrowth. Although the ability of antibiotics to bind specific bacterial chemical targets desirably limits their toxicity, it also narrows the susceptibility of bacterial species and strains to a given antibiotic—and contributes significantly to development of multi-drug resistant bacteria [14]. In contrast, antiseptics such as silver are broad spectrum agents that are less likely to promote bacterial resistance because silver non-selectively targets many cellular processes [14,23,45].

Silver has been used for centuries in water recycling and sanitization and for treatment of wound infections due to its broad antibacterial spectrum [23,30]. With the development of modern antibiotics, silver use for infection control declined significantly. However, beginning in the late 1960s, silver experienced wide use as an antimicrobial in cutaneous wounds [23]. Modern uses of silver include a variety of silver-based dressings in the form of creams, foams, hydrogels, hydrocolloids, polymeric films, and meshes [23]. In addition, silver is used to reduce bacterial colonization/infection in a broad range of devices such as vascular and urinary catheters, endotracheal tubes, and implantable prostheses [24,25]. In the orthopaedic area, electrically generated silver ions have been successfully used to treat chronic osteomyelitis and infected non-unions [26–28]. Mechanistically, silver-based antimicrobials are thought to attach to specific thiol groups containing sulfur and hydrogen found in a variety of structural and functional bacterial proteins; however, they may differ in the reservoir form for the active silver [14]. Ionic reservoir form of silver, such as silver nitrate ($AgNO_3$) and silver sulfate (Ag_2SO_4), were previously used to protect against bacterial infection [30,46,47]. However, inadequate local retention and severe cytotoxic effects limited the clinical use

of ionic silver for bone grafts despite its good short-term antibacterial activity [46–48]. Fortunately, recent developments in nanotechnology have made the creation of new biomedical materials possible, including generation of nanosilver particles. Compared to non-nanoscale silver, nanosilver particles provide a larger surface area to interface with the environment. Previous studies have demonstrated that 5–50 nm size nanosilver particles are bactericidal [20]. Further investigation suggested that the greater the surface area of nanosilver particle the greater the antibacterial activity [22,49–52]. However, the nanosilver particles used are commonly synthesized through chemical reduction of a silver salt solution by a reducing agent, leading to residual chemical impurities and wide distribution of particle sizes that can confound interpretation of the antibacterial performance of nanosilver particles [22,53]. To minimize this, highly purified (>99.9% pure), 20–40 nm nanosilver particles produced through a novel, non-chemically based, proprietary process (QSI-Nano® Silver; USPTO 7,282,167) were used in this study. The active surface of QSI-Nano® Silver (15–25 m^2/g) is much greater compared to commercial non-nanoscale silver powder (1–2 m^2/g) and previously *in vitro* studied nanosilver particles (4 m^2/g, [20]), which suggests that QSI-Nano® Silver may have better antibacterial activity. In this study, we demonstrated that NS/PLGA grafts have excellent antibacterial activity against proliferation of *S. aureus*, which is the bacterial pathogen responsible for ~80% of all cases of human osteomyelitis [54]. The absence of *in vitro* and *in vivo* cytotoxicity of NS/PLGA bone grafts was also shown. Thus, an NS/PLGA graft is particularly promising for use in bone regeneration of contaminated wounds due to its potential effectiveness against multi-drug resistant bacteria that cannot be achieved by available antibiotic agents.

In the creation of a BMP-2/NS/PLGA composite graft, the effect of nanosilver particle on BMP-2 was also considered, as nanosilver particles could possibly interfere with essential cellular elements relating to BMP-2 osteoinductivity when it binds to thiol groups. Fortunately, up to 2.0% concentration of nanosilver particles did not interrupt bone regeneration induced by BMP-2 either *in vitro* or *in vivo* as shown in this study. Not surprisingly, infected defects healed slower compared to non-infected defects, although much faster than infected controls treated without nanosilver. The slower healing time could be attributed to partial BMP-2 loss and depletion by bacteria so that the actual BMP-2 dose is effectively decreased in an infected defect compared to a non-infected one. Future studies using an alternative system for controlled BMP-2 delivery and release, such as via microsphere [33], should be considered to overcome this problem.

In summary, employing nanosilver particles, we have successfully regenerated bone in a 6-mm critical-sized defect (total volume ~75 μl) infected with 10^8 CFU vancomycin-resistant MRSA strain Mu50 (i.e., ~10^9 CFU/ml bacteria, which far exceeds the typical 10^5 CFU/ml criteria for invasive tissue infection [55]).

5. Conclusions

In this study, BMP-2/NS/PLGA composite grafts exhibited significant antibacterial and osteoinductive activity. Our results demonstrated that nanosilver is an effective antimicrobial that is non-toxic, and does not interfere with BMP-2 induced bone formation. In addition, our results also showed that the efficacy of nanosilver is dose dependent, raising the possibility that by using surfactant to minimize NS aggregation, we can fabricate BMP-2/NS/PLGA scaffolds with even higher silver concentrations than the present 2% NS to provide even more potent antibacterial activity.

Disclosure

Dr. D. Carpenter is inventor on non-chemically based processing nanosilver patent (QSI-Nano® Silver; USPTO 7,282,167).

Acknowledgements

This research was supported by US DoD Grant 07128099. The authors would like to thank Dr. Michael Chiang from the Department of Craniofacial Research Institute, University of California, Los Angeles for assisting in microCT scanning and analysis.

Appendix. Supplementary information

Supplementary information associated with this article can be found in the online version at doi:10.1016/j.biomaterials.2010.08.041.

Appendix

Figures with essential colour discrimination. Fig. 6 of this article has parts that are difficult to interpret in black and white. The full colour images can be found in the online version, at doi:10.1016/j.biomaterials.2010.08.041.

References

[1] Farooq AH, Dabke HV, Majeed MA, Carbarns NJ, Mackie IG. Clostridial wound infection following reconstruction of the anterior cruciate ligament using bone-patella-bone autograft. J Coll Physicians Surg Pak 2007;17:369–70.
[2] Journeaux SF, Johnson N, Bryce SL, Friedman SJ, Sommerville SM, Morgan DA. Bacterial contamination rates during bone allograft retrieval. J Arthroplasty 1999;14:677–81.
[3] Bruce JN, Bruce SS. Preservation of bone flaps in patients with postcraniotomy infections. J Neurosurg 2003;98:1203–7.
[4] Mader JT, Shirtliff ME, Bergquist SC, Calhoun J. Antimicrobial treatment of chronic osteomyelitis. Clin Orthop Relat Res 1999;360:47–65.
[5] Lane JM, Tomin E, Bostrom MP. Biosynthetic bone grafting. Clin Orthop Relat Res 1999;367:S107–17.
[6] Arrington ED, Smith WJ, Chambers HG, Bucknell AL, Davino NA. Complications of iliac crest bone graft harvesting. Clin Orthop Relat Res 1996;329:300–9.
[7] Damien CJ, Parsons JR. Bone graft and bone graft substitutes: a review of current technology and applications. J Appl Biomater 1991;2:187–208.
[8] Yu D, Li Q, Mu X, Chang T, Xiong Z. Bone regeneration of critical calvarial defect in goat model by PLGA/TCP/rhBMP-2 scaffolds prepared by low-temperature rapid-prototyping technology. Int J Oral Maxillofac Surg 2008;37:929–34.
[9] Jain RA. The manufacturing techniques of various drug loaded biodegradable poly(lactide-*co*-glycolide) (PLGA) devices. Biomaterials 2000;21:2475–90.
[10] Putney SD, Burke PA. Improving protein therapeutics with sustained-release formulations. Nat Biotechnol 1998;16:153–7.
[11] Kang Q, Sun MH, Cheng H, Peng Y, Montag AG, Deyrup AT, et al. Characterization of the distinct orthotopic bone-forming activity of 14 BMPs using recombinant adenovirus-mediated gene delivery. Gene Ther 2004;11:1312–20.
[12] Govender S, Csimma C, Genant HK, Valentin-Opran A, Amit Y, Arbel R, et al. Recombinant human bone morphogenetic protein-2 for treatment of open tibial fractures: a prospective, controlled, randomized study of four hundred and fifty patients. J Bone Joint Surg Am 2002;84:2123–34.
[13] Van de Belt H, Neut D, Schenk W, van Horn JR, van der Mei HC, Busscher HJ. Infection of orthopedic implants and the use of antibiotic-loaded bone cements. A review. Acta Orthop Scand 2001;72:557–71.
[14] Ovington LG. The truth about silver. Ostomy Wound Manage 2004;50:1S–10S.
[15] Kilgus DJ, Howe DJ, Strang A. Results of periprosthetic hip and knee infections caused by resistant bacteria. Clin Orthop Relat Res 2002;404:116–24.
[16] Josefsson G, Kolmert L. Prophylaxis with systematic antibiotics versus gentamicin bone cement in total hip arthroplasty. A ten-year survey of 1,688 hips. Clin Orthop Relat Res 1993;292:210–4.
[17] Hirakawa K, Stulberg BN, Wilde AH, Bauer TW, Secic M. Results of 2-stage reimplantation for infected total knee arthroplasty. J Arthroplasty 1998;13:22–8.
[18] James PJ, Butcher IA, Gardner ER, Hamblen DL. Methicillin-resistant *Staphylococcus epidermidis* in infection of hip arthroplasties. J Bone Joint Surg Br 1994;76:725–7.
[19] Hope PG, Kristinsson KG, Norman P, Elson RA. Deep infection of cemented total hip arthroplasties caused by coagulase-negative staphylococci. J Bone Joint Surg Br 1989;71:851–5.

[20] Alt V, Bechert T, Steinrucke P, Wagener M, Seidel P, Dingeldein E, et al. An in vitro assessment of the antibacterial properties and cytotoxicity of nanoparticulate silver bone cement. Biomaterials 2004;25:4383–91.
[21] Lok CN, Ho CM, Chen R, He QY, Yu WY, Sun H, et al. Silver nanoparticles: partial oxidation and antibacterial activities. J Biol Inorg Chem 2007; 12:527–34.
[22] Martinez-Castanon GA, Nino-Martinez N, Martinez-Gutierrez F, Martinez-Mendoza JR, Ruiz F. Synthesis and antibacterial activity of silver nanoparticles with different sizes. J Nanopart Res 2008;10:1343–8.
[23] Leaper DJ. Silver dressings: their role in wound management. Int Wound J 2006;3:282–94.
[24] Seymour C. Audit of catheter-associated UTI using silver alloy-coated foley catheters. Br J Nurs 2006;15:598–603.
[25] Hardes J, Ahrens H, Gebert C, Streitbuerger A, Buerger H, Erren M, et al. Lack of toxicological side-effects in silver-coated megaprostheses in humans. Biomaterials 2007;28:2869–75.
[26] Tamura K. Some effects of weak direct current and silver ions on experimental osteomyelitis and their clinical application. Nippon Seikeigeka Gakkai Zasshi 1983;57:187–97.
[27] Webster DA, Spadaro JA, Becker RO, Kramer S. Silver anode treatment of chronic osteomyelitis. Clin Orthop Relat Res 1981;161:105–14.
[28] Nand S, Sengar GK, Jain VK, Gupta TD. Dual use of silver for management of chronic bone infections and infected non-unions. J Indian Med Assoc 1996;94:91–5.
[29] Schreurs WJ, Rosenberg H. Effect of silver ions on transport and retention of phosphate by *Escherichia coli*. J Bacteriol 1982;152:7–13.
[30] Silver S, Phung le T, Silver G. Silver as biocides in burn and wound dressings and bacterial resistance to silver compounds. J Ind Microbiol Biotechnol 2006;33:627–34.
[31] Zheng Z, Deng Y, Lin XS, Zhang LX, Chen GQ. Induced production of rabbit articular cartilage-derived chondrocyte collagen II on polyhydroxyalkanoate blends. J Biomat Sci-Polym E 2003;14:615–24.
[32] Deng Y, Lin XS, Zheng Z, Deng JG, Chen JC, Ma H, et al. Poly(hydroxybutyrate-co-hydroxyhexanoate) promoted production of extracellular matrix of articular cartilage chondrocytes in vitro. Biomaterials 2003;24:4273–81.
[33] Lee M, Li WM, Siu RK, Whang J, Zhang XL, Soo C, et al. Biomimetic apatite-coated alginate/chitosan microparticles as osteogenic protein carriers. Biomaterials 2009;30:6094–101.
[34] Bechert T, Steinrucke P, Guggenbichler JP. A new method for screening anti-infective biomaterials. Nat Med 2000;6:1053–6.
[35] Evangelista MB, Hsiong SX, Fernandes R, Sampaio P, Kong HJ, Barrias CC, et al. Upregulation of bone cell differentiation through immobilization within a synthetic extracellular matrix. Biomaterials 2007;28:3644–55.
[36] Gough JE, Jones JR, Hench LL. Nodule formation and mineralisation of human primary osteoblasts cultured on a porous bioactive glass scaffold. Biomaterials 2004;25:2039–46.
[37] Muller R, Ruegsegger P. Micro-tomographic imaging for the nondestructive evaluation of trabecular bone architecture. Stud Health Technol Inform 1997;40:61–79.
[38] Gauthier O, Muller R, von Stechow D, Lamy B, Weiss P, Bouler JM, et al. In vivo bone regeneration with injectable calcium phosphate biomaterial: a three-dimensional micro-computed tomographic, biomechanical and SEM study. Biomaterials 2005;26:5444–53.
[39] Foot NC. The Masson trichrome staining methods in routine laboratory use. Stain Technol 1933;8:101–10.
[40] Taylor RD. Modification of Brown and Brenn gram stain for differential staining of gram-positive and gram-negative bacteria in tissue sections. Am J Clin Pathol 1966;46:472.
[41] Bobryshev YV, Killingsworth MC, Lord RSA. Spatial distribution of osteoblast-specific transcription factor Cbfa1 and bone formation in atherosclerotic arteries. Cell Tissue Res 2008;333:225–35.
[42] Kasai R, Bianco P, Robey PG, Kahn AJ. Production and characterization of an antibody against the human bone gla protein (Bgp/Osteocalcin) propeptide and its use in immunocytochemistry of bone-cells. Bone Miner 1994;25:167–82.
[43] Jonsson P, Lindberg M, Haraldsson I, Wadstrom T. Virulence of *Staphylococcus aureus* in a mouse mastitis model – studies of alpha-hemolysin, coagulase, and protein-A as possible virulence determinants with protoplast fusion and gene cloning. Infect Immun 1985;49:765–9.
[44] Peschel A, Jack RW, Otto M, Collins LV, Staubitz P, Nicholson G, et al. *Staphylococcus aureus* resistance to human defensins and evasion of neutrophil killing via the novel virulence factor MprF is based on modification of membrane lipids with L-lysine. J Exp Med 2001;193:1067–76.
[45] Gupta A, Phung LT, Taylor DE, Silver S. Diversity of silver resistance genes in IncH incompatibility group plasmids. Microbiology 2001;147:3393–402.
[46] Vik H, Andersen KJ, Julshamn K, Todnem K. Neuropathy caused by silver absorption from arthroplasty cement. Lancet 1985;1:872.
[47] Sudmann E, Vik H, Rait M, Todnem K, Andersen KJ, Julsham K, et al. Systemic and local silver accumulation after total hip replacement using silver-impregnated bone cement. Med Prog Technol 1994;20:179–84.
[48] Drewa T, Szmytkowska K, Chaberski M. The short term exposition of $AgNO_3$ on 3T3 mouse fibroblasts cell line. Acta Pol Pharm 2007;64:175–8.
[49] Jeong SH, Yeo SY, Yi SC. The effect of filler particle size on the antibacterial properties of compounded polymer/silver fibers. J Mater Sci 2005;40: 5407–11.
[50] Jeong SH, Hwang YH, Yi SC. Antibacterial properties of padded PP/PE nonwovens incorporating nano-sized silver colloids. J Mater Sci 2005;40: 5413–8.
[51] Thiel J, Pakstis L, Buzby S, Raffi M, Ni C, Pochan DJ, et al. Antibacterial properties of silver-doped titania. Small 2007;3:799–803.
[52] Martinez-Gutierrez F, Olive PL, Banuelos A, Orrantia E, Nino N, Sanchez EM, et al. Synthesis, characterization, and evaluation of antimicrobial and cytotoxic effect of silver and titanium nanoparticles. Nanomedicine: Nanotechnol Biol Med; 2010 [Epub ahead of print].
[53] Panacek A, Kvitek L, Prucek R, Kolar M, Vecerova R, Pizurova N, et al. Silver colloid nanoparticles: synthesis, characterization, and their antibacterial activity. J Phys Chem B 2006;110:16248–53.
[54] Ellington JK, Harris M, Webb L, Smith B, Smith T, Tan K, et al. Intracellular *Staphylococcus aureus*. A mechanism for the indolence of osteomyelitis. J Bone Jt Surg Br 2003;85:918–21.
[55] Calandra T, Cohen J, Infect ISFD. The international sepsis forum consensus conference on definitions of infection in the intensive care unit. Crit Care Med 2005;33:1538–48.

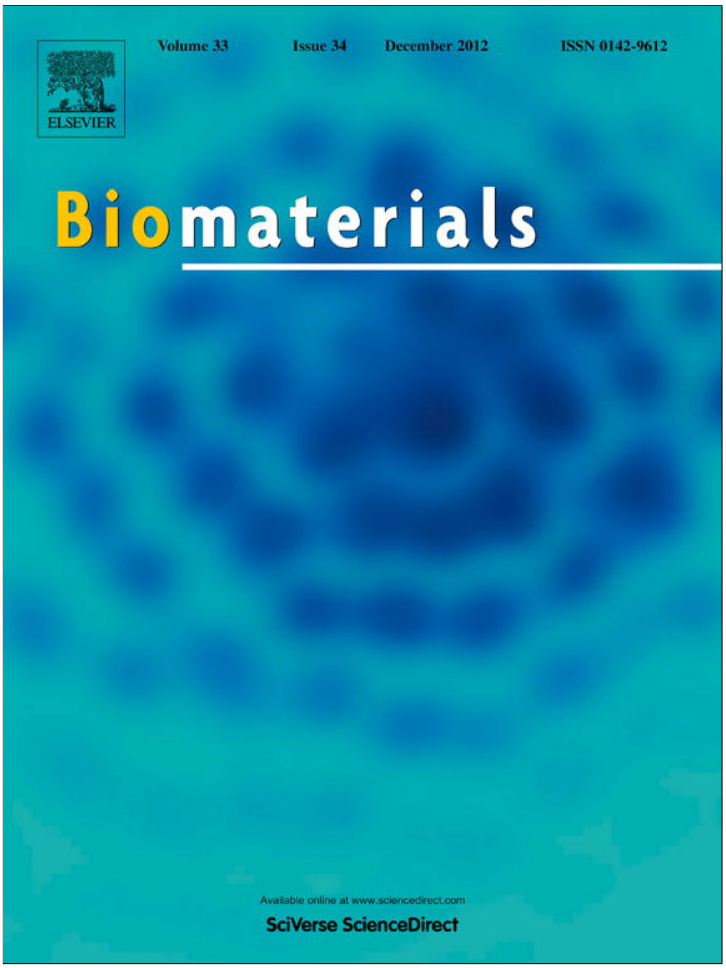

Biomaterials 33 (2012) 8745–8756

Contents lists available at SciVerse ScienceDirect

Biomaterials

journal homepage: www.elsevier.com/locate/biomaterials

The antimicrobial and osteoinductive properties of silver nanoparticle/poly (DL-lactic-*co*-glycolic acid)-coated stainless steel

Yi Liu [a,b,1], Zhong Zheng [b,1], Janette N. Zara [c], Chingyun Hsu [b], Donnalisa E. Soofer [d], Kevin S. Lee [b], Ronald K. Siu [c], Lloyd S. Miller [e,f], Xinli Zhang [b], Doug Carpenter [g], Chunling Wang [a,**], Kang Ting [b,**], Chia Soo [e,*]

[a] *Shandong Provincial Laboratory of Oral Biomedicine, School and Hospital of Stomatology, Shandong University, Jinan, Shandong 250012, PR China*
[b] *Dental and Craniofacial Research Institute and Section of Orthodontics, School of Dentistry, University of California, Los Angeles, CA 90095, USA*
[c] *Department of Bioengineering, University of California, Los Angeles, CA 90095, USA*
[d] *College of Science and Health, Charles R.Drew University of Medicine and Science, Los Angeles, CA 90059, USA*
[e] *UCLA and Orthopaedic Hospital, Department of Orthopaedic Surgery and the Orthopaedic Hospital Research Center, University of California, Los Angeles, MRL 2641, Box 951759, 675 Charles E Young Drive, South, Los Angeles, CA 90095-1759, USA*
[f] *Division of Dermatology, Department of Medicine, David Geffen School of Medicine at University of California, Los Angeles, CA 90095, USA*
[g] *QuantumSphere, Inc., Santa Ana, CA 92705, USA*

ARTICLE INFO

Article history:
Received 6 June 2012
Accepted 5 August 2012
Available online 7 September 2012

Keywords:
Silver nanoparticle
Poly(DL-lactic-*co*-glycolic acid) (PLGA)
Silver nanoparticle/poly(DL-lactic-*co*-glycolic acid)-coated stainless steel alloy (SNPSA)
Implant-associated infections
Antimicrobial osteoinductive

ABSTRACT

Implant-associated bacterial infections are one of the most serious complications in orthopedic surgery. Treatment of these infections often requires multiple operations, device removal, long-term systemic antibiotics, and extended rehabilitation, and is frequently ineffective, leading to worse clinical outcomes and increased financial costs. In this study, we evaluated **s**ilver **n**anoparticle/**p**oly(DL-lactic-*co*-glycolic acid) (PLGA)-coated stainless **s**teel **a**lloy(SNPSA) as a potential antimicrobial implant material. We found that SNPSA exhibited strong antibacterial activity *in vitro* and *ex vivo*, and promoted MC3T3-E1 pre-osteoblasts proliferation and maturation *in vitro*. Furthermore, SNPSA implants induced osteogenesis while suppressing bacterial survival in contaminated rat femoral canals. Our results indicate that SNPSA has simultaneous antimicrobial and osteoinductive properties that make it a promising therapeutic material in orthopedic surgery.

Published by Elsevier Ltd.

1. Introduction

Implant associated bacterial infections are one of the most serious complications in orthopedic surgery because they are extremely difficult to treat and result in increased morbidity and substantially worse outcomes [1–6]. Despite a recent focus on aseptic surgical and procedural techniques, catheter- and surgical implant-associated infections account for nearly half of the 2 million cases of nosocomial infections in the United States per year [1,2,7], representing a significant healthcare and economic burden.

Management of an implant-associated infection typically requires device removal, multiple debridement surgeries, and long-term systemic antibiotic therapy, despite the associated side effects and additional complications [8–10]. However, these additional surgical procedures and medical therapies not only increase the healthcare costs, but also result in an increased rate of recurrence, particularly because it is difficult to clear the infection from devascularized bone and other necrotic tissues [2,3]. Soon after introduction of an implant, a conditioning layer composed of host-derived adhesins (including fibrinogen, fibronectin, collagen, *etc.*) covers the surface of the implant [2]. This layer promotes adherence of free-floating (planktonic) bacteria, which subsequently form a three dimensional (3D), extracellular polysaccharide biofilm [2]. Once a biofilm forms, it is extremely difficult to treat these infections because the biofilm blocks the penetration of both host immune cells (such as macrophages) and systemic antibiotics, promoting further bacterial survival [2,11,12]. Given the difficulties in treating implant-associated infections, strategies aimed at preventing the infection and biofilm formation during surgery and in the immediate postoperative period may serve as more effective alternative that can prevent these infections altogether. The development of implant materials or coatings that resist infection while simultaneously promoting bone growth would be particularly advantageous for orthopedic surgery applications.

* Corresponding author. Tel.: +1 310 794 5479; fax: +1 310 206 7783.
** Corresponding authors.
E-mail address: bsoo@ucla.edu (C. Soo).
[1] Yi Liu and Zhong Zheng contributed equally to this study.

0142-9612/$ – see front matter Published by Elsevier Ltd.
http://dx.doi.org/10.1016/j.biomaterials.2012.08.010

Prior studies have coated or covalently-linked antibiotics onto prosthetic materials to prevent bacterial infection during surgical implantation [13–16]. However, efficacy of local therapies are limited by the sensitivity of a given bacterial species to a specific antibiotic used [19]. As implant-related infections can be caused by a wide spectrum of bacteria, including Gram-positive *Staphylococcus aureus*, *Staphylococcus epidermidis* and *Streptococci* species, and Gram-negative *Pseudomonas* and *Enterobacter* species [17,18], the use of narrow-spectrum antibiotics may inadequately cover infecting bacterial species, while the use of broad-spectrum antibiotics can contribute to the development of antibiotic resistance, which is especially relevant as there is an increasing number of infections caused by methicillin-resistant *S. aureus* (MRSA) and methicillin-resistant *S. epidermidis* (MRSE) strains [19].

As an alternative, broad-spectrum antiseptics such as silver have long been used in various fields of medicine [19]. For example, continuous application of electrically active silver dressings is an effective adjunct in the treatment of chronic bone infection when combined with adequate surgical debridement, thereby reducing the need for prolonged systemic antibiotics [19]. Though at present much remains still to be understood and clarified about the primary mechanism of action of silver nanoparticles, it is thought that silver targets a broad spectrum of Gram-positive and -negative bacteria mainly by attaching to specific thiol groups found in a variety of structural and functional bacterial proteins [19]. In addition, silver resistance requires at least three separate mutations in three different bacterial systems—all within one generation of bacteria; thus, silver-resistant bacteria are rarely observed in hospital microbial germ flora [19]. Pure silver particles can now be produced in a nanoscale form. Due to their greater surface-to-mass ratio, silver nanoparticles exhibit greater solubility, chemical reactivity, and antibacterial activity compared to conventional silver preparations [19]. Previously, we have demonstrated *in vitro* that silver nanoparticles are non-toxic and effective as antimicrobials, and that silver nanoparticle-based bone grafts combined with bone morphogenetic protein 2 (BMP-2) successfully regenerate bone *in vivo* in a rat femoral segmental defect (FSD) infected with *S. aureus* Mu50, an MRSA strain with intermediate vancomycin resistance [19].

In this study, we evaluated the antibacterial properties of silver nanoparticle/poly(DL-lactic-*co*-glycolic acid) (PLGA)-coated stainless steel alloy (SNPSA) *in vitro*, *ex vivo*, and *in vivo* to assess its potential as an implant material in orthopedic surgery. Furthermore, we studied the osteoinductive properties of SNPSA *in vitro* and *in vivo*.

2. Materials and methods

2.1. Stainless steel alloy coating

20-40 nm-diameter spherical silver nanoparticles (QSI-Nano® Silver, QuantumSphere, Inc., Santa Ana, CA) were thoroughly mixed with 17.5% (w/v) PLGA (lactic: glycolic = 85:15, inherent viscosity: 0.64 dl/g in chloroform; Durect Co., Pelham, AL) solution [19]. The proportion of silver nanoparticles refers to the weight ratio of silver nanoparticles to PLGA. 316L stainless steel alloy Kirschner (K)-wire (length: 1 cm, diameter: 0.6 mm; Synthes. Monument, CO) and discs (thickness: 1.59 mm, diameter: 6.35 mm; Applied Porous Technologies, Inc., Tariffville, CT) were soaked in the silver nanoparticle/PLGA-chloroform solution for 30 s and air-dried completely. The soak-dry process was repeated three times for each SNPSA implant. After incubating for 12 h at 37 °C to ensure a uniform coating, SNPSAs were stored at −20 °C until use. Morphology of the SNPSA was evaluated by scanning electron microscopy (SEM; Nova NanoSEM 230-D9064, FEI Company, Hillsboro, OR) (Fig. 1 and Supplemental Fig. 1) [19].

2.2. Surface free energy

Surface free energy of SNPSAs was obtained from contact angle measurements. Contact angles of multiple standard liquids on the tested SNPSAs were measured using a contact angle analyzer (FTA125; First Ten Ångstroms, Portsmouth, VA). In order to obtain an accurate description of the wetting behavior of various SNPSAs,

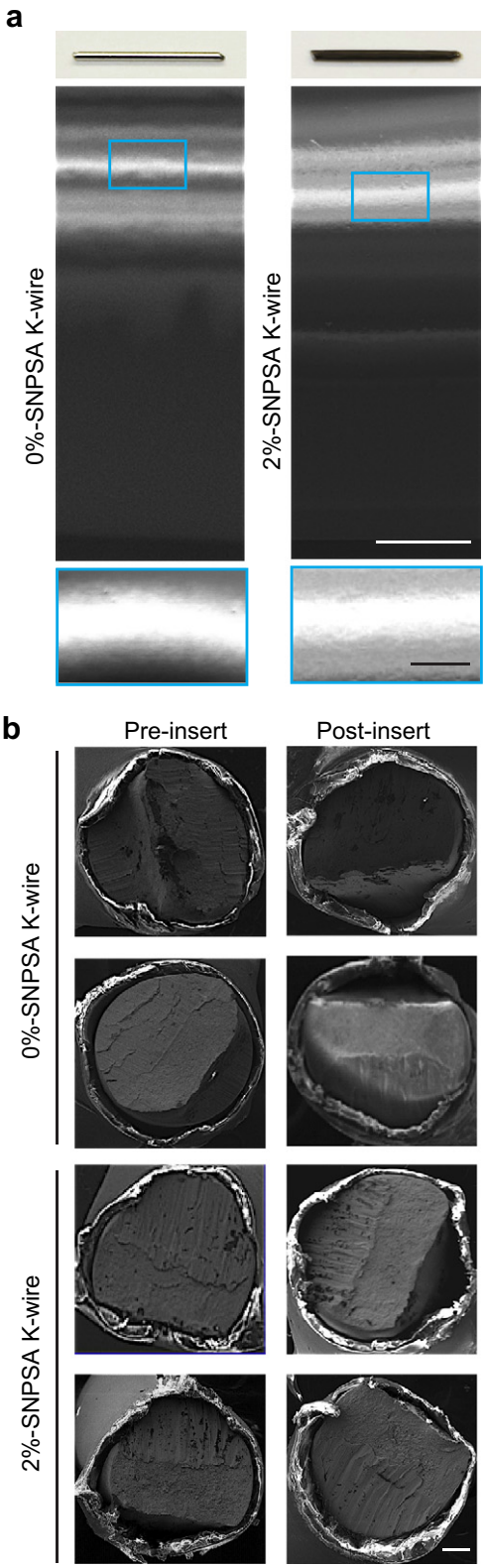

Fig. 1. SEM images of SNPSA K-wires. A uniform layer of silver nanoparticle/PLGA composite was observed on the surface of stainless steel alloy. Aggregates of silver nanoparticles were not found in silver nanoparticle/PLGA composite layers containing up to 2% silver nanoparticles (a). Light microscope images of SNPSA K-wires appear in the top panel. The thickness of silver nanoparticle/PLGA composite layer was 43.36 ± 0.08 μm (b). Blue box shows the area magnified in the bottom panel. Placing SNPSA K-wires into the pre-reamed intramedullary canal did not considerably damage the coating. White scale bar = 100 μm; black scale bar = 25 μm. (For interpretation of the references to colour in this figure legend, the reader is referred to the web version of this article.)

the surface free energy of the solid (γ_s) was considered to be the sum of separate dispersion (γ_S^d) and non-dispersion (γ_S^{nd}) contributions [20]. From this two-component model, the following relationship was derived from the dispersion γ^d and non-dispersion (also known as 'polar') γ^{nd} interactions between liquids and solids [20,21].

$$\gamma_L \times (\cos\theta + 1) = 2 \times \left(\gamma_L^d \times \gamma_S^d\right)^{1/2} + 2 \times \left(\gamma_L^{nd} \times \gamma_S^{nd}\right)^{1/2} \quad (1)$$

Eq. (1), known as the geometric mean model [20,21], allows the calculation of the solid surface free energy using the contact angle (θ) and the surface tension components of the standard liquids, where γ_L, γ_L^d ,and γ_L^{nd} represent the surface tension and its dispersion and non-dispersion components of the standard liquids, respectively [20–22]. The surface tension components of the standard liquids are listed in Supplementary Table 1 [23].

2.3. In vitro antimicrobial activity

The Gram-positive vancomycin-intermediate *S. aureus* (VISA/MRSA) strain Mu50 (ATCC 700699) was cultured in brain heart infusion broth (BHIB; BD, Sparks, MD) at 37 °C [19]; while biofilm-forming, Gram-negative opportunistic pathogen *Pseudomonas aeruginosa* PAO-1 (ATCC 15692) [24,25] was cultured in Luria Bertani broth (LB; Fisher Scientific, Hampton, NH) at 30 °C. 10^3, 10^4, and 10^5 colony forming units (CFU) of bacteria were suspended in 1 ml culture broth and incubated with the SNPSA K-wires at 225 rpm on a shaker for 1, 2, 6, and 24 h. At the end of the incubation, *S. aureus* Mu50 and *P. aeruginosa* PAO-1 bacteria attached to the surface were collected in sterile 0.9% saline solution by sonication for 30 s at 0.6 power with an intermediate size probe (Artek Sonic Dismembrator; Dynatech Laboratories, Chantilly, VA) [26] and plated onto 10-cm BHIB or LB culture medium plates overnight, respectively [27]. After 18 h incubation, the number of colonies on each plate was quantitated following protocols set forth by the U.S. Food and Drug Administration (FDA) in their Bacteriological Analytical Manual – Aerobic Plate Count Method. (http://www.fda.gov/Food/ScienceResearch/LaboratoryMethods/BacteriologicalAnalyticalManualBAM/ucm063346.htm). Briefly, the total number of bacteria collected in 1 ml saline solution were plated onto the plates and diluted as necessary for the quantitation. If resultant colonies per plate were within 25–250, the undiluted colony numbers were utilized for quantitation. If there were over 250 colonies per plate, the bacterial solution was diluted by factors of 10 (*e.g.*, 1:10, 1:100, 1:1000 dilutions) until resultant colonies per plate were again within 25–250, and colony numbers were then calculated accordingly. Figures with undiluted bacteria are documented for visualization purposes only.

2.4. Ex vivo antimicrobial activity

Femurs isolated from 12-week old male 129/sv mice were used to assay SNPSA antimicrobial activity *ex vivo*. Briefly, after locating the femoral intercondylar notch, an intramedullary canal was manually reamed into the distal femur with a 25-gauge needle. A SNPSA K-wire was then placed into the intramedullary canal with 2 μl Mu50 or PAO-1 bacteria suspended in phosphate buffered saline (PBS, pH 7.2; Invitrogen, Carlsbad, CA) [16]. Femurs with implants were then placed on 100 μm cell strainers (BD) inside 6-well culture plates containing 2 ml α-minimal essential medium (α-MEM; Invitrogen) supplemented with 1% HT supplement (Invitrogen) and fetal bovine serum (FBS; Invitrogen). In order to avoid direct contact between SNPSAs and cell culture medium, the distal femur with a protruding SNPSA was angled superiorly, and the proximal femur was soaked in culture medium (Supplementary Fig. 2). After 18 h of incubation at 37 °C, 5% CO_2, and 95% humidity, SNPSAs were removed from the intramedullary canal and incubated in 1 ml nutrient PBS (1 x PBS with 0.25% glucose, 0.2% ammonium sulfate, and 1% sterile bacterial growth broth) for 18 h. During this second incubation step, the viable bacteria attached to the SNPSAs began to multiply and release colonial counterparts into the nutrient PBS. 100 μl of released bacteria was transferred into a 96-well microplate and amplified by adding 100 μl fresh bacterial culture broth for another 40 h. Proliferation of the released daughter cells was monitored at a wavelength of 595 nm using an Infinite f200 microplate reader (Tecan, Durham, NC) to generate a time-proliferation curve for each well of the microplate, as previously described [19], every *ex vivo* antimicrobial test was replicated three times. In this assay, lagging or absent bacterial growth was diagnostic of partial or complete inhibition by the SNPSA, such that only a few or no daughter cells were able to colonize the substrate [19].

2.5. Protein adsorption in vitro

SNPSA discs were incubated at 37 °C for 20 h with 500 μl α-MEM containing 10% FBS and either 0.1 mg/ml bovine serum albumin (BSA; Fisher Scientific) or 0.1 mg/ml BMP-2 (Medtronic, Minneapolis, MN). To harvest all adsorbed proteins, SNPSAs were then incubated in 10 mM TRIS (Fisher Scientific) and 1 mM EDTA (Fisher Scientific) for 6 h at 4 °C. Protein concentration was measured using the Bio-Rad® Protein Assay (Bio-Rad, Hercules, CA) with the Tecan Infinite f200 microplate reader [25,28].

2.6. In vitro osteoinductivity

2×10^3 pre-osteoblastic MC3T3-E1 murine cells (passage 18, subclone 4, ATCC CRL-2593) were seeded on SNPSA discs with 500 μl osteogenic medium (α-MEM supplied with 10% FBS, 1% HT supplement, 100 unit/ml penicillin, 100 μg/ml streptomycin, 50 μg/ml ascorbic acid and 10 mM β-glycerophosphate) in 24-well plates at 37 °C, 5% CO_2, and 95% humidity. All media for cell culture were purchased from Invitrogen. Cell proliferation was estimated using the Vybrand® MTT Cell Proliferation Assay Kit (Invitrogen). Alkaline phosphatase (ALP) activity and degree of mineralization (assessed by Alizarin Red staining) were used to quantify the effect of silver nanoparticle/PLGA-coated stainless steel alloy on osteoblastic differentiation [19].

2.7. Rat femoral canal (FC) model

All surgical procedures were approved by the UCLA Office of Animal Research Oversight (protocol #2008-073). Using aseptic technique, a 25–30 mm longitudinal incision was made over the anterolateral aspect of the left femur of 12-week old male Sprague-Dawley (SD) rats. The femoral shaft was then exposed by separating the vastus lateralis and biceps femoral muscles. Using a micro-driver (Stryker, Kalamazoo, MI), four canals were drilled on each femur with 2 mm interface. SNPSA K-wires were implanted into each predrilled canal. For bacterial inoculation, 10^3 CFU *S. aureus* Mu50 or *P. aeruginosa* PAO-1 in 10 μl PBS (10^5 CFU/ml) was pipetted into the canal before implantation. After inoculation, the overlying muscle and fascia were closed with 4-0 Vicryl absorbable suture to secure the implant in place. Following surgery, the animals were housed in separate cages and allowed to eat and drink *ad libitum*. Weight bearing was started immediately postoperatively, and the animals were monitored daily. Buprenorphine was administered for 2 days as an analgesic, but no antibiotic was administered. Three rats were used in every treatment group.

2.8. Radiograph and micro-computed tomography scanning

At 2, 4, 6, and 8 weeks post-surgery, high-resolution lateral radiographs were obtained while the animals were under isoflurane anesthesia. The animals were euthanized at 8 weeks post-implantation. Operated femurs were dissected, harvested, and fixed in 10% buffered formalin (Fisher Scientific). Following 48 h fixation, samples were scanned using high-resolution micro-computed tomography (microCT; Skyscan 1172, Skyscan, Belgium) at an image resolution of 20.0 μm (55kVp and 181 μA radiation source with 0.5 mm aluminum filter). 2D and 3D high-resolution reconstruction images were acquired using the software provided by the manufacturer [19].

2.9. Histological and immunohistochemical (IHC) evaluation

After 3D microCT scanning, the specimen was decalcified using 10% EDTA solution (pH 7.4, Fisher Scientific, Hampton, NH) for 21 days [29], washed with running tap water for 3–4 h, transferred to a 75% ethanol solution, and embedded in paraffin. 5-μm sagittal sections of each specimen were collected [19]. Hematoxylin and eosin (H&E) staining and Masson's Trichrome staining were used to assess morphology. Taylor-modified Brown and Brenn Gram staining [19] and Giemsa staining were used to assess bacterial contamination and inflammation, respectively. In addition, IHC staining for osteocalcin (OCN, Santa Cruz Biotechnology, Santa Cruz, CA) was applied to evaluate new bone generation.

2.10. Statistical analysis

All results are presented as mean ± standard error of mean (s.e.m.). Statistical significance was computed using one-way ANOVA and independent-samples *t*-test (Origin 8; OriginLab Corp., Northampton, MA). $P < 0.05$ was considered statistically significant. All statistical analyses in this manuscript were conducted per consultation with the UCLA Statistical Biomathematical Consulting Clinic (SBCC).

3. Results

3.1. Characterization of SNPSAs

SNPSA was produced by repeated incubations of 316L steel alloy in silver nanoparticle/PLGA-chloroform solution. A uniform layer of silver nanoparticle/PLGA composite was observed on the surface of the stainless steel alloy (Fig. 1 and Supplementary Fig. 1). In addition, aggregates of silver nanoparticles sintered together were not observed in silver nanoparticle/PLGA layers containing up to 2.0% silver nanoparticles (Fig. 1a and Supplementary Fig. 1). SEM revealed that the thickness of silver nanoparticle/PLGA layer coated on K-wires was 43.36 ± 0.08 μm (Fig. 1b; $N = 8$). Densities of coated silver nanoparticle/PLGA composite were 0.263 g/cm^3, 0.278 g/cm^3,

Table 1
Contact angles of the standard liquids on the SNPSAs.

Silver proportion (%)	Contact angle θ (°) Before incubation[a]			
	Water	Glycerol	Formamide	Ethylene glycol
0%	48.6 ± 0.1	51.9 ± 0.1	45.1 ± 0.2	43.0 ± 0.2
1%	49.7 ± 0.1	54.0 ± 0.2	48.3 ± 0.2	44.1 ± 0.1
2%	50.3 ± 0.1	57.3 ± 0.2	50.1 ± 0.2	48.7 ± 0.2
Silver proportion (%)	Contact angle θ (°) After incubation in osteogenic medium[a,b]			
	Water	Glycerol	Formamide	Ethylene glycol
0%	47.0 ± 0.2	52.5 ± 0.1	40.6 ± 0.1	43.8 ± 0.2
1%	36.1 ± 0.2	51.4 ± 0.1	37.4 ± 0.2	37.4 ± 0.1
2%	27.9 ± 0.2	50.1 ± 0.1	35.4 ± 0.2	29.2 ± 0.2

[a] Data were shown as mean ± SEM ($N = 6$).
[b] SNPSAs were incubated in osteogenic medium for 9 days.

and 0.293 g/cm^3, for 0%, 1%, and 2% silver nanoparticles, respectively; thus, the overall doses of silver nanoparticle-coated on the K-wires were: $\pi \times [(\text{Thickness}_{\text{silver nanoparticle/PLGA}} + \text{Radius}_{\text{Alloy}})^2 - \text{Radius}^2_{\text{Alloy}}] \times \text{Density}_{\text{silver nanoparticle/PLGA}} \times \text{Proportion}_{\text{silver nanoparticle}} = 0$ μg/cm, 2.44 μg/cm, and 5.14 μg/cm for 0%, 1%, and 2% SNPSA, respectively.

3.2. Contact angle and surface free energy of SNPSAs

The contact angles on the SNPSAs obtained before and after incubation in osteogenic medium are summarized in Table 1. Notably, the values of contact angle for the liquids applied on 0%-SNPSA differed only slightly before and after incubation in osteogenic medium. In contrast, the values of contact angle for the liquids applied on 1%- and 2%-SNPSAs dramatically changed after the incubation (Table 1).

Using the contact angle values and Eq. (1) [20,21], surface free energy and its dispersion and non-dispersion components of SNPSAs were calculated (Fig. 2). The presence of silver nanoparticles had minimal effect on the surface free energy of SNPSAs before incubation in osteogenic medium; however, the surface free energy of SNPSAs increased significantly as a function of silver proportion after 9 days of incubation in osteogenic medium (Fig. 2a). Interestingly, the dispersion component γ_S^d decreased with increasing silver proportion (Fig. 2b) but remained quite small compared to the non-dispersion component γ_S^{nd} (Fig. 2c); moreover, incubation in osteogenic medium further decreased γ_S^d (Fig. 2b). In contrast, the non-dispersion (or 'polar') component γ_S^{nd} increased with silver proportion, and incubation in osteogenic medium resulted in more dramatically increased γ_S^{nd} as a function of silver proportion (Fig. 2c). As a result, the polarity of SNPSAs, defined as $\frac{\gamma_S^{nd}}{\gamma_S}$ x 100%, increased with silver proportion (Fig. 2d). It is noteworthy that incubation in osteogenic medium did not influence the polarity of PLGA-coated alloy without silver nanoparticles (0%-SNPSA), but the same incubation resulted in significantly increased polarity of both 1%- and 2%-SNPSAs (Fig. 2d).

3.3. In vitro antimicrobial activity of SNPSAs

Analysis of bacterial colonization showed that, when compared to 0%-SNPSA, 1%- and 2%-SNPSAs inhibited the initial adherence of *S. aureus* Mu50 (Fig. 3) and *P. aeruginosa* PAO-1 (Fig. 4) after 1 h incubation in the bacterial broth in a silver-proportion-dependent manner. Quantification of CFU formation demonstrated that, when 0%-SNPSA was incubated with 10^3 CFU *S. aureus* Mu50, almost all the bacteria initially adhered to the alloy surface within the first hour of incubation, and the number of bacteria markedly increased with incubation time (Fig. 3a). This result suggested that *S. aureus* Mu50 proliferated extensively on 0%-SNPSA surface after adherence. 1% silver nanoparticles slightly reduced initial adherence of 10^3 CFU *S. aureus* Mu50 but significantly inhibited its proliferation on the coated alloy (Fig. 3a). Initial adherence of 10^3 CFU *S. aureus* Mu50 to 2%-SNPSA was less than 5% (Fig. 3a). Furthermore, no bacteria survived at an initial inoculum of 10^3 CFU after 24 h incubation with 2%-SNPSA (Fig. 3a). In addition, 2%-SNPSA presented similar antibacterial properties against the adherent bacteria from 10^3 CFU *P. aeruginosa* PAO-1 as those from the same initial inoculum of *S. aureus* (Fig. 4a).

When the initial inocula of both species were increased to 10^4 and 10^5 CFU, about 2×10^3 bacteria initially adhered to the 0%-SNPSA and proliferated during the incubation (Fig. 3b and c, and Fig. 4b, and c). In contrast, only about 1×10^3 bacteria initially adhered to the 1%-SNPSA, and their extended proliferation was significantly decreased (Fig. 3b and c, and Fig. 4b, and c). Remarkably, at the established ceiling of 2% silver [19], initial bacterial adherence was significantly inhibited (Fig. 3b and c, and Fig. 4b, and c). Although 2%-SNPSA was not enough to kill all adherent bacteria from 10^4 or 10^5 CFU inoculum within 24 h, less than 1% of adherent bacteria survived (Fig. 3b and c, and Fig. 4b and c).

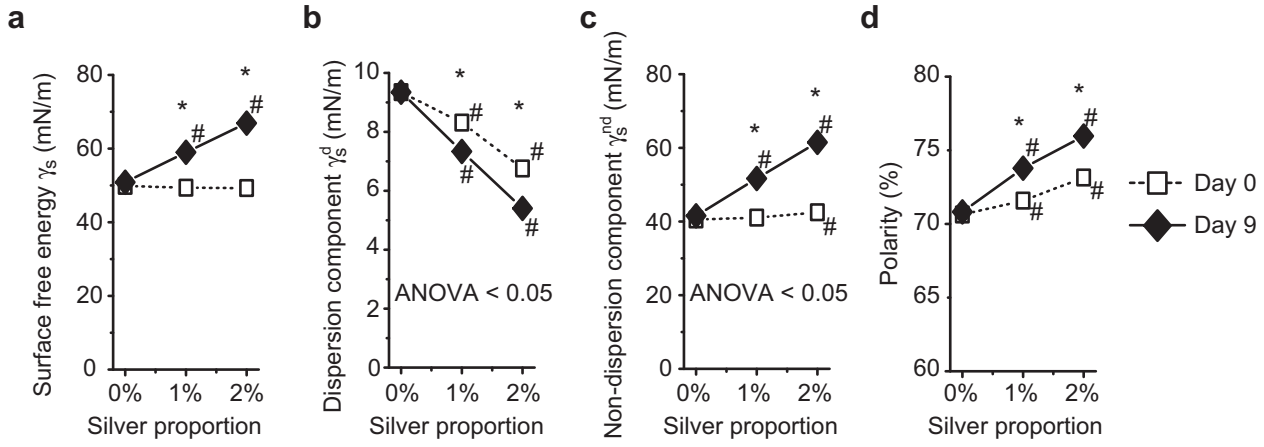

Fig. 2. Surface free energy of SNPSAs. Dependency of the total surface free energy (a, γ_S)the dispersion component (b, γ_S^d) the non-dispersion component (c, γ_S^{nd})and the polarity (d, $\frac{\gamma_S^{nd}}{\gamma_S}$. 100%) on the silver proportion of various SNPSAs during the 9-day incubation in osteogenic medium *in vitro*. $N = 6$; #, significant difference compared to 0%-SNPSA, ANOVA < *0.05*; *, significant difference between before and after incubation in osteogenic medium, $P < 0.05$; error bars were too small to show.

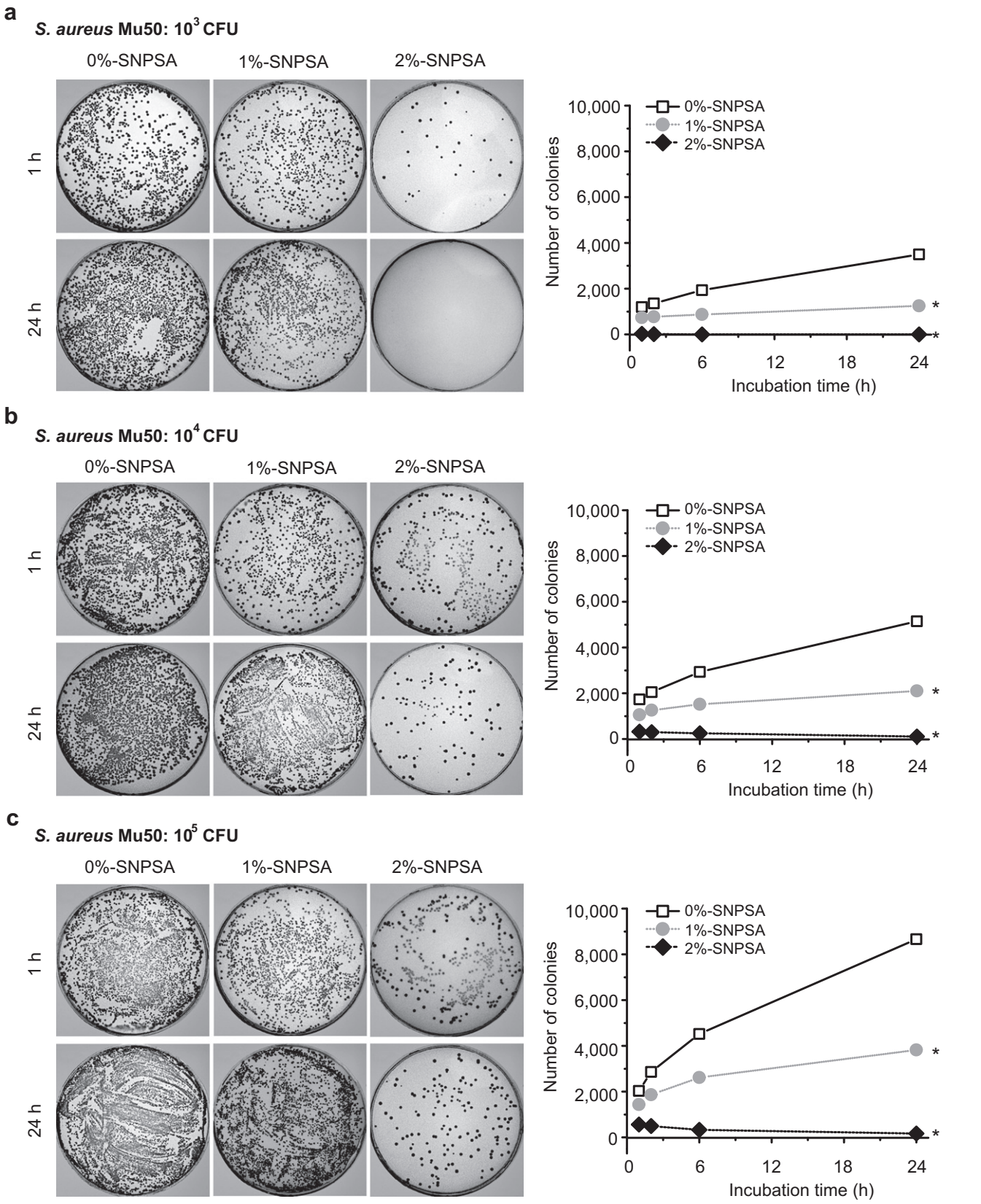

Fig. 3. *In vitro* bacterial colonization analysis of *S. aureus* Mu50. Antimicrobial activity of SNPSAs against 10^3 (a), 10^4 (b), and 10^5 (c) CFU *S. aureus* Mu50 was evaluated. SNPSA inhibited *S. aureus* Mu50 initial adherence and extended proliferation in a silver-proportion-dependent manner *in vitro*. $N = 4$; *, significant difference compared to 0%-SNPSA, ANOVA < 0.05; error bars were too small to show.

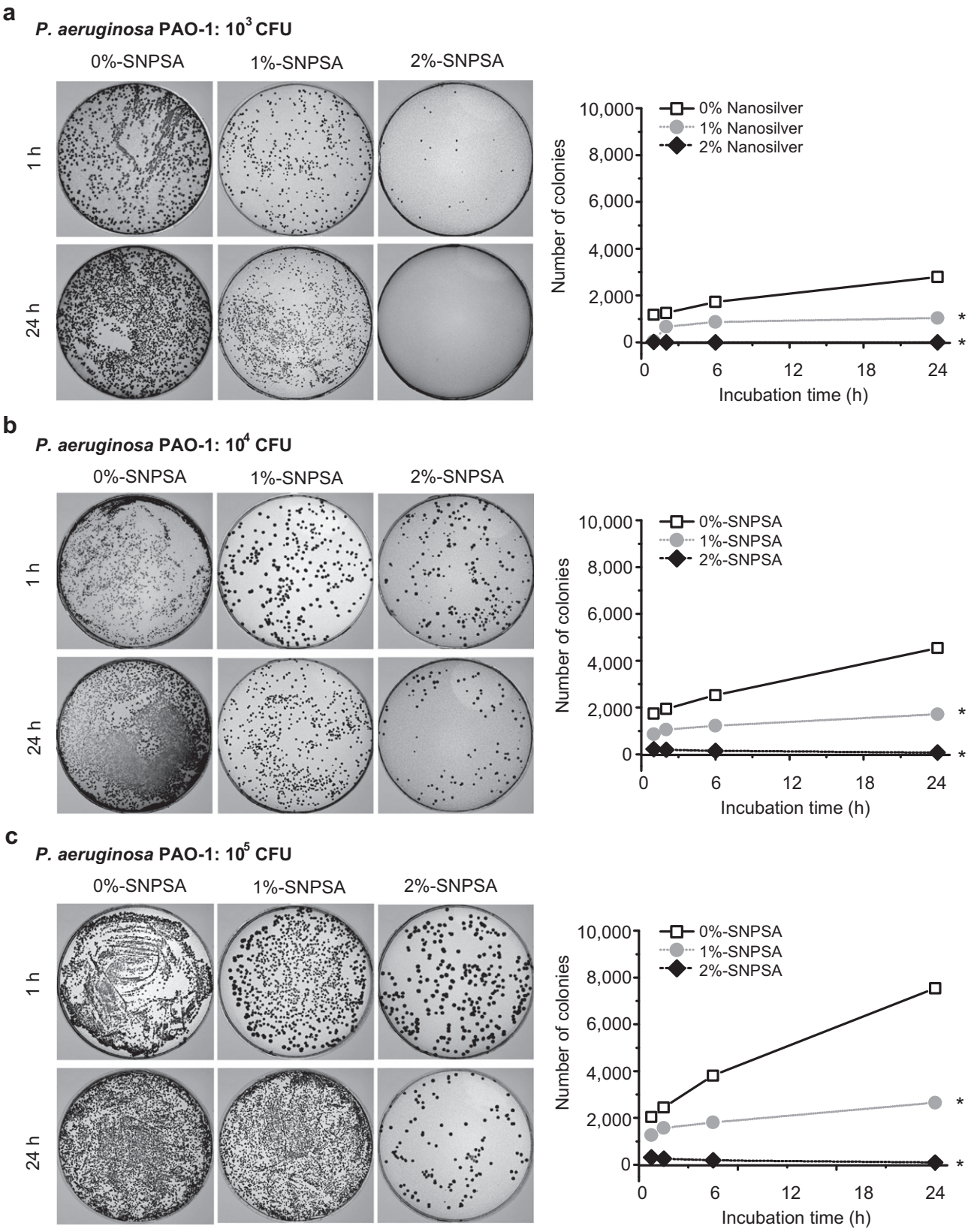

Fig. 4. *In vitro* bacterial colonization analysis of *P. aeruginosa* PAO-1. Antimicrobial activity of SNPSAs against 10^3 (a), 10^4 (b), and 10^5 (c) CFU *P. aeruginosa* PAO-1 was evaluated. SNPSA inhibited *P. aeruginosa* PAO-1 initial adherence and extended proliferation in a silver-proportion-dependent manner *in vitro*. $N = 4$; *, significant difference compared to 0%-SNPSA, ANOVA < 0.05; error bars were too small to show.

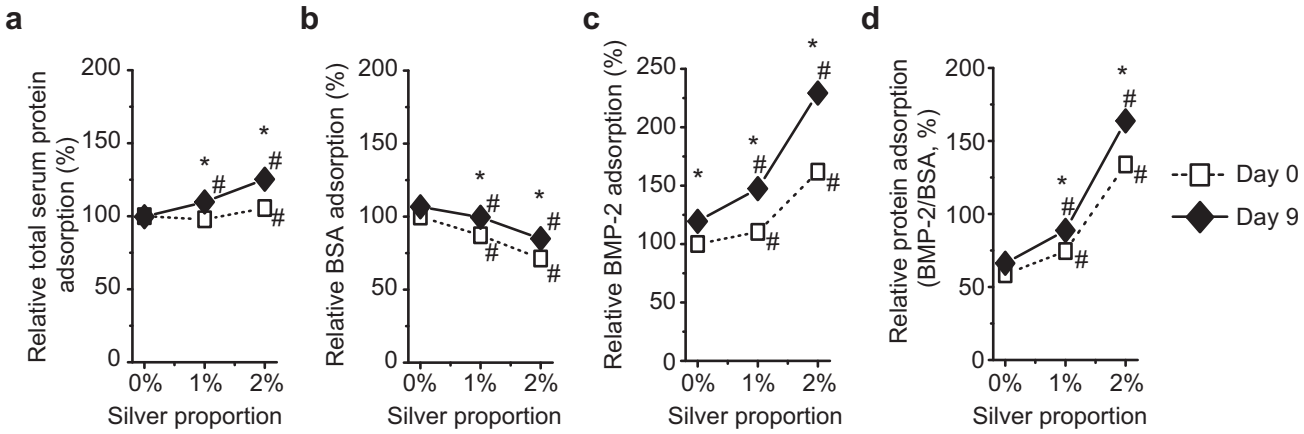

Fig. 5. *In vitro* protein adsorption of SNPSAs. Adsorption of the total serum protein (a), BSA (b), and BMP-2 (c) was measured after 0 and 9 h of incubation in osteogenic medium. The ratio of protein adsorption of BMP-2/BSA is also shown (d). Data normalized to 0%-SNPSA on day 0. $N = 6$; #, significant difference compared to 0%-SNPSA, ANOVA < 0.05; *, significant difference before and after incubation in osteogenic medium, $P < 0.05$; error bars were too small to show.

3.4. Ex vivo antimicrobial activity of SNPSAs

In order to further evaluate the effect of silver nanoparticle/PLGA coating on preventing bacterial adherence and biofilm formation on the surface of implants, an *ex vivo* contamination model (Supplementary Fig. 2) was employed with a previously reported microplate proliferation assay [19]. The *ex vivo* model was used to observe the antibacterial activity of SNPSA independently of host immunological responses and to compare its antibacterial activity with that observed in the *in vivo* contamination model of rat FCs. SEM revealed that placing the SNPSA K-wires into the pre-reamed intramedullary canal did not damage the coating significantly (Fig. 1b).

Control 0%-SNPSA did not inhibit *ex vivo* bacterial adherence or proliferation, while silver-proportion-dependent antimicrobial activity was observed in 1%- and 2%-SNPSAs (Supplementary Fig. 3). 1%-SNPSAs significantly inhibited 10^3–10^5 CFU *S. aureus* Mu50 *ex vivo* growth on the coated alloy surface (Supplementary Fig. 3a–c). However, the inhibition against 10^3 CFU *P. aeruginosa* PAO-1 growth by 1%-SNPSA was minimal (Supplementary Fig. 3d), and no considerable effects of 1% silver nanoparticle against 10^4 or 10^5 CFU *P. aeruginosa* PAO-1 were observed *ex vivo* (Supplementary Fig. 3e, and f). Higher silver proportion at 2% silver nanoparticle was more effective against *ex vivo* growth of 10^4 or 10^5 CFU *S. aureus* Mu50 (Supplementary Fig. 3b, and c) and *P. aeruginosa* PAO-1 (Supplementary Fig. 3e, and f), respectively. Furthermore, *ex vivo* growth of 10^3 CFU *S. aureus* Mu50 and *P. aeruginosa* PAO-1 was completely inhibited by 2%-SNPSA (Supplementary Fig. 3a, and d).

3.5. Protein adsorption on SNPSAs in vitro

Protein adsorption was detected on SNPSAs (Fig. 5). Clearly, a positive correlation between surface free energy and the total serum protein adsorption was observed: the higher the surface free energy, the more protein adsorbed onto the SNPSA surfaces and *vice versa* (Figs. 2 and 5a). Surprisingly, SNPSAs exhibited selective protein adsorption in a silver-proportion-dependent manner: as silver proportion increased in SNPSAs, adsorption of the control protein BSA decreased (Fig. 5b) while that of the osteoinductive growth factor BMP-2 increased (Fig. 5c). This selectivity was more significant after the incubation in osteogenic medium (Fig. 5d).

3.6. Osteogenic activity of SNPSAs in vitro

The MTT assay was used to compare mouse MT3T3-E1 pre-osteoblastic cell proliferation on different SNPSAs (Fig. 6a). Generally, silver nanoparticles resulted in increased MC3T3-E1 cell proliferation on SNPSAs in a silver-proportion-dependent manner (Fig. 6a). Interestingly, along with the culture time, SNPSAs with higher silver proportions promoted cell proliferation more potently (Fig. 6a). For example, cell proliferation on 2%-SNPSA was 1.17, 1.63, and 1.88 times greater than that on control 0%-SNPSA after 3, 6, and 9 days in osteoblastic differentiation medium, respectively. To assay osteoblastic cell function, ALP activity in MC3T3-E1 cells was measured after 9 days in osteoblastic differentiation medium. SNPSAs significantly increased ALP activity of ongrowth cells compared to 0%-silver nanoparticle controls (Fig. 6b). Furthermore, SNPSAs also significantly promoted ongrowth terminal differentiation of osteoblasts, as indicated by mineralization, during the 21-day culture period (Fig. 6c). Therefore, SNPSAs exhibited osteoinductive properties in a silver-proportion-dependent manner *in vitro*.

3.7. Effects of SNPSA implants in rat FCs

3.7.1. Radiography

No obvious radiographic signs of bone formation were observed in rat FCs implanted with either uncontaminated (Supplementary Fig. 4) or bacterially contaminated (Fig. 7) 0%-SNPSAs up to 8 weeks post-surgery; instead, radiographic evidence of osseous destruction was detected in the contaminated 0%-SNPSA group (Fig. 7). In contrast, significant bone formation surrounding 2%-SNPSAs implants in rat FCs was observed despite the initial contamination with 10^3 CFU bacteria (Fig. 7 and Supplementary Fig. 4). In addition, no osteolysis was observed in the contaminated 2%-SNPSAs group (Fig. 7). Radiographic findings of bone formation surrounding contaminated 2%-SNPSA implants in rat FCs were also confirmed by 3D microCT analysis (Fig. 7).

Supplementary video related to this article can be found online at 10.1016/j.biomaterials.2012.08.010.

3.7.2. Histological and IHC evaluation

Microscopic examination revealed bacterial persistence (Fig. 8a) accompanied by many inflammatory cells (Fig. 8b) in the intramedullary tissues around 0%-SNPSA implants in rat FCs 8 weeks after implantation with 10^3 CFU initial bacterial inoculum. In

contrast, no bacterial survival was evident around 2%-SNPSA implants under the same conditions (Fig. 8a), and inflammatory cell infiltration in the intramedullary tissues around the implants was minimal (Fig. 8b). Thus, 2%-SNPSA implants markedly inhibited bacterial invasion without evoking significant host inflammatory responses *in vivo*.

Newly formed bone around SNPSA implants was further evaluated by H&E staining, Trichrome staining, and IHC staining with an antibody against OCN, a marker of mature differentiated osteoblasts, at 8 weeks after implantation with 10^3 CFU initial bacterial inoculum. Only minimal bone formation around the 0%-SNPSA groups was observed (Fig. 8c and d). On the other hand, consistent with radiographic analyses, significant bone formation was detected around 2%-SNPSA implants (Fig. 8c and d), and intense OCN staining signified that new bone formation was still active around 2%-SNPSA implants at week 8 after implantation (Fig. 8e). Taken together, 2%-SNPSA implants exhibited significant osteoinductive as well as antibacterial effects *in vivo*.

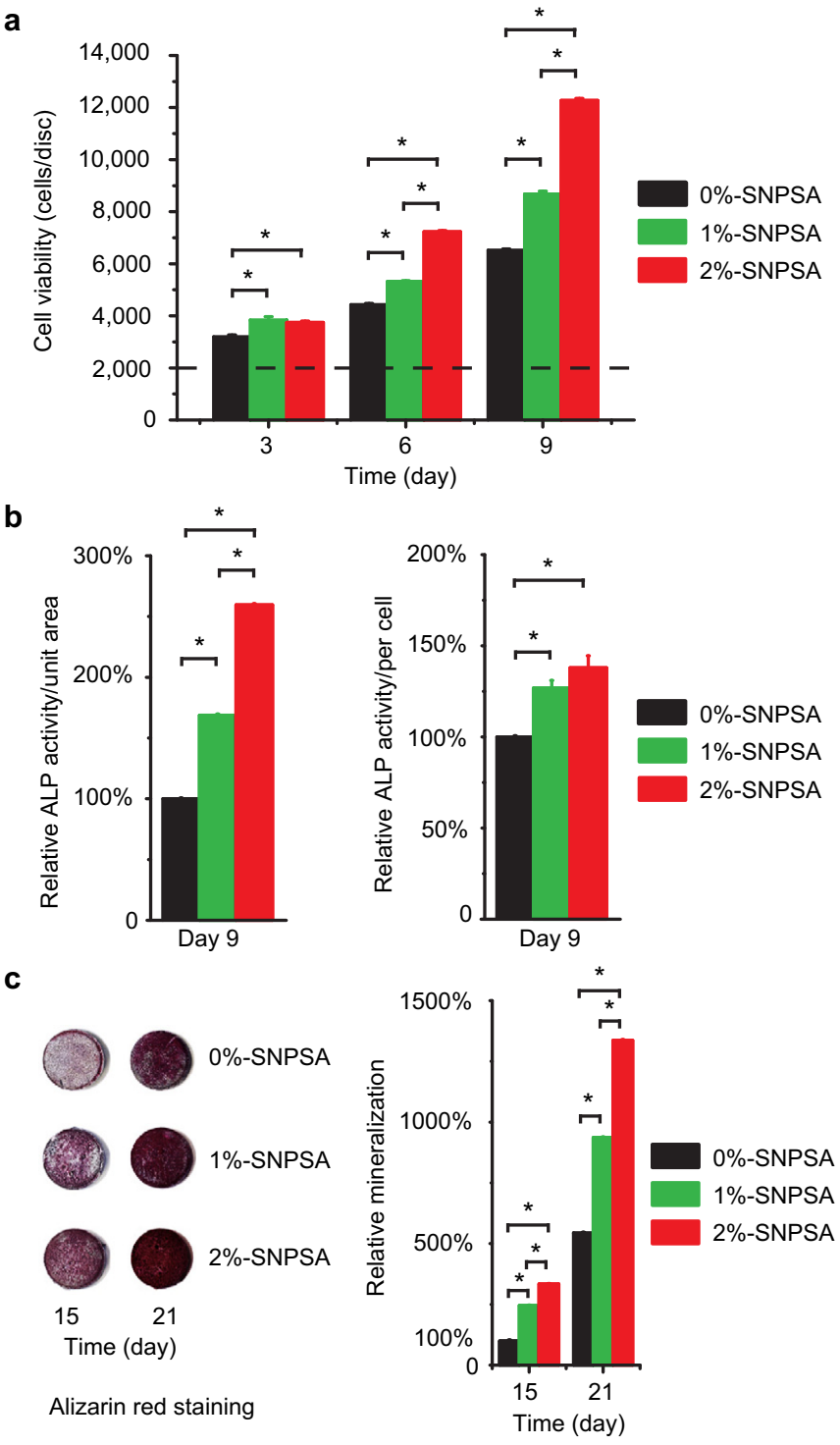

Fig. 6. *In vitro* osteoinductive activity of SNPSAs. SNPSAs significantly promoted MC3T3-E1 cell proliferation (a), ALP activity (b), and mineralization (c). Data normalized to 0%-SNPSA on day 9 (b) And on day 15 (c). $N = 6$; *, $P < 0.05$.

4. Discussion

Since the first applications of surgically-implanted materials in humans, bacterial infections have represented a common and challenging problem [1,2,7]. Bacterial adherence to the foreign implanted materials and subsequent biofilm formation are hallmarks of implant-associated infections [2,14,30–32]. As a result, prevention of bacterial colonization and biofilm formation on implants by administration of prophylactic antibiotics has been extensively studied [13–16]. Interestingly, most of these studies are focused on preventing *S. aureus* contamination [13–16], as this species is the leading cause of implant-associated infections due to its high affinity to bone, rapid induction of osteonecrosis, and resorption of bone matrix [5,33,34]. However, other bacterial species, including *P. aeruginosa*, *S. epidermidis*, *Klebsiella ozaenae*, and *Escherichia coli*, are also commonly involved in implant-associated infections in orthopedic surgery [5,8,33,35–38], and some studies have even reported *P. aeruginosa* as a major isolated organism [38]. Because pathogens involved in implant-associated infections are diverse, and bacteria in biofilms are protected from the host immune responses and antibiotics [2,11,12,31], the restricted activity of antibiotics against implant infections limits their clinical effectiveness. This is especially the case in infections involving antibiotic-resistant bacterial strains (*e.g.* MRSA strains), which are increasing in both healthcare and community settings and are becoming a major threat to public health.

Because of its antimicrobial properties, silver has been extensively used in water recycling and sanitization and for treatment of wound infections [19]. Currently, silver is gaining renewed attention as a medical antimicrobial agent due to its broad antibacterial spectrum and the difficulty of developing bacterial resistance to silver [19]. For instance, silver is used to reduce bacterial colonization in a variety of pharmaceutical devices including vascular and urinary catheters, endotracheal tubes, and implantable prostheses [19]. Mechanistically, silver prevents cell division and transcription by binding to and disrupting multiple components of bacterial structure and metabolism, including cellular transport, essential enzyme systems such as the respiratory cytochromes, and synthesis of cell wall components, DNA and RNA; nevertheless, the reservoir form of the active silver form may be diverse [19]. Previously, ionic reservoir forms of silver such as silver nitrate ($AgNO_3$) and silver sulfate (Ag_2SO_4) have been used to provide protection against bacterial infections [19]. However, despite its effective short-term antibacterial activity, inadequate local retention and severe cytotoxic effects of ionic silver (Ag^+) have made it undesirable for continually preventing bacterial colonization on the implants [19]. Recent reports have shown that that 20–25 nm silver nanoparticles effectively inhibit microorganisms without causing significant cytotoxicity [19], and that 10–20 nm silver nanoparticles are nontoxic in mice and guinea pigs when administered by the oral, ocular and dermal routes [39]. These findings suggest silver nanoparticles of the size evaluated in the present study are appropriate for therapeutic application from a safety standpoint.

In addition, the preparation and stabilization of silver nanoparticles remain challenging due to their tendency to aggregate. Several polymers have been used to stabilize silver nanoparticles, including polyethyleneimine [40], polyallylamine [41], poly(vinylpyrrolidone) [42], and chitosan [43]. The nucleophilic character of these polymers, albeit minor, is sufficient for them to bind to the metal particles by donating electrons [44]. The FDA-approved, biodegradable and biocompatible polymer PLGA has been chosen in this study because its hydrolyzable ester bonds are subject to nucleophilic interactions with incorporated components [45] such as silver particles. Another advantage of PLGA is that it could be applied onto implants using solvent casting techniques, which allow coating of alloys and even plastic surfaces with polished, irregular or porous materials. For instance, up to 2% silver nanoparticles were coated onto 316L stainless steel alloy within PLGA without aggregation (Fig. 1 and Supplementary Fig. 1). In addition, PLGA degradation is based on hydrolytic splitting of the polymer backbone into oligomers and release of lactic acid and glycolic acid, two byproducts of various metabolic pathways in the body under normal physiological conditions. Thus, a local delivery system that incorporates silver nanoparticles into the polymer coating ensures not only high local concentrations around the implant for long periods but also reduced risks and side effects for the host organism compared to systemic drug application [46].

In this study, the results from *in vitro* and *ex vivo* assays demonstrated that 2%-silver nanoparticle/PLGA coating effectively prevented bacterial adherence and biofilm formation on the stainless steel alloy implants (Figs 3 and 4, and Supplementary Fig. 3). Using a rat FC model, we also found that 2%-SNPSA displayed significant antibacterial activity against contamination with 10^5 CFU/ml Gram-positive *S. aureus* Mu50 or Gram-negative *P. aeruginosa* PAO-1 (Figs 7 and 8), a bacterial burden typical of invasive tissue infection [19]. In addition, by employing BMP-2-coupled silver nanoparticle/PLGA composite grafts, we successfully regenerated bone formation in a 6-mm critical-sized rat FSD grossly infected with 10^9 CFU/mlVISA/MRSA strain Mu50 [19]. Collectively, our findings support the application of silver nanoparticle/PLGA composite for localized prophylaxis of implant-associated infections.

Notably, surface free energy of SNPSA, especially its non-dispersion component γ_S^{nd} ,increases with silver proportion after incubation in osteogenic medium (Fig. 5c). Silver nanoparticles in SNPSA may have contributed to the non-dispersion component of surface free energy by progressively releasing cationic silver [Ag^+, *i.e.* ionic silver Ag(I)] and/or exposing partially oxidized silver nanoparticles with Ag^+ chemisorbed to the surface of SNPSA during the incubation [19]. As a result, the non-dispersion component of surface free energy, the total surface free energy, and the polarity are all increased after incubation in osteogenic medium in a silver-proportion-dependent manner (Fig. 2). In turn, the increased surface free energy, especially its non-dispersion component, imparts higher bioactivity and increased total protein adsorption to the material after incubation in osteogenic medium (Fig. 5a). Surprisingly, adsorption of BMP-2 on the SNPSA surface is positively correlated with the non-dispersion component of surface free energy, which increases along with the silver proportion and incubation time in osteogenic medium; conversely, adsorption of BSA decreases slightly with increased silver proportion and is not significantly affected by the incubation (Fig. 5b). This result suggests that SNPSAs may have the ability to adsorb proteins selectively in a silver-proportion-dependent manner, which may explain their markedly osteoinductive activity *in vitro* (Fig. 6) and *in vivo* (Figs 7 and 8) when BMP-2 is applied. However, further investigation is necessary to determine the mechanism of this selectivity and the effect of incubation.

In summary, we demonstrated that SNPSA successfully inhibited bacterial adherence and biofilm formation in a silver-proportion-dependent manner. Unexpectedly, we also found that SNPSA materials promoted MC3T3-E1 pre-osteoblast proliferation and maturation *in vitro*. Finally, we used a rat FC model to show that 2%-SNPSA implants have significantly induced bone generation despite bacterial contamination, even at a bacterial inoculum that could cause invasive tissue infection.

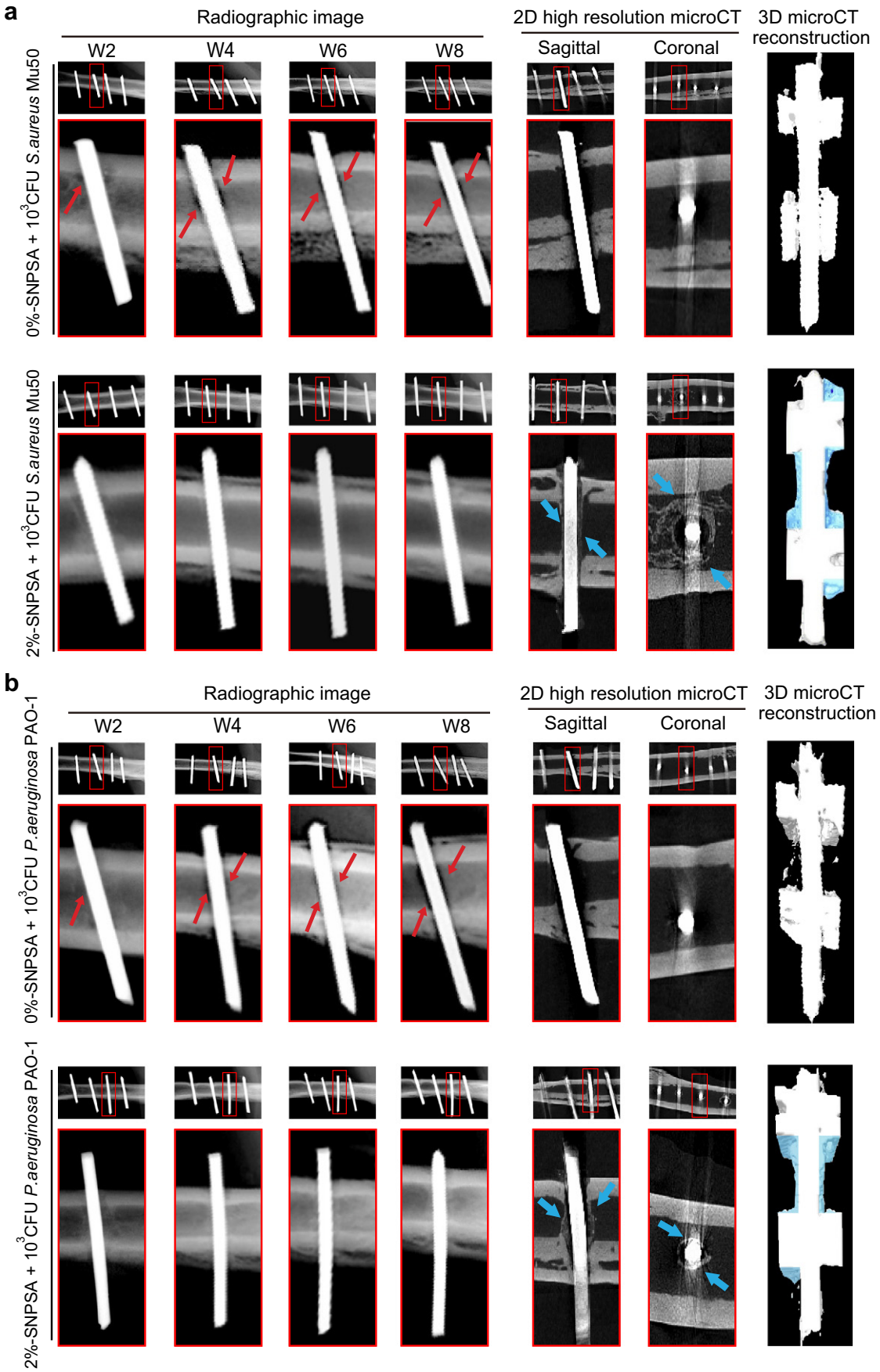

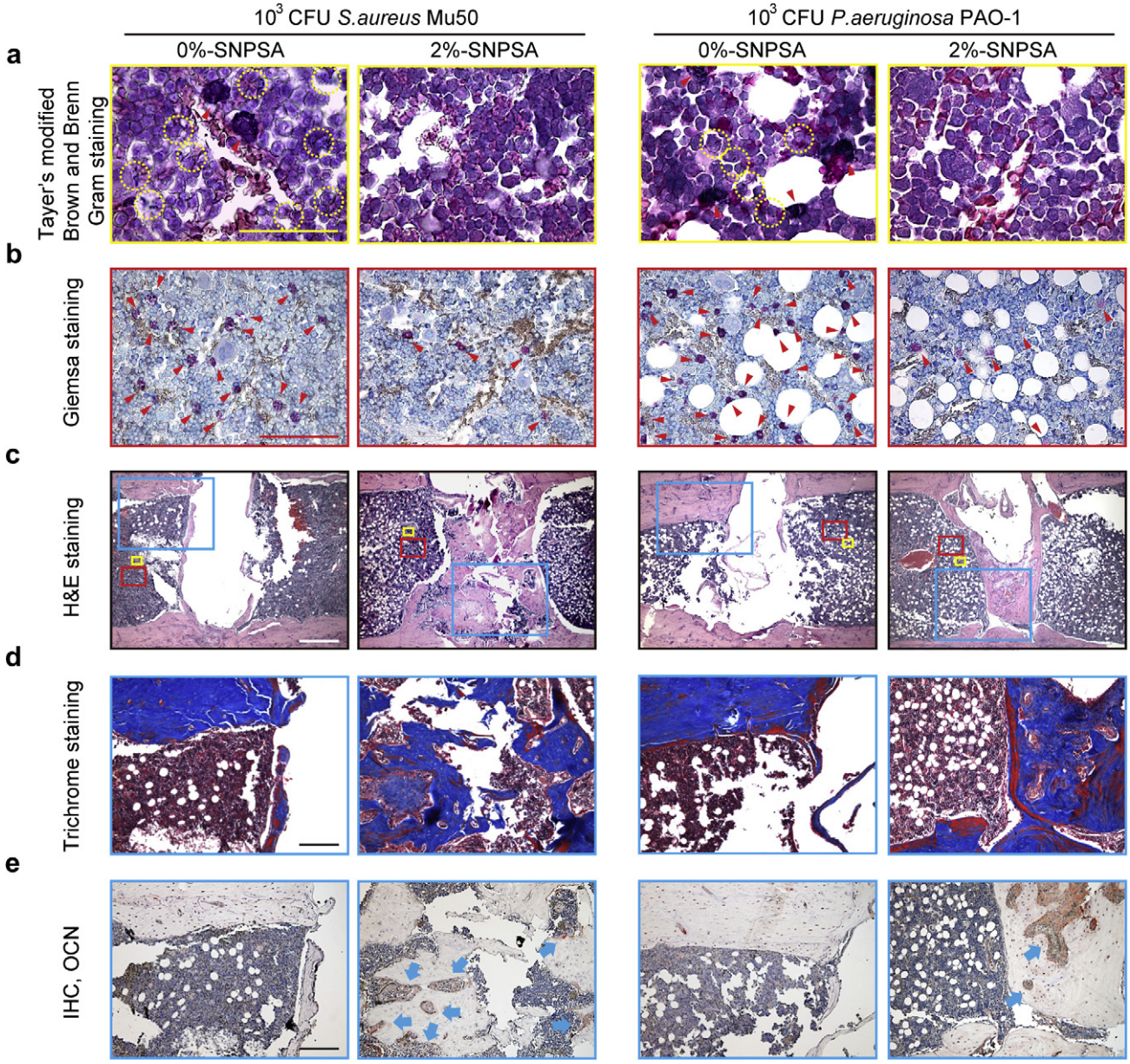

Fig. 8. Histological and IHC analysis of contaminated 0%- and 2%-SNPSA implants in rat FCs at 8 weeks after implantation. 10^3 CFU *S. aureus* Mu50 or *P. aeruginosa* PAO-1 in 10 μl PBS (10^5 CFU/ml) was pipetted into the canal before implantation for bacterial invasion. Taylor-modified Brown and Brenn Gram staining (a) And Giemsa staining (b) Revealed bacterial persistence (yellow dotted circles) with massive inflammatory cell infiltration (red arrowheads) in the intramedullary tissue around 0%-SNPSA implants in rat FCs. In contrast, no bacterial survival was evident around 2%-SNPSA implants in the same situation, and inflammatory cell infiltration in the intramedullary tissues around the implants was minimal. Consistent with the radiographic analysis, only minimal bone formation around the 0%-SNPSA groups was observed, whereas significant bone formation (blue arrows) was detected around 2%-SNPSA implants, as shown by H&E staining (c), Masson's Trichrome staining (d), and immunostaining of high-intensity OCN signals (e). Yellow scale bar = 50 μm; red scale bar = 100 μm; white scale bar = 500 μm; black scale bar = 200 μm.

5. Conclusions

From a materials and device development perspective, SNPSA exhibited strong bactericidal and osteoinductive properties that make it a promising pharmaceutical material in orthopedic surgery. Our results also indicated that silver nanoparticle/PLGA coating is a practical process that is non-toxic, easy to operate, and free of silver nanoparticle aggregation. In addition, our results revealed that the antibacterial and osteoinductive activities of SNPSA are silver-proportion-dependent, raising the interest in increasing the silver proportion of the coating in future investigations. Further improvement of interfacial adhesion of silver nanoparticle/PLGA coating to different metal surfaces, such as stainless steel alloys, titanium and titanium-based alloys, and cobalt alloys, should be

Fig. 7. Radiographic images of contaminated 0%- and 2%-SNPSA implants in rat FCs. 10^3 CFU *S. aureus* Mu50 (a) or *P. aeruginosa* PAO-1 (b) In 10 μl PBS (10^5 CFU/ml) was pipetted into the canal before implantation for bacterial invasion. Radiographic evidence of osseous destruction (red arrows), without any obvious signs of bone formation up to 8 weeks post-surgery, was detected in the contaminated 0%-SNPSA group. In contrast, significant bone formation surrounding 2%-SNPSAs implanted in rat FCs at week 8 post-implantation (shown as blue arrows in 2D resolution microCT images), without significant osteolysis, was detected. Newly formed bone around 2%-SNPSA implants was highlighted in 3D microCT reconstruction images (blue shading) and videos (Supplementary Videos). (For interpretation of the references to colour in this figure legend, the reader is referred to the web version of this article.)

made for clinical application of silver nanoparticle/PLGA-coated implants in orthopedic surgery, especially when permanent implants such as pins for the fixation of bone fracture are indicated.

Disclosure

D. C. is inventor on non-chemically based processing silver nanoparticle patent (QSI-Nano® Silver; USPTO 7,282,167). K. T., C. S., and Z. Z. are inventors of silver nanoparticle-related patents filed from UCLA.

Acknowledgments

This research is supported by the US DoD Grant 07128099. Y. L. is supported by the China Scholarship Council (CSC). The authors would like to thank Dr. Wei Yuan from the Department of Orthopaedic Surgery, Zhongshan Hospital, Fudan University, Shanghai 200032, PR China and Dr. Michael Chiang from the Dental and Craniofacial Research Institute and Section of Orthodontics, School of Dentistry, University of California, Los Angeles for assistance in surgery and microCT scanning, and the Translational Pathology Core Laboratory (TPCL) and Surgical Pathology divisions of the UCLA Department of Pathology and Laboratory Medicine for histology processing.

Appendix A. Supplementary data

Supplementary data related to this article can be found at http://dx.doi.org/10.1016/j.biomaterials.2012.08.010.

References

[1] Gomez J, Rodriguez M, Banos V, Martinez L, Claver MA, Ruiz J, et al. Orthopedic implant infection: prognostic factors and influence of long-term antibiotic treatment on evolution. Prospective study, 1992–1999. Enferm Infecc Microbiol Clin 2003;21:232–6.
[2] Darouiche RO. Treatment of infections associated with surgical implants. N Engl J Med 2004;350:1422–9.
[3] Giavaresi G, Borsari V, Fini M, Giardino R, Sambri V, Gaibani P, et al. Preliminary investigations on a new gentamicin and vancomycin-coated PMMA nail for the treatment of bone and intramedullary infections: an experimental study in the rabbit. J Orthop Res 2008;26:785–92.
[4] Shirai T, Tsuchiya H, Shimizu T, Ohtani K, Zen Y, Tomita K. Prevention of pin tract infection with titanium-copper alloys. J Biomed Mater Res B Appl Biomater 2009;91:373–80.
[5] Khosravi AD, Ahmadi F, Salmanzadeh S, Dashtbozorg A, Montazeri EA. Study of bacteria isolated from orthopedic implant infections and their antimicrobial susceptibility pattern. Res J Microbiol 2009;4:158–63.
[6] Campoccia D, Montanaro L, Arciola CR. The significance of infection related to orthopedic devices and issues of antibiotic resistance. Biomaterials 2006;27:2331–9.
[7] Schierholz JM, Beuth J. Implant infections: a haven for opportunistic bacteria. J Hosp Infect 2001;49:87–93.
[8] Sanderson PJ. Preventing infection in orthopedic implants. J Antimicrob Chemother 1989;24:277–80.
[9] Toma MB, Smith KM, Martin CA, Rapp RP. Pharmacokinetic considerations in the treatment of methicillin-resistant Staphylococcus aureus osteomyelitis. Orthopedics 2006;29:497–501.
[10] Winkler H, Kaudela K, Stoiber A, Menschik F. Bone grafts impregnated with antibiotics as a tool for treating infected implants in orthopedic surgery - one stage revision results. Cell Tissue Bank 2006;7:319–23.
[11] Habash M, Reid G. Microbial biofilms: their development and significance for medical device-related infections. J Clin Pharmacol 1999;39:887–98.
[12] Costerton JW, Lewandowski Z, Caldwell DE, Korber DR, Lappin-Scott HM. Microbial biofilms. Annu Rev Microbiol 1995;49:711–45.
[13] Alt V, Bitschnau A, Osterling J, Sewing A, Meyer C, Kraus R, et al. The effects of combined gentamicin-hydroxyapatite coating for cementless joint prostheses on the reduction of infection rates in a rabbit infection prophylaxis model. Biomaterials 2006;27:4627–34.
[14] Antoci Jr V, King SB, Jose B, Parvizi J, Zeiger AR, Wickstrom E, et al. Vancomycin covalently bonded to titanium alloy prevents bacterial colonization. J Orthop Res 2007;25:858–66.
[15] Darouiche RO, Mansouri MD, Zakarevicz D, Alsharif A, Landon GC. In vivo efficacy of antimicrobial-coated devices. J Bone Jt Surg Am 2007;89:792–7.
[16] Bernthal NM, Stavrakis AI, Billi F, Cho JS, Kremen TJ, Simon SI, et al. A mouse model of post-arthroplasty Staphylococcus aureus joint infection to evaluate in vivo the efficacy of antimicrobial implant coatings. PLoS One 2010;5:e12580.
[17] Bouza E, Muñoz P. Micro-organisms responsible for osteo-articular infections. Baillieres Best Pract Res Clin Rheumatol 1999;13:21–35.
[18] Moojen DJ, Spijkers SN, Schot CS, Nijhof MW, Vogely HC, Fleer A, et al. Identification of orthopaedic infections using broad-range polymerase chain reaction and reverse line blot hybridization. J Bone Jt Surg Am 2007;89:1298–305.
[19] Zheng Z, Yin W, Zara JN, Li W, Kwak J, Mamidi R, et al. The use of BMP-2 coupled-nanosilver-PLGA composite grafts to induce bone repair in grossly infected segmental defects. Biomaterials 2010;31:9293–300.
[20] Vakula VL, Pritykin LM. Polymer adhesion, basic physiochemical principles. New York: Ellis Horwood; 1991.
[21] Persin Z, Stana-Kleinschek K, Sfiligoj-Smole M, Kreze T, Ribitsch V. Determining the surface free energy of cellulose materials with the powder contact angle method. Text Res J 2004;74:55–62.
[22] Zheng Z, Bei FF, Tian HL, Chen GQ. Effects of crystallization of polyhydroxyalkanoate blend on surface physicochemical properties and interactions with rabbit articular cartilage chondrocytes. Biomaterials 2005;26:3537–48.
[23] Good RJ. Contact angle, wetting, and adhesion: a critical review. J Adhes Sci Technol 1992;6:1269–302.
[24] Holloway BW. Genetic recombination in Pseudomonas aeruginosa. J Gen Microbiol 1955;13:572–81.
[25] Shan Z, Xu H, Shi X, Yu Y, Yao H, Zhang X, et al. Identification of two new genes involved in twitching motility in Pseudomonas aeruginosa. Microbiology 2004;150:2653–61.
[26] Hughes MS, Moghadamian ES, Yin LY, Della Rocca GJ, Crist BD. Comparison of bulb syringe, pressurized pulsatile, and hydrosurgery debridement methods for removing bacteria from fracture implants. Orthopedics 2012;35:e1046–50.
[27] Chai H, Guo L, Wang X, Fu Y, Guan J, Tan L, et al. Antibacterial effect of 317L stainless steel contained copper in prevention of implant-related infection in vitro and in vivo. J Mater Sci Mater Med 2011;22:2525–35.
[28] De Bartolo L, Morelli S, Bader A, Drioli E. Evaluation of cell behaviour related to physico-chemical properties of polymeric membranes to be used in bioartificial organs. Biomaterials 2002;23:2485–97.
[29] Alers JC, Krijtenburg PJ, Vissers KJ, van Dekken H. Effect of bone decalcification procedures on DNA in situ hybridization and comparative genomic hybridization. EDTA is highly preferable to a routinely used acid decalcifier. J Histochem Cytochem 1999;47:703–10.
[30] Gristina AG. Biomaterial-centered infection: microbial adhesion versus tissue integration. Science 1987;237:1588–95.
[31] Gristina AG. Implant failure and the immuno-incompetent fibro-inflammatory zone. Clin Orthop Relat Res 1994;298:106–18.
[32] Pribaz JR, Bernthal NM, Billi F, Cho JS, Ramos RI, Guo Y, et al. Mouse model of chronic post-arthroplasty infection: noninvasive in vivo bioluminescence imaging to monitor bacterial burden for long-term study. J Orthop Res 2012;30:335–40.
[33] Eron LJ. Prevention of infection following orthopedic surgery. Antibiot Chemother 1985;33:140–64.
[34] Littlewood-Evans AJ, Hattenberger MR, Luscher C, Pataki A, Zak O, OReilly T. Local expression of tumor necrosis factor alpha in an experimental model of acute osteomyelitis in rats. Infect Immun 1997;65:3438–43.
[35] Barth E, Myrvik QM, Wagner W, Gristina AG. In vitro and in vivo comparative colonization of Staphylococcus aureus and Staphylococcus epidermidis on orthopaedic implant materials. Biomaterials 1989;10:325–8.
[36] von Eiff C, Proctor RA, Peters G. Coagulase-negative staphylococci. Pathogens have major role in nosocomial infections. Postgrad Med 2001;110:63–4. 69–70, 73–6.
[37] Ehrman JD, Bender ET, Stojilovic N, Sullivan T, Ramsier RD, Buczynski BW, et al. Microbial adhesion to zirconium alloys. Colloids Surf B Biointerfaces 2006;50:152–9.
[38] Mousa HA. Infection following orthopaedic implants and bone surgery. East Mediterr Health J 2001;7:738–43.
[39] Maneewattanapinyo P, Banlunara W, Thammacharoen C, Ekgasit S, Kaewamatawong T. An evaluation of acute toxicity of colloidal silver nanoparticles. J Vet Med Sci 2011;73:1417–23.
[40] Dai J, Bruening ML. Catalytic nanoparticles formed by reduction of metal ions in multilayered polyelectrolyte films. Nano Lett 2002;2:497–501.
[41] Kuo PL, Chen WF. Formation of silver nanoparticles under structured amino groups in pseudo-dendritic poly(allylamine) derivatives. J Phys Chem B 2003;107:11267–72.
[42] Yu H, Xu XY, Chen X, Lu T, Zhang P, Jing X. Preparation and antibacterial effects of PVA-PVP hydrogels containing silver nanoparticles. J Appl Ploym Sci 2007;103:125–33.
[43] Travan A, Pelillo C, Donati I, Marsich E, Benincasa M, Scarpa T, et al. Non-cytotoxic silver nanoparticle-polysaccharide nanocomposites with antimicrobial activity. Biomacromolecules 2009;10:1429–35.
[44] Henglein A. Physicochemical properties of small metal particles in solution: "microelectrode" reactions, chemisorption, composite metal particles, and the atom-to-metal transition. J Phys Chem 1993;97:5457–71.
[45] Houchin ML, Topp EM. Chemical degradation of peptides and proteins in PLGA: a review of reactions and mechanisms. J Pharm Sci 2008;97:2395–404.
[46] Cowsar DR. Introduction to controlled release. Adv Exp Med Biol 1974;47:1–13.

Toll-like receptor 9 inhibition improves immune response in late posttraumatic mice

Xiangcai Ruan, Sophie Darwiche MD, Melanie Scott PhD, Timothy R Billiar MD, FACS
Univerisity of Pittsburgh, Pittsburgh, PA

INTRODUCTION: To investigate the role of TLR9 in the immune response following severe trauma, we analysis the resistance of TLR9 knockout mice as well as inhibitory CpG injected C57BL/6 (WT) mice to immunosuppression in our novel pseudofracture (PFx) model.

METHODS: Male TLR9 knockout and WT mice were randomly assigned to sham operation or PFx. PFx was induced by crushed bone solution injection and soft tissue injury to the thigh musculature bilaterally. For the effects of inhibitory CpG sequence, WT mice were injected with inhibitory or control CpG 100μg/day for 2 days, and then assigned to sham or PFx groups. Serum IL-6 and IL-10 level and splenocytes peroliferation were assesed at 6 h and 48 h following PFx.

RESULTS: PFx increased serum il-6 and il-10 level at 6h, and returned to sham level at 48h posttraumatically in all groups. In WT mice, PFx decreased stimulated T cell proliferation by 45.9% (with concanavalin A, stimulated B cell proliferation by 45.0% (with LPS). In TLR9 knockout mice and inhibitory CpG injected WT mice, the inhibitory effects of PFx on splenocytes proliferation were abrogated, resulting in T and B cell proliferation similar to sham group. Levels of il-6 were significantly increased by PFx in the supernatant of stimulated WT splenocytes, but not in that of TLR9 knockout and inhibitory CpG injected WT splenocytes.

CONCLUSIONS: TLR9 signaling plays a key role in immnosuppression of T and B lymphocytes in late posttraumatic model. TLR9 blockade may be a potential strategy for the treatment of immunosuppression in human severe trauma.

Nanosilver particles with BMP2 improve bone repair of contaminated segmental defects

Janette N Zara MD, Zhong Zheng PhD, Wei Yin MD, Min Lee PhD, Jin Hee Kwak DDS, Ronald Siu MS, Xinli Zhang MD, PhD, Ben Wu DDS, PhD, Kang Ting DMD, DMedSci, Chia Soo MD, FACS*
University of California-Los Angeles, Los Angeles, CA

INTRODUCTION: Healing of contaminated segmental bone defects is a serious clinical problem. Prevalence of multi-antibiotic resistant organisms such as methicillin-resistant Staphylococcus aureus has renewed interest in the use of antiseptic silver as an effective, but less toxic antimicrobial with decreased potential for bacterial resistance. We hypothesize that silver in nanocrystalline form has bactericidal effects that can be combined with BMP2 to treat contaminated bone defects.

METHODS: In vitro microplate proliferation assays of 20-40 nm nanocrystalline silver particles (nanosilver) were performed. MC3T3-E1 pre-osteoblasts were cultured on 0, 1, and 2% nanosilver coupled poly (lactic-co-glycolic acid) (PLGA) scaffolds to determine its toxicity and effects. Nanosilver PLGA scaffolds + BMP2 or PLGA only scaffolds + BMP2 were implanted into 6 mm rat femoral defects contaminated with 10^8 S. aureus Mu50 to determine effects on BMP2 osteoinductivity.

RESULTS: Nanosilver exhibited strong antibacterial properties in vitro and in vivo. Nanosilver coupled PLGA scaffolds did not inhibit adherence, proliferation, ALP activity, or mineralization of MC3T3-E1 pre-osteoblasts compared to uncoupled PLGA scaffold controls. Furthermore, nanosilver did not affect the in vivo osteoinductivity of BMP2. The nanosilver PLGA scaffolds + BMP2 treated femoral defects healed in 8 weeks without evidence of residual bacteria. In contrast, the PLGA only scaffolds + BMP2 group failed to heal due to presence of continued bacteria.

CONCLUSIONS: Our results indicate that nanosilver of defined particle size is bactericidal without discernable in vitro or in vivo osteoblast toxicity or negative effects on BMP2 osteoinductivity, making it an ideal antimicrobial for bone regeneration in infected wounds.

Increased fetal tendon wound size results in a transition from scarless regeneration to scar formation and is associated with upregulation of genes regulating inflammation and cell migration

Myron Allukian MD, Benjamin J Herdrich MD, Dustin M Bermudez MD, Bianca C Chin MD, Louis J Soslowsky PhD, Zhe Zhang PhD, Marc E Mitchell MD, Kenneth W Liechty MD
Hospital of the University of Pennsylvania, Philadelphia, PA

INTRODUCTION: The fetal response to tendon injury is regenerative and scarless, while the adult response results in contracture, scarring and decreased mobility. We have shown that as fetal tendon wound size increases, a transition occurs from regenerative healing to scar formation. This is associated with increased inflammatory gene expression. Normal wound healing consists of 3 phases: inflammatory, proliferative, and remodeling. We hypothesized that increased gene expression of factors involved in cellular migration, proliferation, and regulation of the extracellular matrix may also be involved in this change.

METHODS: In our fetal sheep model, small wounds (50% tenotomy) heal regeneratively whereas large wounds (50% tenotomy with a 2mm excision) heal reparatively. Wounds were harvested 3 days after injury and RNA isolated. An ovine-specific microarray gene chip was used to analyze gene expression for the groups "migration", "proliferation", and "extracellular matrix" selected from the gene ontology database. Genes were considered differentially-expressed between small and large wounds if there was at least a two-fold change and p-value of t-test <0.05.

RESULTS: Large fetal tendon wounds, which heal with inflammation and scar formation, demonstrated significantly higher levels of gene expression for factors involved in cellular migration ($p<0.02$), but not proliferation or regulation of the extracellular matrix, which may explain the increased recruitment of inflammatory cells observed during scar formation.

ISSN 1072-7515/10/$34.00

Infected Femoral Segmental Defect Model: Effects of Nanosilver in Re-Establishing BMP-2 Osteoinductivity in Infected Wounds

[1]Zara J N; [1]Zheng Z; [1]Yin W; [1]Li W M; [1]Siu R K; [1]Kwak J; [1]Ngo R; [1]Chiang M; [1]Zhang X; [1]Ting K, +[1]Soo C
[1]University of California, Los Angeles, Los Angeles, CA
bsoo@ucla.edu

INTRODUCTION:

Bone graft materials are placed in a variety of skeletal defects to promote bony union. Infection of bone graft devices are devastating complications that require multiple debridement surgeries, systemic antibiotic treatment, and may result in osseous non-union. Besides significant medical costs, there are also high costs from lost productivity and function. It is therefore critical to develop a systematic approach to study and treat bone graft infections. The aim of this study is to establish an infected segmental defect model to simulate acute bacterial infections in the setting of a critical-sized, segmental bone loss, and to use this model to test BMP2 efficacy with antibactericidal treatment. *Staphylococcus aureus (S. aureus)* was used in this model because it is the bacterial pathogen responsible for ~80% of all cases of human osteomyelitis. Silver in nano particle size (nanosilver; Ag^{NANO}), rather than an antibiotic, was used in this study because antiseptics such as silver are broad spectrum, potentially low cytotoxicity agents that non-selectively target many bacterial cellular activities and are thus less likely to promote bacterial resistance. We hypothesize that *S. aureus* can effectively create an acute osteomyelitic model without use of sclerosing agents and that nanosilver can restore BMP2 efficacy in osteomyelitic bone defects.

METHODS:

Acute infection model. In order to establish an acute infection model, a 6 mm critical sized femoral segmental defect (FSD) was created in 3 month old male Sprague Dawley rats. All surgical procedures were approved by the UCLA Chancellor's Animal Research Committee. A polyethylene plate (23 x 4 x 4 mm dimension) was fixed on each femur using six 0.9 mm diameter threaded Kirschner wires. 10^6, 10^7, 10^8, 10^9, or 10^{12} standard *S. aureus* (strain SA113) or vancomycin- and methicillin-resistant *S. aureus* (Mu50) inoculated on Gelfoam were implanted into the defect prior to closure. After two weeks, the wounds were opened and degree of infection through bacterial culture and straining for bacterial residue were performed, as well as assessment of hardware fixation stability. *Nanosilver cytotoxicity and bactericidal testing*. Bacteria were inoculated onto nanosilver-loaded poly (lactic-co-glycolic acid) (PLGA) scaffolds of the exact dimension to be implanted for reconstructing the FSD. Cytoxicity testing was performed on 3D PLGA scaffold rather than under 2D culture conditions because 3D conditions more closely simulate *in vivo* conditions and can improve cellular survival with cytotoxic agents. Bactericidal testing was also performed on the PLGA scaffold to better assess whether nanosilver coating effectively prevented infected nidus formation in the PLGA. Cytotoxicity testing was performed by seeding 5,000 passage 18 MC3T3-E1 cells onto 0%, 0.5%, 1%, 1.5%, and 2% Ag^{NANO}-PLGA cylinders in 96-well plates containing maintenance medium. Viable cell density and proliferation on days 2, 4 and 6 were assayed using the MTT Cell Proliferation Assay Kit. Bactericidal testing of nanosilver was performed using bacterial microplate proliferation assays. *Nanosilver and BMP2 efficacy in vivo*. Using our developed acute infected FSD model infected with 10^8 *S. aureus* Mu50, nanosilver PLGA scaffolds + BMP2 or PLGA only scaffolds + BMP2 were implanted into the defects. High resolution faxitron imaging were performed at week 0, 2, 4, 6, 8, 10, and 12. Femurs were harvested at 12 weeks. Histomorphometric assessment including microCT imaging and histological staining to evaluate bone formation were performed.

RESULTS:

Acute infection model. We observed that 10^8 *S. aureus* Mu50 resulted in abundant pus and was the highest inoculum possible without hardware fixation loss, excessive osteolysis, or animal mortality. *S. aureus* Mu50 was superior, as the SA113 strain inconsistently produced infection at similar inoculum doses. *Nanosilver cytotoxicity and bactericidal testing*. Nanosilver exhibited strong antibacterial properties *in vitro* and *in vivo*. Nanosilver coupled PLGA scaffolds did not inhibit adherence, proliferation, alkaline phosphatase activity, or mineralization of MC3T3-E1 pre-osteoblasts compared to uncoupled PLGA scaffold controls. Nanosilver *in vitro* assays showed that 0.1% Ag^{NANO}-PLGA delayed 10^6 CFU *S. aureus* SA113 growth, while 0.5%, 1.0%, 1.5%, and 2% Ag^{NANO}-PLGA 2.0% inhibited 10^6 and 10^7 CFU *S. aureus* SA113 growth completely. Furthermore, 2.0% Ag^{NANO} was the most effective bactericidal dose, consistently killing both 10^7 and 10^8 CFU of the more virulent *S. aureus* Mu50, while lower doses were only variably bactericidal. *Nanosilver and BMP2 efficacy in vivo*. Nanosilver did not affect the in vivo osteoinductivity of BMP2. 20-40% of the animals implanted with 2% Ag^{NANO}-BMP2-PLGA group healed by 8 weeks and ~60% of the animals healed by 10 weeks as assessed by high resolution imaging (**Fig 1**). A mineralized bony bridge connecting the two defect ends was clearly identified by both Masson's trichrome staining and osteocalcin (OCN) immunohistochemistry staining (**Fig 1**). High intensity OCN signals signify active bone formation in the defect area. In contrast, 0% and 1% Ag^{NANO}-BMP2-PLGA groups exhibited no healing. Furthermore, no *S. aureus* Mu50 survival was evident in the contaminated femurs implanted with 2% Ag^{NANO}-BMP2-PLGA bone grafts after 12 weeks. By eliminating bacteria in the defect, 2% Ag^{NANO}-BMP2-PLGA grafts promoted significantly more bone formation compared to the control group.

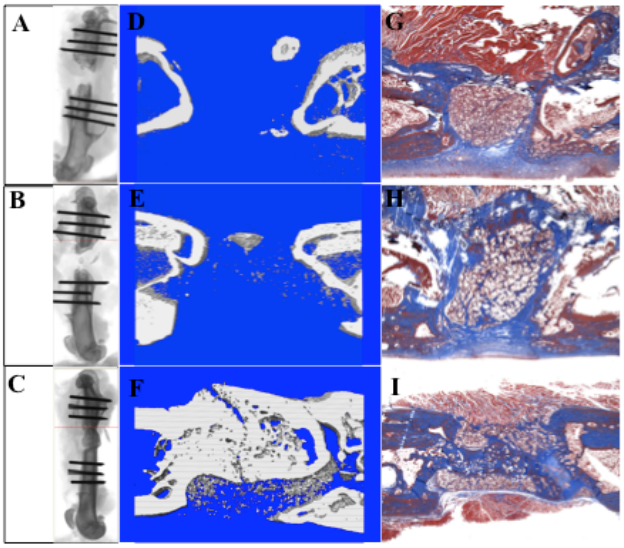

Figure 1. Left column; Representative 2D high resolution imaging of 0, 1, and 2% Ag^{NANO} treated femoral defects at 12 weeks post-operation (**A, B, C**). Middle column; 3D microCT reconstruction of femoral defects, showing bridging bone in the 2% Ag^{NANO} group (**F**) with little or no bone formation in the 0% and 1% groups (**D, E**). Right column; Trichrome staining showing bridging bone in the 2% Ag^{NANO} group (**I**).

CONCLUSION(S):

In this study, we established a consistent acute FSD infection model using Mu50 *S. aureus* without the use of sclerosing agents. Our results using this model indicate that nanosilver of defined particle size is bactericidal without discernable negative effects *in vitro* or *in vivo* on osteoblast toxicity or BMP2 osteoinductivity, making it an ideal antimicrobial for bone regeneration in infected wounds. These results show that it is possible to integrate robust bactericidal and osteoinductive components in one scaffold. This approach shows great promise in shifting the clinical osteomyelitic treatment paradigm from staged debridement and reconstructive surgeries to a single-staged surgery allowing debridement and immediate reconstruction.

RESULTS: 61 (51%) patients received blocks. Total OME ranged from 0 to 5,355 mg, mean 809 mg (Sd: 1025 mg). Mean LOS was 3.8 days (Sd: 3.0). Patients receiving a block were more likely to have insurance vs. none (56% vs. 29%, $p = 0.02$) and surgery for reconstruction (73%) vs. trauma (44%) or infection (32%) ($p = 0.003$). A shorter LOS (3.0 days) was found for patients receiving a nerve block vs none (4.6 days) ($p = 0.002$). Nerve block remained a significant predictor of LOS, after controlling for age, injury severity, insurance status, surgery type, and comorbidities.

CONCLUSIONS: Nerve blocks appear to reduce LOS in patients with TLEI. Additional prospective research is needed to examine outcomes across types of nerve block (single injection vs. continuous) and to assess their impact following upper-extremity traumatic injury.

Synergistic effects of BMP2 and Nell-1, with nanosilver for the healing of infected long bone defects

Yi Liu DDS DNB, Virgnia T Nguyen BSc, Janette N Zara MD, MS, Aaron W James MD, Michael Chiang DDS DNB, Wei Yuan MD, Zhong Zheng PhD, Xinli Zhang MD, PhD, C Soo MD, FACS, Kang Ting DMD, D Med Sci
University of California-Los Angeles, Los Angeles, CA

INTRODUCTION: BMP2-coupled Nanosilver-PLGA composite grafts have been shown to successfully repair grossly infected segmental defects. However, BMP2–regenerated bone are known to have cyst-like bone voids and extensive amounts of fatty tissue. In this study, we hypothesize that addition of the osteoinductive growth factor Nell-1 to the BMP2-coupled Nanosilver-PLGA composite grafts will achieve higher quality bone and faster rates of fusion.

METHODS: Nell-1+BMP2 were added to Nanosilver PLGA scaffolds and implanted into 6 mm rat femoral defects contaminated with 108 S. aureus Mu50. High resolution faxitron images were obtained at 2, 4, 6, 8, 10, and 12 weeks. Femurs were harvested at 12 weeks post-operation. MicroCT analysis, histology, and immunohistochemistry were performed.

RESULTS: Nell-1+BMP2 showed faster healing of femoral defects by 8 weeks post-operation compared to 12 weeks in the previous study with BMP2 alone. Progressive mineralization was seen starting at 4 weeks, with 100% fusion achieved by 8 weeks. microCT 3D reconstructions showed robust bone formation with no cyst formation. Histology showed densely packed woven and lamellar bone.

CONCLUSIONS: Nell-1+BMP2 appear to have synergistic effects. The combination of BMP2+Nell-1 improved bone formation over either cytokine alone, and is a promising combination therapy for faster healing of contaminated bone loss.

Human perivascular stem cells are superior to stromal vascular fraction in ectopic bone formation

Janette N Zara MD, MS, Aaron W James MD, Virginia T Nguyen BSc, Mirko Corselli PhD, Michael Chiang DDS DNB, Xinli Zhang MD, PhD, David Stoker MD, Kang Ting DMD, D Med Sci, Bruno Peault PhD, Chia Soo MD, FACS
University of California-Los Angeles, Los Angeles, CA

INTRODUCTION: Adipose tissue is a promising source of stem cells for skeletal tissue regeneration. However, traditionally derived ASCs (adipose stromal cells) are a heterogeneous cell population of which only a subset are able to undergo osteogenesis. PSCs (perivascular stem cells) are a FACS (fluorescence activated cells sorting) based subset of ASCs, which are a more highly purified cell population with potential utility for bone regeneration.

METHODS: Traditionally derived SVF (stromal vascular fraction) and PSCs were isolated from fresh lipoaspirate as previously described. 2.5×105 cells of SVF and PSCs were combined with 100 uL of demineralized bone matrix putty (DBX) and implanted in the femoral muscle of nude mice, bilaterally. DBX alone was used as control. Samples were harvested at 4 weeks post-operation. Analysis was by microCT, histology, histomorphometry, and immunohistochemistry.

RESULTS: PSC implantation resulted in significantly higher bone formation compared to SVF and DBX control as shown by microCT analysis of bone volume and bone mineral density. Histomorphometric analysis of serial sections of aniline blue slides showed greater bone area of osteoid stained pixels of high power images. Immunochemistry for bone sialoprotein and osteocalcin also showed increased staining in PSCs compared to SVF and DBX control.

CONCLUSIONS: PSCs showed robust bone formation and were superior to SVF in forming bone. PSC homogeneity is ideal for defining their potency and dose response when combined with osteoinductive growth factors. Future studies will examine PSC bone formation within a defect site rather than ectopic site.

Hydrogel barrier for preventing adhesion formation in a sheep lumbar fusion revision model

Bauer Sumpio MD, PhD, FACS, James Yue MD, Anthony Simon Turner BSc, MA, Ann Prewett PhD, Alan Chen MEng(Hon)
Yale University School of Medicine, New Haven, CT, Colorado State University, Fort Collins, CO

INTRODUCTION: Despite the potential for vascular complications, the anterior approach to the lumbar spine is becoming a preferred option when treating degenerative or neoplastic spinal conditions. Revision anterior surgery is even more difficult due to extensive scar formation which may prevent mobilization of the great vessels at the spine levels to be revised. PTFE barriers(Gore Preclude®) are sometimes used to form a plane of separation to facilitate access to the revision site. The aim of this study was to evaluate a hydrogel-cloth (EnGuard™) as an alternative barrier in an animal survival study.

METHODS: Sheep (n=6, 60kg) lumbar spine levels were exposed using a retroperitoneal approach. Interbody fusion, L2/L3 and L4/L5 levels, was performed using autograft and commercial PEEK spacers (Synthes). At alternating levels within the same sheep, the fusion site was covered with hydrogel cloth or PTFE. Sheep were euthanized at 7 and 30 days and a strain gauge quantified the force (N) to release the barrier sheets from the fusion site and the mean $\pm$SD calculated. Barriers were stained with Hematoxylin/Eosin for histological analysis.

The Use of Nanosilver-Containing Materials for Orthopedic Application

Zhong Zheng[1], Janette N. Zara[2], Yi Liu[1], Min Lee[2], Ching-Yun Hsu[1], Kevin S. Lee[1], Xinli Zhang[1], Kang Ting[1], Chia Soo[3]

[1]Dental and Craniofacial Research Institute and Section of Orthodontics, School of Dentistry, [2]Department of Bioengineering, [3]Department of Surgery and Orthopaedic Surgery, David Geffen School of Medicine, University of California, Los Angeles, CA 90095

INTRODUCTION

Blast weapons such as improvised explosive devices (IEDs) can cause devastating soft and hard tissue extremity injuries and significant wound contamination that lead to secondary infection. Here, we tested the antimicrobial property, cytotoxicity, and osteoinductive activity of nanosilver-containing materials in infected bone regeneration models. Bone morphogenetic protein 2 (BMP2)-coupled nanosilver (with a size of 20-40 nm)/PLGA [poly(DL-lactic-*co*-glycolic acid)] composite graft induced bone regeneration in grossly contaminated bone defects. In addition, **s**ilver **n**anoparticle/**P**LGA-coated stainless **s**teel **a**lloy (SNPSA) suppressed biofilm formation that could cause implant infection and induced osteogenesis.

METHODS

Antimicrobial activity was assayed by bacterial colonization and microplate proliferation assay *in vitro* and *ex vivo*, and by Taylor-modified Brown and Brenn's Gram staining *in vivo*. *In vivo* bone formation was evaluated by radiograph, 3D micro-computed tomography (CT) scanning and immunohistological staining.

RESULTS

Nanosilver exhibited strong antibacterial properties *in vitro* and *in vivo* without cytotoxicity against osteoblasts. Grossly contaminated rat femur implanted with BMP2-coupled nanosilver/PLGA composite grafts healed in 12 weeks without evidence of residual bacteria, while the control implanted with BMP2-coupled PLGA failed to heal due to the presence of continued bacterial infection (**Figure 1**). In addition, SNPSA exhibited strong osteoinductive and antibacterial properties, which resulted in bone formation without bacterial survival *in vivo* (**Figure 2**).

CONCLUSIONS

In this study, we have successfully regenerated bone in a 6-mm critical-sized defect (total volume ~75 µl) infected with 10^8 CFU bacteria (~10^9 CFU/ml, which far exceeds the typical 10^5 CFU/ml criteria for invasive tissue infection). Meanwhile, nanosilver/PLGA-coated stainless steel alloy was antibacterial, promoting significant *in vivo* bone formation in the presence of bacterial infection. Our results indicate that nanosilver of defined particle size is bactericidal without discernible osteoblast toxicity or negative effects on osteoinductivity, making it an ideal antimicrobial and osteoinductive agent for bone regeneration in infected wounds.

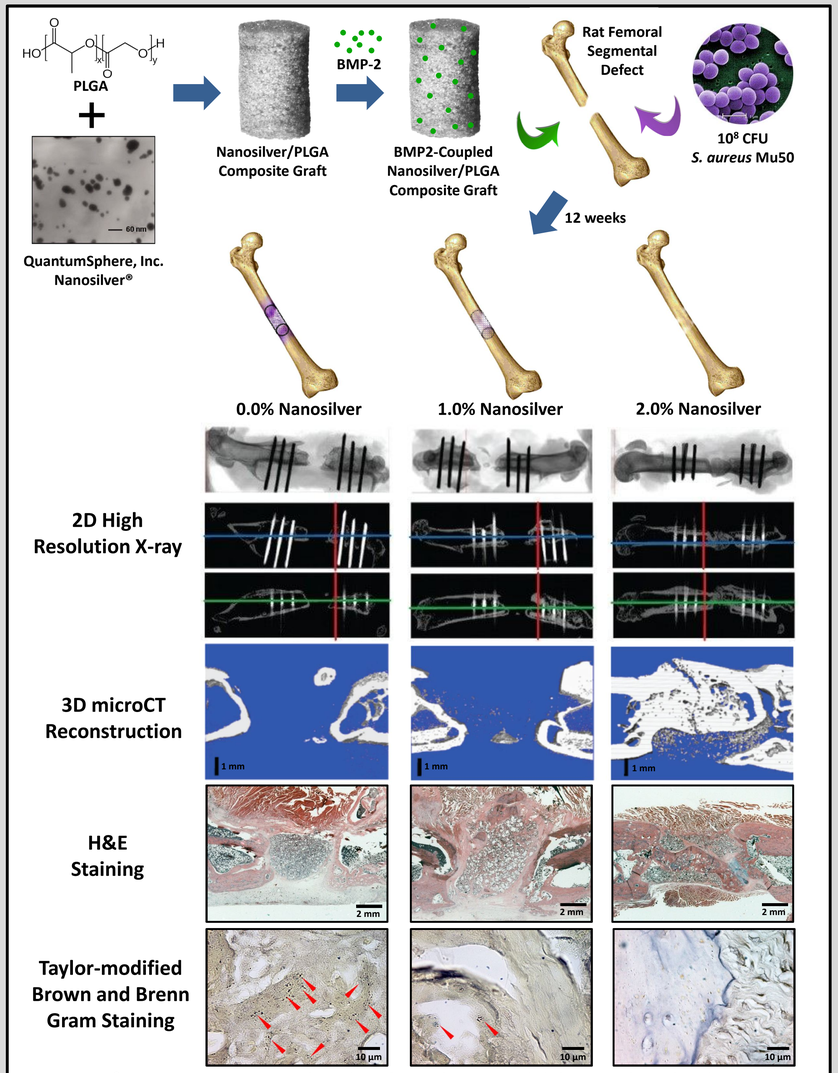

Figure 1. 10^8 CFU *S. aureus* Mu50 infected rat femoral segmental defects implanted with 0.0%, 1.0%, and 2.0% nanosilver/PLGA bone grafts coupled with 30 µg/ml BMP2, at 12 weeks post-implantation. The schematic illustrations, 2D high resolution X-ray and 3D microCT reconstruction images, and H&E and Taylor-modified Brown and Brenn Gram staining showed that almost no bone regenerated in BMP2/0.0%-NS/PLGA groups with obvious bacterial contamination (red arrows). BMP2/2.0%-NS/PLGA grafts promoted significantly greater bone formation to form a bony bridge between the two defect ends by eliminating bacteria. [*Biomaterials* 31 (2010) 9293-9300.]

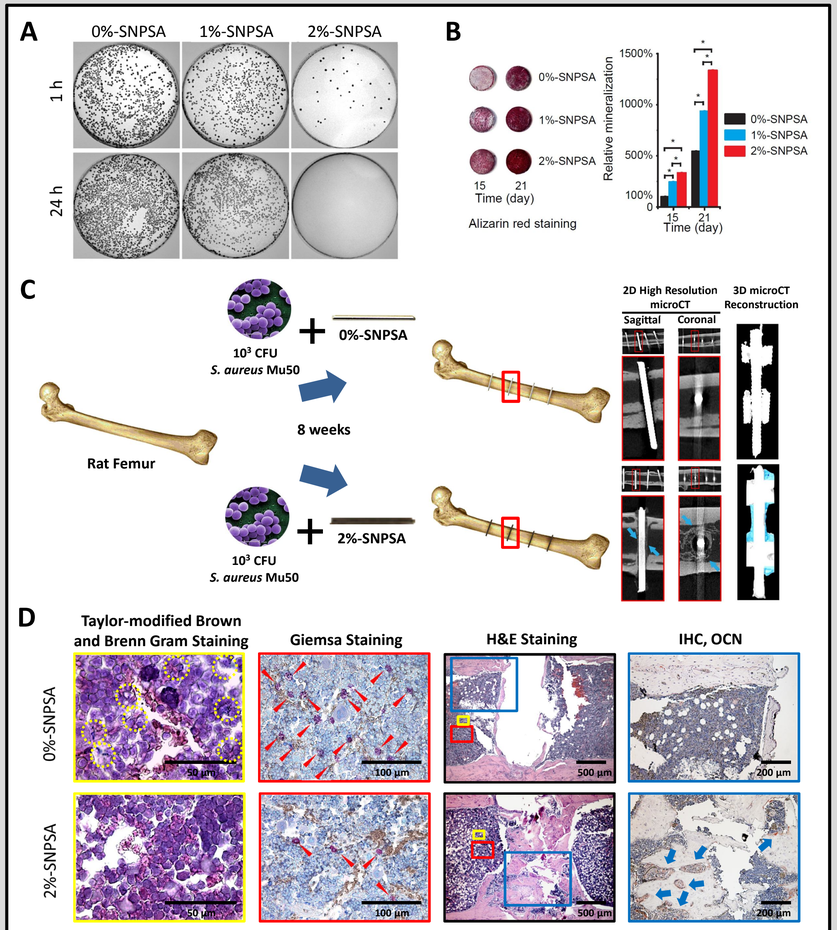

Figure 2. (**A**) SNPSAs inhibited 10^3 CFU *S. aureus* Mu50 adherence and proliferation in a silver-proportion-dependent manner *in vitro*. N = 4; *, P < *0.05*. (**B**) SNPSAs significantly promoted mineralization of mouse osteoblasts *in vitro*. Data normalized to 0%-SNPSA on day 15. N = 6; *, *P < 0.05*. (**C**) Schematic illustrations and microCT images of 0%- and 2%-SNPSA implants in rat femoral canals (FCs) contaminated with 10^3 CFU *S. aureus* Mu50 at 8 weeks post-implantation. (**D**) Taylor-modified Brown and Brenn Gram and Giemsa staining revealed bacterial persistence (yellow dotted circles) with massive inflammatory cell infiltration (red arrows) around 0%-SNPSA implants in rat FCs. In contrast, no bacterial survival was evident around 2%-SNPSA implants, and inflammatory cell infiltration was minimal. H&E staining and immunostaining of high-intensity OCN signals showed only minimal bone formation around 0%-SNPSA implants but significant bone formation (blue arrows) around 2%-SNPSA implants. [*Biomaterials* (2012) In press.]

DISCLOSURE

K. T., C. S., and Z. Z. are inventors of silver nanoparticle-related patents filed from the UC Regents.

This study was funded by US DoD Grant 07128099.

SP20 | 9:45 - 11:15 am
General Surgery II
Location: W 187

TRACK: GEN

MODERATOR: Barbara L. Bass, MD, FACS, *Houston, TX*

Do Small Bowel Serosal Tears Perforate under Physiological Conditions?
Ming-Chih Tsai, MB, BCh; Andrew Grieve; Martin Brand; Geoffrey Candy. *University of Witwatersrand, Johannesburg, South Africa.*

Predicting Midline Fascial Re-approximation with Component Separation in Complex Ventral Hernias: Maximizing the Utility of Preoperative Computed Tomography
Parag Bhanot, MD; Brenton Franklin, MD; Ketan M. Patel, MD; Laura E. Baldassari, MD; Maurice Y. Nahabedian, MD, FACS. *Georgetown University Hospital, Washington, DC.*

Functional Polymorphism in CYP2E1 Is Associated With the Development, Progression, and Poor Outcome of Gastric Cancer
Zekuan Xu, MD; Jin Feng; Xiaolin Pan; Bin Wang. *The First Affiliated Hospital of Nanjing Medical University, Nanjing, China.*

Predictors of Discharge Disposition on Mortality in Octogenarians Undergoing Major Abdominal Surgery
Josh Knudson, MD; Sarah McDonough; Justin Gregg. *TriHealth, Cincinnati, OH.*

Incisional Hernia Repair after Abdominal Operations: Long-Term Follow-up of Multiple Surgical Procedure Types
Benjamin K. Poulose, MD, MPH; Benjamin K. Poulose, MD, MPH; Sharon Phillips, MSPH; William Beck, MD; Julia Shelton, MD, MPH; Kenneth W. Sharp, MD, FACS; William Nealon, MD, FACS; Michael D. Holzman, MD, FACS. *Vanderbilt University Medical Center, Nashville, TN.*

Nanosilver-Coated Stainless Steel: An Antimicrobial and Osteoinductive Material for Orthopedic Device Fabrication
Zhong Zheng, PhD; Yi Liu, DDS; Janette N. Zara, MD; Michael Chiang, BDS; Wei Yuan, MD; Ching Yun Hsu, BDS; Donnalisa Soofer; Xinli Zhang, MD, PhD; Kang Ting, DMD, DMedSci; Chia Soo, MD. *University of California, Los Angeles, Los Angeles, CA.*

Appendectomy Gone Wrong: The Who and Where of Accidental Puncture of Laceration during a Procedure
Justin Lee, MD; Peter Miller, MD; Reza Kermani, MD; Alan Hackford, MD, FACS. *St. Elizabeth Medical Center, Tufts University School of Medicine, Boston, MA.*

Nanosilver coated stainless steel: an antimicrobial and osteoinductive material for orthopedic device fabrication

Authors
Zhong Zheng, Ph.D., Yi Liu, D.D.S., Janette N. Zara, M.D., Michael Chiang, B.D.S., Wei Yuan, M.D., Ching Yun Hsu, B.D.S., Donnalisa Soofer, B.S., Xinli Zhang, M.D., Ph.D, Kang Ting, D.M.D., D.Med.Sci., Chia Soo, M.D.

Abstract
INTRODUCTION: To date, bacterial infections remain one of the most serious complications after orthopedic device implantation. Treatment of orthopedic implant infections generally requires removal of the infected device, multiple debridement surgeries, and long-term systemic antibiotic therapy—with resultant prolonged healing times or development of bony nonunions. Previously, we described successful repair of grossly infected segmental bone defects using BMP2-coupled nanosilver-poly($_{DL}$-lactic-*co*-glycolic acid)(PLGA) composite grafts. In this study, we hypothesize that nanosilver coated stainless steel implants will have both bactericidal and osteoinductive effects.

METHODS: *In vitro* and *ex vivo* bactericidal properties of 20-40 nm nanosilver particle-coated stainless 316L steel Kirschner (K)-wires against gram-positive vancomycin-resistant MRSA *Staphylococcus aureus* Mu50 and gram-negative *Pseudomonas aeruginosa* PAO-1 were assessed by microplate proliferation assays. Nanosilver-coated K-wires were implanted into rat femurs with 1,000 CFU bacteria to determine *in vivo* antibacterial and osteoinductive effects. MC3T3-E1 pre-osteoblasts were also cultured on 0, 1, and 2% nanosilver coupled 316L steel K-wires and pl ates (without bacteria) to evaluate combined nanosilver/steel toxicity and osteoinductivity.

RESULTS: Nanosilver coated K-wires exhibited strong antibacterial properties *in vitro*, *ex vivo*, and *in vivo*. Nanosilver-coated stainless steel K-wires significantly promoted bone regeneration at 8 weeks after implantation. Interestingly, *in vitro* nanosilver coated stainless steel surfaces increased MC3T3-E1 pre-osteoblasts proliferation, ALP activity, and mineralization compared to uncoated steel controls.

CONCLUSION(S): Nanosilver coated stainless steel implants are potently bactericidal, promoting significant *in vivo* bone formation in the presence of gram-positive or gram-negative infection. Excitingly, nanosilver/steel implants may also possess novel osteoinductive properties distinct from its antimicrobial effects.